Fall 12-2016

Doppler Temperature Coefficient Calculations Using Adjoint-Weighted Tallies and Continuous-Energy Cross Sections in MCNP6

Matthew A. Gonzales

Matthew Alejandro Gonzales

Candidate

Nuclear Engineering

Department

This dissertation is approved, and it is acceptable in quality and form for publication:

Approved by the Dissertation Committee:

Prof. Anil K. Prinja , Chairperson

Dr. Gary Cooper

Dr. Forrest Brown

Prof. Brian Kiedrowski

Doppler Temperature Coefficient Calculations Using Adjoint-Weighted Tallies and Continuous Energy Cross Sections in MCNP6

by

Matthew Alejandro Gonzales

B.S., Regis University, 2009
M.S., Engineering, University of New Mexico, 2012

DISSERTATION

Submitted in Partial Fulfillment of the
Requirements for the Degree of

Doctor of Philosphy
Engineering

The University of New Mexico

Albuquerque, New Mexico

December, 2016

Dedication

To my parents, for their continued support throughout my career as a student. To my wife and daughter, whose inspiration has been priceless.

Acknowledgments

I would like to thank my advisor, Professor Anil K. Prinja, for his support and constant encouragement. There were many hours spent on the board discussing this research; his patience and attention to detail were paramount to my success. I would also like to thank Professor Brian Kiedrowski for his ideas and helpfulness. Brian's feedback was always held in high regard and I am very thankful for having him as a mentor throughout my development as a researcher. Thanks also goes to Dr. Forrest Brown for his continued support through my masters work on up to this dissertation. His help with MCNP has given me the confidence to work with a production level code and become proficient in code development. If it wasn't for these people I would not have had the opportunity to fulfill this work, I am ever thankful for their help and support.

Doppler Temperature Coefficient Calculations Using Adjoint-Weighted Tallies and Continuous Energy Cross Sections in MCNP6

by

Matthew Alejandro Gonzales

B.S., Regis University, 2009
M.S., Engineering, University of New Mexico, 2012
Ph.D., Engineering, University of New Mexico, 2016

Abstract

The calculation of the thermal neutron Doppler temperature reactivity feedback coefficient, a key parameter in the design and safe operation of advanced reactors, using first order perturbation theory in continuous energy Monte Carlo codes is challenging as the continuous energy adjoint flux is not readily available. Traditional approaches of obtaining the adjoint flux attempt to invert the random walk process as well as require data corresponding to all temperatures and their respective temperature derivatives within the system in order to accurately calculate the Doppler temperature feedback.

A new method has been developed using adjoint-weighted tallies and On-The-Fly (OTF) generated continuous energy cross sections within the Monte Carlo N-Particle (MCNP6) transport code. The adjoint-weighted tallies are generated during the continuous energy k-eigenvalue Monte Carlo calculation. The weighting is based upon

the iterated fission probability interpretation of the adjoint flux, which is the steady state population in a critical nuclear reactor caused by a neutron introduced at that point in phase space. The adjoint-weighted tallies are produced in a forward calculation and do not require an inversion of the random walk. The OTF cross section database uses a high order functional expansion between points on a user-defined energy-temperature mesh in which the coefficients with respect to a polynomial fitting in temperature are stored. The coefficients of the fits are generated before runtime and called upon during the simulation to produce cross sections at any given energy and temperature. The polynomial form of the OTF cross sections allows the possibility of obtaining temperature derivatives of the cross sections on-the-fly.

The use of Monte Carlo sampling of adjoint-weighted tallies and the capability of computing derivatives of continuous energy cross sections with respect to temperature are used to calculate the Doppler temperature coefficient in a research version of MCNP6. Temperature feedback results from the cross sections themselves, changes in the probability density functions, as well as changes in the density of the materials. The focus of this work is specific to the Doppler temperature feedback which result from Doppler broadening of cross sections as well as changes in the probability density function within the scattering kernel. This method is compared against published results using Mosteller's numerical benchmark to show accurate evaluations of the Doppler temperature coefficient, fuel assembly calculations, and a benchmark solution based on the heavy gas model for free-gas elastic scattering.

An infinite medium benchmark for neutron free gas elastic scattering for large scattering ratios and constant absorption cross section has been developed using the heavy gas model. An exact closed form solution for the neutron energy spectrum is obtained in terms of the confluent hypergeometric function and compared against spectra for the free gas scattering model in MCNP6. Results show a quick increase in convergence of the analytic energy spectrum to the MCNP6 code with increasing tar-

get size, showing absolute relative differences of less than 5% for neutrons scattering with carbon. The analytic solution has been generalized to accommodate piecewise constant in energy absorption cross section to produce temperature feedback. Results reinforce the constraints in which heavy gas theory may be applied resulting in a significant target size to accommodate increasing cross section structure. The energy dependent piecewise constant cross section heavy gas model was used to produce a benchmark calculation of the Doppler temperature coefficient to show accurate calculations when using the adjoint-weighted method. Results show the Doppler temperature coefficient using adjoint weighting and cross section derivatives accurately obtains the correct solution within statistics as well as reduce computer runtimes by a factor of 50.

Contents

List of Figures

List of Tables

List of Tables

List of Tables

Chapter 1

Introduction

Reactor design and analysis require the characterization of certain safety parameters. One of these safety parameters, the Doppler temperature coefficient, involves the temperature feedback resulting in the operation of nuclear reactors. In order to obtain this value, it requires an accurate evaluation of the neutron transport equation. As a result, much effort has been put into resolving the double differential scattering kernel which contributes to the temperature feedback and accounts for those neutrons which have collided into the phase space in question. This work is specifically concerned with neutron elastic scattering using the free-gas scattering model under the conditions when the relative speed is small enough to consider the target as stationary yet large enough to ignore any crystalline lattice effects. Free-gas scattering in the thermal energy range for heavy and intermediate-mass isotopes assumes an isotropic Maxwellian velocity distribution to describe the agitation of the atoms in the target[4]. This method of characterizing the scattering kernel is employed in all deterministic and stochastic transport codes currently used in the nuclear industry. The total scattering cross section is typically assumed to be constant but recent work has considered techniques to relax this restriction[5][6]. The formulation of the Doppler-broadened transfer kernel derived in Ref[5] shows that

the neutron energy spectrum is strongly dependent on the medium temperature and the presence of scattering resonances in certain isotopes.

Research efforts over the last several years have focused on Doppler broadening of the scattering kernel in an attempt to accurately calculate the change in reactivity due to temperature feedback. Earlier works [7],[8] focused on the proof and development of the concept in the model given by Ref.[5], while more recent efforts have focused on the deterministic[9],[10],[11],[12],[13],[14] and stochastic[15],[6],[16],[17],[18] implementation of Doppler broadened kernels. Inherent to all of these efforts is the use of calculating the Doppler temperature coefficient to quantify differences between the different models. This work will focus on enhancing the computation of the Doppler coefficient in the MCNP6 Monte Carlo code by reducing the computer runtime of current methods while still maintaining accurate results providing a more efficient alternative to comparing the various Doppler broadened kernels.

In order to verify the changes in the reactivity due to changes in temperature a numerical benchmark[19] was constructed and approved by the Joint Benchmark Committee of the Mathematics and Computation Division of the American Nuclear Society. For Monte Carlo codes, this benchmark has been employed in works[6][20][21] previously described in order to quantify Doppler broadening of the cross sections and their associated probability functions. This benchmark calculates the Doppler-defect by a direct subtraction method in which two reactivity values are calculated at two different fuel temperatures resulting in a finite-difference approximation of the reactivity temperature derivative. This requires two separate calculations at two separate temperatures, which leads to a time-consuming estimate of the Doppler temperature coefficient. In order to improve the efficiency in quantifying the Doppler temperature feedback, recent work [22], provides an alternative method to estimating the Doppler temperature coefficient requiring only one calculation. Reference [22] and [23] take advantage of recent advancements in Monte Carlo perturbation meth-

ods and sensitivity calculations[24],[21],[25]. Reference [22] uses an adjoint-weighted correlated sampling method[20] in order to predict the reactivity change due to fuel temperature variations as accurately as the conventional direct subtraction method, yet requires direct differencing during the calculation which leads to significant data requirements and also limits the calculation to a fixed temperature. This dissertation will add to this field of study by using an adjoint-weighted methodology which uses cross section derivatives requiring only a single set of data per nuclide and allows for an unlimited variation in temperature.

In order to contribute to this field of study, the following work was produced. First, completing the efficient computation of the Doppler temperature coefficient will be presented which will include the contribution of cross sections and probability distributions to the change in reactivity with respect to temperature. This new method takes advantage of adjoint-weighted tallies and continuous-energy cross section data sets in MCNP6. Unlike the direct subtraction method, only one calculation is needed to approximate the Doppler temperature coefficient. Further, this new method may handle multiple temperatures for multiple materials with no significant increase in cross section data libraries. While a numerical benchmark does exist, investigation into an analytic benchmark was made and produced based on the heavy gas model. The heavy gas model produced an analytic expression of the temperature dependent reactivity eigenvalue k and is used to benchmark the reactivity temperature derivative.

Relevant definitions, an explanation of first-order perturbation theory applied to this problem, as well as cross section temperature derivatives are discussed in Chapter 2 & Chapter 4. A discussion of the temperature sensitivities with respect to cross sections and probability distributions, along with preliminary results showing comparable results with respect to the conventional direct subtraction method are presented in Chapter 4. Discussion of the analytic representation of free-gas scatter-

ing using the heavy-gas model is made in Chapter 5 as well as a comparison of the Doppler temperature coefficient obtained with the heavy-gas model and MCNP6.

Concluding discussions will consist of the continued research, which include discussions on expanding this dissertation work as well as a potential pathway for calculating the scattering kernel using a non-constant cross section model.

Chapter 2

Monte Carlo Neutron Transport for Reactor Analysis

The fundamental understanding of reactor design and analysis requires the evaluation of a neutron population within a system. The evaluation of neutron population falls under the field of study known as particle transport. Particle transport for charged and neutral particles is a broad field and many techniques have been developed to simulate particle movement within specific systems. Areas of study include, but are not limited to, medical physics, radiation shielding, radiation protection and dosimetry, fission and fussion reactor design and radiation detector analysis. Neutron transport phenomena in various media is characterized by the Boltzman transport equation and was originally developed to study the kinetic theory of gases[26]. The Boltzman transport equation describes the behavior of neutrons with respect to seven dimensions of phase-space, position(3-dimensional Cartesian space), angle(polar and azimuthal), energy and time. While the time-dependent Boltzman transport equation lends itself to a specific realm of reactor analysis, i.e. transient analysis of reactors, the focus of this dissertation is with respect to the steady-state or time-independent equation.

The steady-state neutron Boltzman transport equation is given by:

$$\vec{\Omega} \cdot \nabla\psi(\vec{r},\vec{\Omega},E) + \Sigma_t\left(\vec{r},E\right)\psi\left(\vec{r},\vec{\Omega},E\right) = \int_0^{\infty}\int_0^{4\pi}\Sigma_s\left(\vec{\Omega}'\cdot\vec{\Omega},E'\to E\right)\psi\left(\vec{r},\vec{\Omega}',E'\right)d\vec{\Omega}'dE' + Q\left(\vec{r},\vec{\Omega},E\right), \tag{2.1}$$

$$\vec{r}\in V, \quad \vec{\Omega}\in 4\pi, \quad 0<E<\infty.$$

The angular flux $\psi\left(\vec{r},\vec{\Omega},E\right)$ describes the expected number of neutrons per unit area per angle per unit energy and is proportional to the neutron density $N\left(\vec{r},\vec{\Omega},E\right)$ which describes the expected number of neutrons per unit volume per angle per unit energy:

$$\psi\left(\vec{r},\vec{\Omega},E\right) = vN\left(\vec{r},\vec{\Omega},E\right) \tag{2.2}$$

where v is the speed of the neutron which is given by $v=\sqrt{\frac{2E}{m}}$ and m is the mass of the neutron. The macroscopic cross sections Σ represent probabilities of interaction per unit length and are used to determine reaction rates with respect to specific interactions. Subscripts represent separate interactions where t, s are respectively the total and scattering reactions.

The spatial vector $\vec{r}$ is represented in three-dimensional Cartesian coordinates by standard notation $\vec{r}=x\hat{i}+y\hat{j}+z\hat{k}$ and represents the position of the neutron shown in Figure 2.1. The angular unit vector $\vec{\Omega}$ is determined by the polar angle, θ and the azimuthal angle φ in which the components of $\vec{\Omega}$ are given by:

$$\begin{aligned}
\vec{\Omega}_x &= (1-\cos\theta)^{1/2}\cos\varphi,\\
\vec{\Omega}_y &= (1-\cos\theta)^{1/2}\sin\varphi,\\
\vec{\Omega}_z &= \cos\varphi, \qquad \theta=[0,\pi], \quad \varphi=[0,2\pi],
\end{aligned} \tag{2.3}$$

representing the direction in which the neutron is headed at the point $\vec{r}$. The variable E represents the energy of the neutron.

Equation 2.1 is a balance equation where the left hand side represents the loss of neutrons in phase-space and the right side of the equation represents the gains within phase-space. The loss terms include, from left to right, the net leakage of neutrons from the system and the total collision rate of neutrons. The gain terms, from left to right respectively, are the in-scattering source neutrons and the source neutrons. The in-scattering source is defined by a double differential cross section which states the probability of some neutron traveling in the direction $\vec{\Omega}'$ with energy E' scatters into some differential $d\vec{\Omega}'$ and dE' about $(\vec{\Omega}, E)$ and is given explicitly as:

$$\Sigma_s \left(\vec{\Omega}' \cdot \vec{\Omega}, E' \rightarrow E\right) = \Sigma_s \left(\vec{\Omega}', E'\right) p_\Omega(\vec{\Omega}' \cdot \vec{\Omega}) p_E(E' \rightarrow E) \tag{2.4}$$

where p_Ω and p_E are probability functions determining the probabilities of the neutron with incoming direction $\vec{\Omega}'$ will have an outgoing direction $\vec{\Omega}$ and a neutron with incoming energy E' will have an outgoing energy E. The scattering cross section is the sum of elastic and inelastic collisions, elastic collisions occur when the momentum and kinetic energy of the neutron and nucleus are conserved before and after a neutron interacts with a target nucleus. Inelastic collisions are those which kinetic energy is not conserved before and after the neutron collision with the nucleus. In an inelastic collision the transfer of energy from the neutron to the nucleus may be absorbed by the nuclei causing an excited state, in which the nucleus will emit a gamma ray to return to it's ground state.

The source definition $Q\left(\vec{r}, \vec{\Omega}, E\right)$ is dependent on the specific problem in question. For fissile materials, $Q\left(\vec{r}, \vec{\Omega}, E\right)$ is given by:

$$Q\left(\vec{r}, \vec{\Omega}, E\right) = \frac{\chi(E)}{4\pi k_{\text{eff}}} \int_0^\infty \int_{4\pi} \nu\Sigma_f(\vec{r}, E') \psi\left(\vec{r}, \vec{\Omega}', E'\right) d\vec{\Omega}' dE' \tag{2.5}$$

where the probability of a fission event is given by Σ_f, the number of neutrons per fission is given by ν, the isotropic distribution of fission neutrons in energy is given by χ, and k is the criticality eigenvalue which is physically interpreted as the

neutron multiplication factor. Reactor calculations which attempt to solve for the k-eigenvalue are known as criticality calculations and use the eigenfunction ψ to determine a unique, positive and nonzero solution. A nuclear reactor is determined to be critical for k exactly equal to one, meaning the number of neutrons produced equals the number of neutrons lost. For k less than one, a reactor is said to be subcritical, meaning the number of neutrons produced is less than the number of neutrons lost. And for k greater than one, a reactor is said to be supercritical, meaning the number of neutrons produced is greater than the number of neutrons lost in the reactor. The calculation of k for varying reactor configurations is one of the most frequent and important calculations in the design and operation of nuclear reactors. In the study of reactor kinetics, the criticality k is sometimes replaced by the reactivity ρ, defined by:

$$\rho = \frac{k-1}{k} \tag{2.6}$$

In order to solve the steady state k-eigenvalue criticality value, boundary conditions must be defined. Analytic solutions to simplified versions of the Boltzman transport equation include but are not limited to reflecting and vacuum boundary conditions[26]. In order to solve more complicated neutron transport problems, deterministic and stochastic numerical methods are employed[26][27][28]. Hybrid methods, a combination of deterministic and stochastic methods, are also a rich research area in which the Boltzman transport equation can be solved.

Each of these methods have their own benefits. Deterministic methods discretize the Boltzman transport equation in space, angle and energy and can be used to calculate global(i.e. k-eigenvalue) and local(i.e. ϕ-eigenfunction) quantities. Discretization of phase-space may result in high numerical error for course grids, yet become computationally expensive for extremely fine grids. As a result, for complex geometries, it is extremely difficult to represent three-dimensional geometries in deterministic codes. Recent research efforts have focused on the development of efficient

algorithms within deterministic neutron transport codes. Furthermore, multigroup calculations suffer from experimental error in the cross sections as well as difficulty characterizing weight-functions associated with multi-group normalizations.

Monte Carlo methods use a stochastic approach to solve the neutron transport equation. This takes advantage of the "random walk" process which neutrons undergo. Since the system is not discretized, the geometry and physics is modeled exactly and therefore, Monte Carlo methods do not suffer from truncation errors rather, Monte Carlo calculates averaged quantities which produce statistical uncertainties. These uncertainties may require long computational time to reduce the statistical noise to predict neutron behavior in a reactor with a high degree of accuracy.

2.1 Neutron Slowing Down and Thermalization

The Doppler temperature coefficient quantifies the change in reactivity with respect to a change in temperature of the system. The scattering of neutrons is directly related to the temperature of the medium and therefore effects the energy of neutrons within a system as they slow down from fission. *Fast neutrons*, which are those born from fission, must scatter down through the epithermal range to thermal energies where they are readily absorbed. The epithermal range of neutrons energy E are given by $0.025\text{eV} \geq \text{E} < 1\text{MeV}$ while thermal energies are given by energies $0.025\text{eV} < \text{E}$. In the *epithermal region*, neutrons are moving fast enough that the thermal motion of the nuclei may be neglected and the nucleus is assumed to be at rest in the laboratory system. As a result, the atoms of the nuclei are treated as free, unbound, due to the insignificance of the binding energy in comparison to the neutron-nucleus interaction. For neutrons with energies comparable to the nuclei, those in the *thermal region*, the motion of the nuclei is no longer insignificant and therefore may no longer

be considered at rest. Unlike the slowing-down of neutrons in the *epithermal region*, if the scattering nucleus is in motion, there is a probability that a neutron may experience an increase in energy during a neutron-nucleus interaction. Furthermore, at low enough neutron energies, chemical binding and crystal lattice effects must also be considered.

Depending on where the neutron is in energy space determines the double differential scattering cross section. In the thermal region, $S(\alpha, \beta)$ probability tables are used which take into account binding and lattice effects. At the upper thermal region on through the epithermal region, the scattering function is defined by a monatomic gas or free gas model. This model assumes the target nuclei are in motion but is considered unbound, meaning the binding energy and crystal lattice effects do not contribute to the scattering of neutrons with the nuclei. For the upper thermal region where neutron energies are significantly higher (400 times the thermal motion of the target) target-at-rest kinematics are used.

2.1.1 Target-at-Rest Kinematics

When the neutron is traveling significantly faster than the target nuclei it is possible to assume the target is stationary and assume the target velocity is zero and elastic scattering is dominate. Consider a neutron with some incident velocity $\mathbf{v}$ and some target with a mass ratio A and velocity $\mathbf{V}$ in the laboratory frame. The center-of-mass velocity is given by:

$$\mathbf{v}_{cm} = \frac{\mathbf{v} + A\mathbf{V}}{A + 1} \tag{2.7}$$

Now consider Figure 2.2 which depicts the laboratory frame versus the center-of-mass frame where velocities in the center-of-mass frame are denoted with c in the subscript and outgoing velocities are denoted by the apostrophe in the superscript.

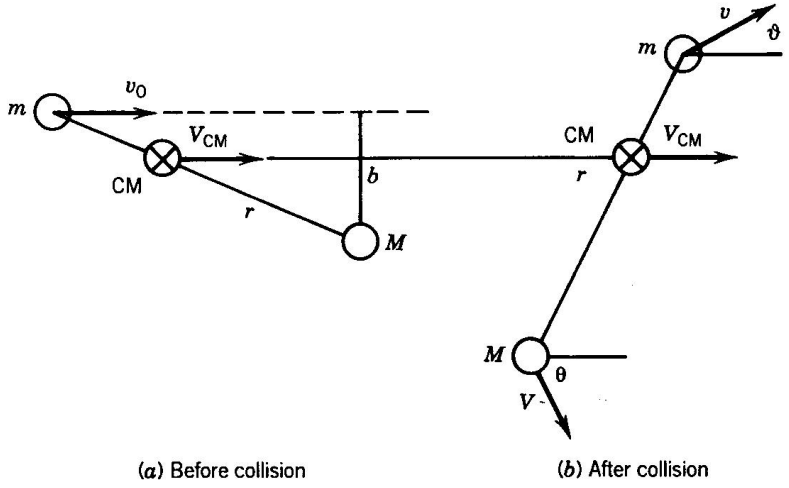

Figure 2.1: Depcition of neutron kinematics in the laboratory frame before and after collision.[1]

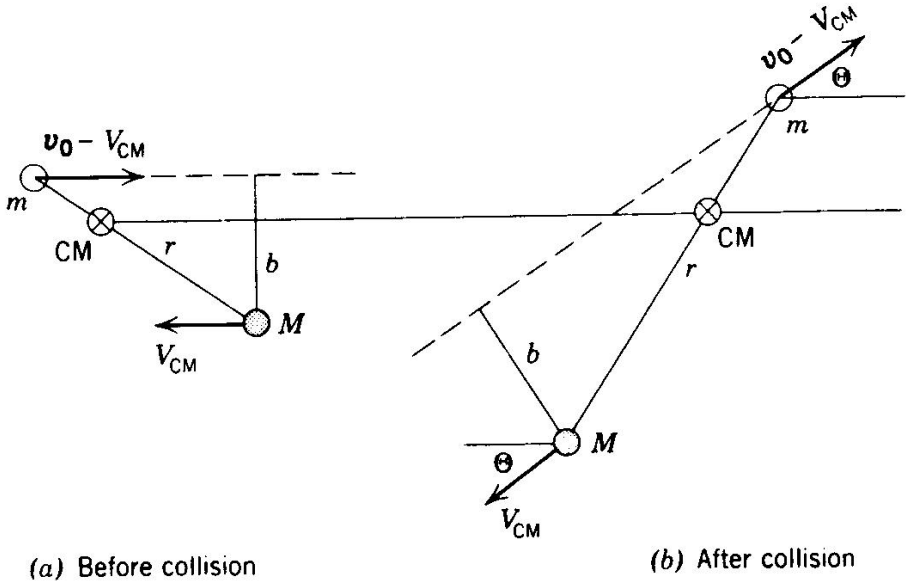

Figure 2.2: Depcition of neutron kinematics in the center-of-mass frame before and after collision.[1]

Scattering in the center-of-mass frame is assumed to be isotropic ($p_\Omega = 1/4\pi$)and elastic collisions conserve both kinetic energy and momentum, as a result the incident

neutron and final neutron speeds v_c, v_c' are equivalent in the center-of-mass system and can be found in terms of the relative speed v_r between the neutron and the nucleus by[26]:

$$v_c = v_c' = \frac{A}{A+1} v_r, \tag{2.8}$$

similarly for the target,

$$V_c = V_c' = \frac{1}{A+1} v_r. \tag{2.9}$$

Since the speeds do not change when in the center-of-mass frame, the neutron and nucleus velocity vectors simply rotated through the center-of-mass scattering angle ϕ_c. The scattering angles in the center-of-mass frame ϕ_c and the lab frame ϕ_l are related by:

$$\tan \phi_l = \frac{\sin \phi_c}{\frac{1}{A} + \cos \phi_l} \tag{2.10}$$

Since cross sections are usually calculated in the center-of-mass frame but are measured in the lab frame, it is important to be able to relate the two frames of reference with their respective differential elastic scattering cross sections. This is explicitly given by[26]:

$$\sigma_l(\phi_l) = \sigma_c(\phi_c) \frac{\left(\frac{1}{A^2} + \frac{2}{A} \cos \phi_c + 1\right)^{3/2}}{1 + \frac{1}{A} \cos \phi_c} \tag{2.11}$$

In terms of outgoing energy E_f, it can be shown using vector analysis and the relationship between energy and velocity to show the outgoing energy can be found from the initial energy E_i of the neutron and the center-of-mass scattering angle ϕ_c and is given by:

$$E_f = \left[\frac{(1+\alpha) + (1-\alpha) \cos \phi_c}{2} \right] E_i \qquad \text{where,} \tag{2.12}$$

$$\alpha = \left(\frac{1-A}{1+A} \right)^2 \tag{2.13}$$

Equation 2.12 shows that the final energy E_f is only dependent on the scattering angle in the center-of-mass and the initial energy E_i of the neutron. When the scattering angle in the center-of-mass $\cos\phi_c = 1$ this means the neutron did not collide with the target and sets the minimum energy loss to zero. The maximum energy loss occurs when the neutron backscatters ($\cos\phi_c = -1$) and the most energy a neutron can lose in a single collision is αE. Further inspection shows a neutron colliding with hydrogen can lose all of its energy in a single collision where heavier targets require more collisions to reduce the neutron energy as the maximum energy loss is inversely related to the target mass ratio. Since the scattering is isotropic in the center-of-mass, the differential elastic scattering cross section for energy is given by

$$\Sigma_s(E' \to E) = \Sigma_s(E')p_E(E' \to E) \qquad \text{where,} \tag{2.14}$$

$$p_E(E' \to E) = \begin{cases} \frac{1}{(1-\alpha)E}, & \text{if } \alpha E' < E < E' \\ 0, & \text{otherwise} \end{cases} \tag{2.15}$$

This probability is only with respect to elastic scattering in which the neutron is traveling fast enough to consider the target to be stationary and is therefore the reason why elastic scattering in the epithermal range is dominant. In the case where the neutron energy is close to thermal energies where the velocity of the nuclei are not stationary different models must be used.

2.1.2 Thermal Neutrons

For neutrons whose kinetic energies are low enough to be near the thermal motion of the target material target-at-rest kinematics no longer are valid. Target-at-rest kinematics assumed isotropic scattering in the center-of-mass as well as the lab frame velocity of the target to be zero which resulted in the impossibility of upscattering, an increase in energy resulting from the scattering event. When the neutron's energy

is near the thermal energy of the target there becomes a probability at which the neutron will not only lose energy (downscatter) but also gain energy (upscatter) in the collision. As a result the model to capture thermal scattering must include probabilities of both upscatter and downscatter. While various models exist, focus of this dissertation is with respect to free gas scattering and only it will be discussed.

When neutrons slow down to thermal energies they take on a distribution similar to that of the thermal distribution of the medium, a Maxwellian distribution and is given by:

$$\phi(E)dE = \phi_{th}M(E,T)dE \qquad \text{where,} \tag{2.16}$$

$$M(E,T) \equiv \frac{E}{(kT)^2}e^{-E/kT} \qquad \text{so that,} \tag{2.17}$$

$$\int_0^\infty M(E,T)dE = 1$$

By considering the infinite medium, time-independent neutron transport equation in the absence of absorption, the distribution of neutrons is a Maxwellian:

$$\Sigma_s(E)M(E,T) = \int\int \Sigma_s(E')p\left(\vec{\Omega}'\cdot\vec{\Omega}, E'\rightarrow E\right)M(E',T)d\vec{\Omega}'dE' \tag{2.18}$$

and this equation must be satisfied. This is results in the following detailed-balance relation:

$$\Sigma_s(E')p\left(\vec{\Omega}'\cdot\vec{\Omega}, E'\rightarrow E\right)M(E',T) = \Sigma_s(E)p(\vec{\Omega}\cdot\vec{\Omega}', E'\rightarrow E)M(E,T) \tag{2.19}$$

This equation states that the rate of neutrons in the direction $\vec{\Omega}'$ with energy E' scattering in the direction $\vec{\Omega}$ with energy E is equal to the rate of neutrons in the direction $\vec{\Omega}$ with energy E will scatter in the direction $\vec{\Omega}'$ with energy E'. Integration over $d\vec{\Omega}$ and dE will recover Equation 2.18. This detailed-balance relation is required for cross sections when dealing with neutrons in a Maxwell distribution and used when obtaining models which approximate the scattering distributions.

One of the simplest scattering models is the free gas scattering model. This scattering model is simple enough to be derived explicitly[4] and is summarized in detail in Appendix A. Also, it is this model that MCNP6 uses for thermal scattering and is also relevant to the work in this dissertation. This model assumes the nuclei are unbound and therefore crystal lattice and binding energy effects are neglected, scattering is isotropic in the center-of-mass and the scattering cross section is independent of energy. Consider again, a collision between a neutron traveling with a velocity $\mathbf{v}$ and a neutron with velocity $\mathbf{V}$ resulting in the relative speed v_r:

$$v_r = \sqrt{v^2 + V^2 - 2vV\mu} \tag{2.20}$$

where v, V are the neutron and nucleus speed and μ is the scattering cosine between the neutron and nucleus velocity vectors. The probability a neutron will collide with a nucleus with some velocity in $d\mathbf{V}$ about $\mathbf{V}$ is given by:

$$\text{Probability of collision per sec} = v_r \Sigma_{s_0} P(\mathbf{V}) d\mathbf{V} \tag{2.21}$$

and the corresponding microscopic scattering cross section is obtained by dividing by v:

$$\Sigma_s(v) = \frac{\Sigma_{s_0}}{v} \int v_r P(\mathbf{V}) d\mathbf{V} \tag{2.22}$$

where $P(\mathbf{V})$ is an isotropic Maxwellian distribution of nuclear velocities given in Appendix A. By integrating over all atom velocities and scattering angles, the differential scattering cross section is given by:

$$\begin{aligned}\Sigma_s(E')p(E' \to E) =& \frac{\Sigma_{s_0}}{E'} \frac{\eta^2}{2} \Bigg\{ \exp\left(\frac{E'}{kT} - \frac{E}{kT}\right) \Bigg[\operatorname{erf}\left(\eta\sqrt{\frac{E'}{kT}} - \rho\sqrt{\frac{E}{kT}}\right) \\ & \pm \operatorname{erf}\left(\eta\sqrt{\frac{E'}{kT}} + \rho\sqrt{\frac{E}{kT}}\right) \Bigg] + \operatorname{erf}\left(\eta\sqrt{\frac{E}{kT}} - \rho\sqrt{\frac{E'}{kT}}\right) \\ & \mp \operatorname{erf}\left(\eta\sqrt{\frac{E}{kT}} + \rho\sqrt{\frac{E'}{kT}}\right)\end{aligned} \tag{2.23}$$

where η and rho are given by,

$$\eta = \frac{A+1}{2\sqrt{A}} \qquad \rho = \frac{A-1}{2\sqrt{A}} \tag{2.24}$$

The upper signs corresponds to upscattered neutrons with energies $E' < E$ and the lower signs corresponds to downscattered neutrons with energies $E' > E$. Equation 2.23 is the explicit scattering model for thermal scattering where a monotonic gas assumption can be made. This scattering model is used in the transport equation to solve reactor problems and is seen to be quite accurate with more complicated models at higher temperatures[29]. This free gas scattering model is the foundation for the heavy gas model which is explained in much more detail in Chapter 4.

2.2 Monte Carlo Basics

This dissertation is focused on obtaining temperature dependent k-eigenvalues in the thermal and epithermal region where free-gas elastic scattering is employed. This section is mainly concerned with these elements of neutron transport and therefore the following section is an overview of Monte Carlo methods along with details about neutron elastic scattering which are a main concern of this thesis.

Monte Carlo neutron transport is based on what is known as the "random walk" of a neutron or the stochastic simulation of a neutron path through a system from birth to termination. This "random walk" is a Markov process, meaning the current state of the neutron is memoryless. Probabilities of the neutron at a single point in phase-space has no dependence on its previous state. Monte Carlo methods take advantage of this property by randomly sampling probabilities which move a neutron through its "random walk" and tally specific information until the life of the neutron has ended or it escapes from the system. Each neutron carries a history, random sampling of multiple histories creates a statistical average. These statistical averages

are only as good as the data and probability distributions that define the physical processes.

The Monte Carlo "random walk" first begins with generating a source neutron by sampling from the source definition. The particle begins its walk by moving a straight distance determined by exponentially sampling a distance to collision. Once moved, the particle then must sample a collision type and collision outcome. This process is repeated until the particle has been lost to the system. The following outline gives a brief overview of the Monte Carlo algorithm:

Monte Carlo algorithm

1. Generate source neutron
2. Sample distance to collision
3. Sample interaction type
4. Sample outgoing direction after elastic collisions
5. Repeat steps 2-4 until neutron is absorbed or has left the system

These steps are discussed in more detail in the following subsections.

2.2.1 Source neutrons

Criticality calculations consist of several sequential fixed source calculations, called cycles (or generations). The first cycle utilizes an arbitrary fission source distribution. After the initial particle history simulation, the fission source distribution for subsequent cycles is defined from the previous cycle fission sites. Before any information is saved during a Monte Carlo simulation, "inactive" cycles are used solely to "converge" the fission source to the true distribution. Subsequent "active" cycles are performed to tally information about the desired quantities.

2.2.2 Sampling distance to collision

Once a neutron has been generated, a distance to collision must be determined. It is assumed that neutrons do not interact with each other, quantum and wave effects are ignored, and there does not exist long-range effects which means neutrons move in straight lines. The distance to collision is based on exponential attenuation given by the probability density function (PDF) $p(x)$:

$$p(x) = \Sigma_t e^{-\Sigma_t x} \tag{2.25}$$

where x is some distance and Σ_t is the total scattering cross section. In order to obtain an expression for the distance to collision d of neutron given the PDF in Eqn. 2.25, a cumulative distribution function (CDF) must be constructed. Integrating Eqn. 2.25 over the interval [0,d] and setting it equal to a random variable ξ will yield the following expression for distance to collision:

$$d = -\frac{\ln \xi}{\Sigma_t} \tag{2.26}$$

where ξ is randomly sampled from 0 to 1. Once the distance to collision is sampled, the particle is moved. If the particle distance to collision is longer than the distance to a boundary through this flight, the particle is moved to the boundary. If the boundary is an external boundary, the particle is said to have left the system and is terminated.

2.2.3 Sample interaction type

After the particle distance to collision has been determined, physical interactions must be determined. The neutron may encounter an absorption(a) which is the sum of fission(f) and capture(c) interactions, or it may encounter a scattering (s) interaction which is the sum of elastic scattering(e) and inelastic scattering(ie). Each

of these probabilities of interaction are given by their respective cross sections:

$$\begin{aligned}\Sigma_t(E) &= \Sigma_a(E) + \Sigma_s(E) \\ \Sigma_a(E) &= \Sigma_f(E) + \Sigma_c(E) \\ \Sigma_s(E) &= \Sigma_e(E) + \Sigma_{ie}(E)\end{aligned} \tag{2.27}$$

In order to determine probabilities of specific interaction, an analog approach is taken in which Eqns. 2.27 are normalized by the total cross section which divide i^{th} interactions into different intervals or probabilities $p_i = \Sigma_i/\Sigma_t$ which account for all of the separate interactions(Eqns 2.28). A random number ξ is chosen between 0 and 1 and simple logic is used to determine the interaction type. For $\xi < p_a$ the interaction is considered absorbed and if $\xi < p_f$ fission is the specific absorption event.

$$\begin{aligned}1 &= p_a + p_s \\ p_a &= p_f + p_c \\ p_s &= p_e + p_{ie}\end{aligned} \tag{2.28}$$

2.2.4 Sample outgoing direction

Once the particle interaction has been determined and the particle was not absorbed, meaning it scattered, an outgoing direction of the particle must be determined. The outgoing direction $(\vec{\Omega}'_x, \vec{\Omega}'_y, \vec{\Omega}'_z)$ is sampled directly from it's incoming direction $(\vec{\Omega}_x, \vec{\Omega}_y, \vec{\Omega}_z)$[30] by uniformly sampling $\mu = \cos\theta$ on the interval [-1,1] and the azimuthal angle uniformly on [0,2π]. The resulting outgoing direction is given

by the equations:

$$\vec{\Omega}'_x = \mu\vec{\Omega}_x + \frac{\sqrt{1-\mu^2}\left(\vec{\Omega}_x\vec{\Omega}_z\cos\gamma - \vec{\Omega}_y\sin\gamma\right)}{\sqrt{1-\vec{\Omega}_z^2}}$$

$$\vec{\Omega}'_y = \mu\vec{\Omega}_y + \frac{\sqrt{1-\mu^2}\left(\vec{\Omega}_y\vec{\Omega}_z\cos\gamma - \vec{\Omega}_x\sin\gamma\right)}{\sqrt{1-\vec{\Omega}_z^2}} \tag{2.29}$$

$$\vec{\Omega}'_z = \mu\vec{\Omega}_z - \cos\gamma\sqrt{1-\mu^2}\sqrt{1-\vec{\Omega}_z^2} \tag{2.30}$$

These equations assume that scattering is elastic and isotropic in the center of mass and therefore the cosine of the polar angle μ may be sampled uniformly on [-1,1].

2.2.5 Monte Carlo tallies

During the "random walk" specific quantities of interest are tallied or scored during a particle history in order to produce a mean value for all the tallies or scores from each neutron history. Quantities of interest include flux, current and reaction rates. The following list of tallies are specific to the Monte Carlo code MCNP6[2]:

- Current on a surface
- Flux on a surface
- Flux in a cell
- Flux at a point or ring detector
- Energy deposition
- Fission energy deposition
- Pulse height tally

Each tally contribution x_n from the n^{th} history is summed up and normalized by the total number of neutron histories N to produce an estimation $\hat{x}$ of the quantity of interest.

$$\hat{x} = \frac{1}{N} \sum_{n=1}^{N} x_n \tag{2.31}$$

For example, in order to obtain a current J over some surface A, each time a neutron passes over that surface tally the respective weight w_n of the neutron. Summing each particle weight and then dividing by the area of the surface along with the total starting weight W produces the current over a surface.

$$J = \frac{1}{A \cdot W} \sum_{n=1}^{N} w_n \tag{2.32}$$

Flux tallies within a cell differ from current tallies since they use a pathlength estimator. In order to obtain the flux ϕ within a volume V, sum up the particle weight of each history multiplied by its respective distance d_n traveled within that volume and divide by the total weight and volume.

$$\phi = \frac{1}{V \cdot W} \sum_{\forall n \in V} w_n \cdot d_n \tag{2.33}$$

Other flux estimators include collision and absorption estimators. These estimators take advantage of the definition of collision and absorption rates in order to estimate the flux. Equations 2.34 and 2.35 are the given collision and absorption estimators for neutrons that respectively collide or are absorbed:

$$\phi = \frac{1}{V \cdot W} \sum_{\forall n_{\text{col}} \in V} \frac{w_n}{\Sigma_t} \tag{2.34}$$

$$\phi = \frac{1}{V \cdot W} \sum_{\forall n_{\text{abs}} \in V} \frac{w_n}{\Sigma_a} \tag{2.35}$$

Error estimation

Since Monte Carlo methods are averaged quantities, a statistical error must accompany each quantity of interest. Statistical error is represented in the form of standard

variation or variance σ. The variance $\sigma_{\hat{x}}$ for some averaged quantity $\hat{x}$ is given by:

$$\sigma = \frac{1}{\sqrt{N-1}}\sqrt{\frac{1}{N}\sum_{n=1}^{N} x_n^2 - \hat{x}^2} \approx \frac{1}{\sqrt{N}}\sqrt{\frac{1}{N}\sum_{n=1}^{N} x_n^2 - \hat{x}^2} \tag{2.36}$$

The variance of the mean describes the precision of the calculated quantity, producing a spread of x_n values about the average $\hat{x}$. From Eqn. 2.36 it is clear that the variance scales by a factor of $1/\sqrt{N}$ which means in order to reduce the variance by a factor of two, four times the original number of particles must be sampled.

2.2.6 Sampling methods

Monte Carlo calculations require a random number generator (RNG) to sample probabilities. Most production-level Monte Carlo codes for particle transport use linear congruential random number generators[31]. MCNP6 specifically uses a multiplicative congruential method whose details are left to the code's manual[30].

There exist many different ways to sample probabilities so only the basics are covered here. It is assumed there exits discrete or continuous probability density functions (PDF) which have been normalized to unity. When possible, PDFs are inverted to become cumulative distribution functions (CDF) in which a direct sampling may be made (see Sec. 2.2.2). Figure 2.4 shows an example of directly sampling from a CDF given some continuous PDF. Since the values of the y-axis are between 0 and 1, any value in-between maps to a specific value on the x-axis picking out a random value. For discrete PDFs, the same process is used and is depicted in Fig. 2.4.

Another helpful method of random sampling is rejection sampling. Figure 2.5 shows a schematic representation of a rejection method for some arbitrary PDF. The idea is to bound the PDF in question by an equation which is easier to sample from, then check if the value is within the PDF in question. If the value is inside the PDF, accept, otherwise reject and choose another value. Rejection methods are considered

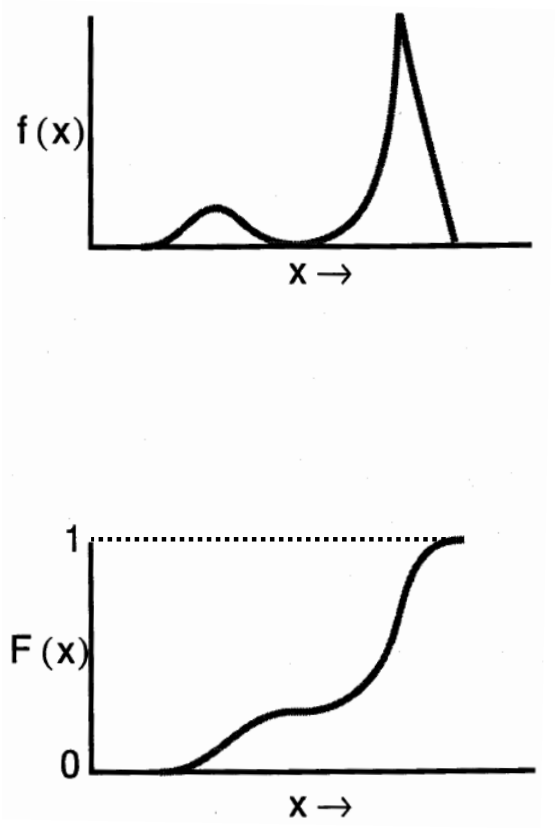

Figure 2.3: Inversion of continuous PDF to CDF (Source: MCNP notes[2])

a "low-order" approach and therefore some rejection schemes may be difficult to follow. Other pitfalls of rejection sampling include inefficient bounding functions. If the boundary equation chosen is much larger than the PDF distribution it will take

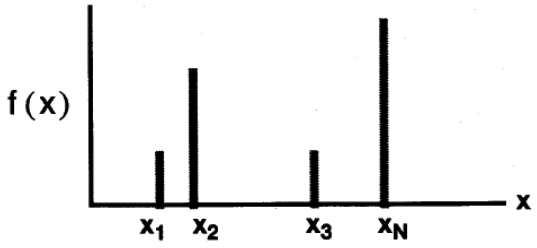

Figure 2.4: Discrete PDF (Source: MCNP notes[2])

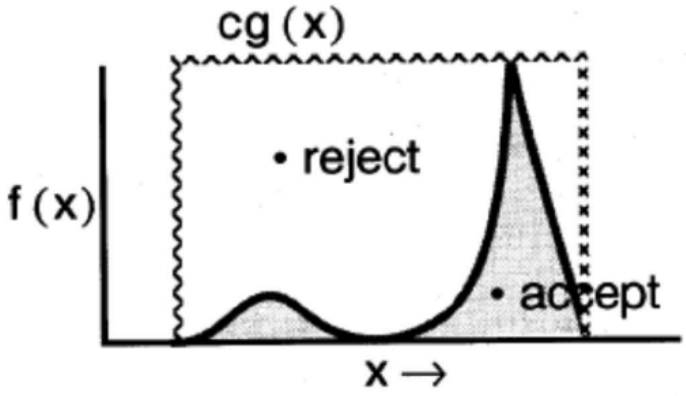

Figure 2.5: Rejection method sampling.

may rejections before an acceptance is made since most of the bounding equation does not cover the PDF.

2.3 Criticality Calculations Using Monte Carlo

Obtaining criticality calculations is crucial to reactor analysis. In the study of the steady-state solution, k_{eff} is the multiplication factor which changes the relative level of the fission source in order to balance the neutron Boltzmann equation. For simplicity, the following matrix notation will be used in order to represent Eqn. 2.1:

$$\begin{aligned}
\mathcal{L} &= \vec{\Omega} \cdot \psi \left(\vec{r}, \vec{\Omega}, E\right) \\
\mathcal{T} &= \Sigma_t \left(\vec{r}, E\right) \psi \left(\vec{r}, \vec{\Omega}, E\right) \\
\mathcal{S} &= \int_0^\infty \int_{4\pi} \Sigma_s \left(\vec{r}, \vec{\Omega}' \cdot \vec{\Omega}, E' \rightarrow E\right) \psi \left(\vec{r}, \vec{\Omega}' \cdot \vec{\Omega}, E' \rightarrow E\right) d\vec{\Omega}' dE' \\
\mathcal{M} &= \frac{\chi(E)}{4\pi} \int_0^\infty \int_{4\pi} \nu\Sigma_f(\vec{r}, E')\psi \left(\vec{r}, \vec{\Omega}', E'\right) d\vec{\Omega}' dE'
\end{aligned} \tag{2.37}$$

and the neutron transport equation (Eqn. 2.1) may be written as:

$$[\mathcal{L}+\mathcal{T}]\,\psi = \left[\mathcal{S}+\frac{1}{k_{\text{eff}}}\mathcal{M}\right]\psi \tag{2.38}$$

where $\mathcal{L}$ is the leakage operator, $\mathcal{T}$ is the collision operator, $\mathcal{S}$ is the scattering-in operator, and $\mathcal{M}$ is the fission multiplication operator. By rearranging Eqn. 2.38 and combining all terms into a single operator $\mathcal{F}$,

$$\begin{aligned}\psi =& \frac{1}{k_{\text{eff}}}\mathcal{M}[\mathcal{L}+\mathcal{T}-\mathcal{S}]^{-1}\psi \\ \psi =& \frac{1}{k_{\text{eff}}}\cdot\mathcal{F}\psi\end{aligned} \tag{2.39}$$

Equation 2.39 is a standard linear algebra eigenvalue equation which is solved numerically by power iteration. Power iteration works by iterating on the eigenfunction or angular flux ψ and the eigenvalue or criticality constant k_{eff} until each of them have reached a specified tolerance. The power iteration algorithm begins with an initial guess on the flux $\psi^{(0)}$and eigenvalue $k_{\text{eff}}^{(0)}$. Next, a Monte Carlo random walk for N particles is simulated to produce fission source points for the next iteration $\psi^{(n+1)}$. During histories for iteration $n+1$, tallies of the neutron production from fission are kept to estimate a new k_{eff}^{n+1}. The following list outlines the power iteration process for Monte Carlo eigenvalue calculations:

1. Initial guess for $k_{\text{eff}}^{(0)}$ and $\psi^{(0)}$
2. Solve for $\psi^{(n+1)}$

   $$\psi^{(n+1)} = \tfrac{1}{k_{\text{eff}}^{(n)}}\cdot\mathcal{F}\psi^{(n)}$$

3. Compute new $k_{\text{eff}}^{(n+1)}$

   $$k_{\text{eff}}^{(n+1)} = \tfrac{1}{k_{\text{eff}}^{(n)}}\cdot\tfrac{\int\mathcal{M}\psi^{(n+1)}d\vec{r}}{\int\mathcal{M}\psi^{(n)}d\vec{r}}$$

4. Repeat 1-3 until both $k_{\text{eff}}^{(n+1)}$ and $\psi^{(n+1)}$ have converged.

5. Continue iterating to compute quantities of interest.

Since the initial guess of the source particles is arbitrary, quantities of interest are not tallied until k_{eff} has reached a reasonable convergence. During the power iteration process fission sites are saved and used as source points for successive iterations. After so many iterations, the source points begin to converge providing a more accurate representation of the system. Figure 2.7 shows a schematic of successive cycles in which neutron fission points are generated from an initial guess to an actual source distribution based on the problem definition. As a result, the Monte Carlo code uses *inactive* cycles before tallying quantities of interest during *active cycles*. Figure 2.6 provides a diagram depicting k_{eff} iteration convergence with respect to n^{th} iterations. It is clear from the diagram, Monte Carlo codes discard initial iterations since the initial tallies are far from the converging solution. The MCNP6 criticality

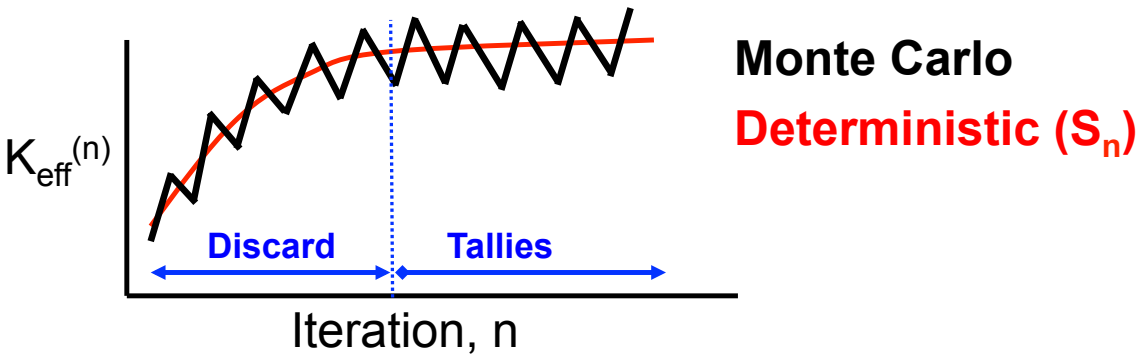

Figure 2.6: Diagram showing inactive and active cycles (Source: MCNP Crit Class[2])

calculations nomenclature uses the following terms which are all equivalent: *batch, cycle, iteration,* and *generation*. Histories are run in batches of N particles and the total weight in each cycle is N. For each n^{th} cycle three separate estimates of k_{eff} are made:

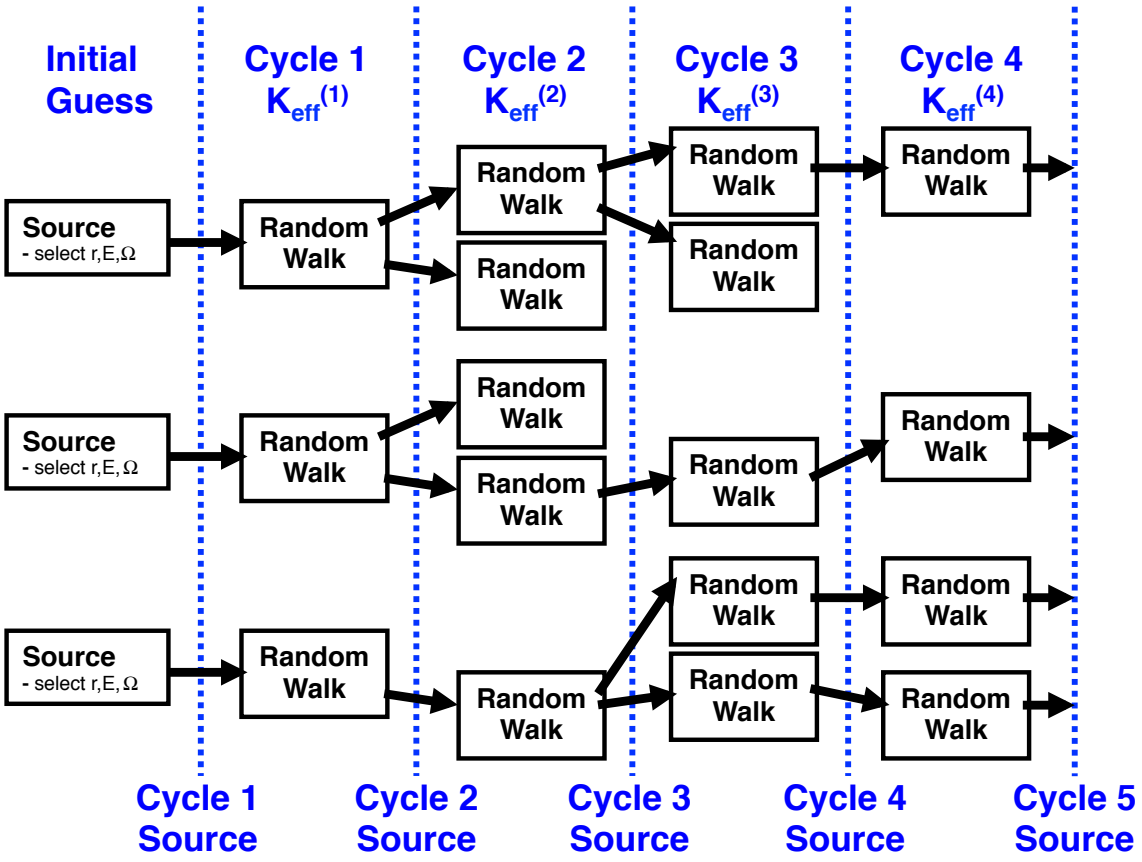

Figure 2.7: Source iteration schematic (Source:MCNP Crit Class[31])

- track-length estimator

$$k_{\text{path}}^{(n)} = \left(\sum_{\forall \text{ flights}} w_j \cdot d_j \cdot \nu\Sigma_f \right) \Big/ N \tag{2.40}$$

- collision estimator

$$k_{\text{col}}^{(n)} = \left(\sum_{\forall \text{ collisions}} \frac{w_j}{\Sigma_t} \cdot \nu\Sigma_f \right) \Big/ N \tag{2.41}$$

- absorption estimator

$$k_{\text{abs}}^{(n)} = \left(\sum_{\forall \text{ aborptions}} \frac{w_j}{\Sigma_a} \cdot \nu\Sigma_f \right) \Big/ N \tag{2.42}$$

While these estimators have been discussed, k_{eff} estimators take advantage of the definition of neutron production rate $\nu\Sigma_f\phi$ in which all of the previously defined estimators are multiplied by the number of neutrons per fission ν and the fission cross section Σ_f. At the end of the problem, all three estimates are combined in which an overall combined cumulative estimate based on all the data is given.

Chapter 3

Temperature Sensitivity Coefficients using Perturbation Theory

One of the main goals of this work is to calculate the Doppler temperature coefficient α_T. The Doppler temperature coefficient gives the change in the reactivity as a result of Doppler broadening of cross sections. The coefficient α_T is given by the derivative of the system reactivity ρ with respect to temperature T,

$$\alpha_T = \frac{d\rho}{dT} \tag{3.1}$$

which can also be written in terms of the criticality eigenvalue k,

$$\rho = \frac{k-1}{k} \implies \frac{d\rho}{dT} = \frac{-1}{k^2}\frac{dk}{dT} \implies \alpha_T = \frac{-1}{k^2}\frac{dk}{dT}$$

Using the neutron transport equation, a derivation of the relative change in the criticality eigenvalue k with respect to a change in temperature T will be shown using a first-order perturbation approximation. This will lead to the formal definition of sensitivity coefficients, which will allow for a mathematical expression of the Doppler temperature coefficient.

3.1 First-Order Perturbation Approximation

This study is concerned with the steady-state Boltzmann neutron transport equation, which satisfies the following balance

$$\mathcal{M}\psi(\vec{r}, E, \vec{\Omega}) = \lambda \mathcal{F}\psi(\vec{r}, E, \vec{\Omega}), \tag{3.2}$$

where $\psi\left(\vec{r}, \vec{\Omega}, E\right)$ is the six-dimensional neutron flux. The eigenvalue term λ is equal to k^{-1}, where k is the criticality eigenvalue descrbing the relative change in the neutron population for subsequent generations. The operator $\mathcal{M}$, which describes neutron streaming, absorption and scattering is given by

$$\begin{aligned}\mathcal{M}\psi = \vec{\Omega} \cdot \nabla\psi\left(\vec{r}, \vec{\Omega}, E\right) + \Sigma_t(\vec{r}, E)\psi\left(\vec{r}, \vec{\Omega}, E\right) \\ - \int_{4\pi} d\hat{\vec{\Omega}}' \int_0^\infty dE' \Sigma_s\left(\vec{r}, \vec{\Omega}' \cdot \vec{\Omega}, E' \to E\right)\psi\left(\vec{r}, \vec{\Omega}', E'\right),\end{aligned} \tag{3.3}$$

where $\Sigma_t(\vec{r}, E)$ and $\Sigma_s(\vec{r}, E' \to E, \hat{\vec{\Omega}}' \cdot \hat{\vec{\Omega}})$ are the total cross section and differential scattering cross section respectively.

The neutron production term $\mathcal{F}$ is given by the sum of all neutrons produced from fission and any fixed source S given by

$$\mathcal{F}\psi = \frac{\chi(\vec{r}, E)}{4\pi} \int_{4\pi} d\hat{\vec{\Omega}}' \int_0^\infty dE' \bar{\nu}\Sigma_f(\vec{r}, E')\psi\left(\vec{r}, \vec{\Omega}', E'\right) + S(\vec{r}, E, \vec{\Omega}), \tag{3.4}$$

where Σ_f is the fission cross section, $\bar{\nu}$ is the number of neutrons emitted per fission and χ is the outgoing fission neutron energy spectrum. For eigenvalue problems it is assumed the neutron source term $S(\vec{r}, E, \vec{\Omega})$ is zero, and it is understood a solution exists for ψ when appropriate boundary conditions are applied.

We define the inner product $< f, g >$ between any two real functions $f(\vec{r})$and $g(\vec{r})$ as

$$< f, g > \equiv \int_V d^3 r f(\vec{r}) g(\vec{r}) \tag{3.5}$$

where V is the volume.

Using this inner product, the adjoint operator $M^\dagger$ is defined by

$$< M^\dagger f, g > = < f, Mg > \tag{3.6}$$

for every $f(\vec{r})$and $g(\vec{r})$ satisfying appropriate boundary conditions.

Now consider the steady-state adjoint equation

$$\mathcal{M}^\dagger \psi^\dagger = \lambda^\dagger \mathcal{F}^\dagger, \tag{3.7}$$

where $\psi^\dagger$ is the six-dimensional angular neutron flux, the adjoint neutron transport collision term $\mathcal{M}^\dagger$ is given by

$$\begin{aligned} \mathcal{M}^\dagger \psi \dagger \left(\vec{r}, \vec{\Omega}, E\right) = -\vec{\Omega} \cdot \nabla \psi^\dagger \left(\vec{r}, \vec{\Omega}, E\right) + \Sigma_t(\vec{r}, E) \psi^\dagger \left(\vec{r}, \vec{\Omega}, E\right) \\ - \int_{4\pi} d\hat{\vec{\Omega}}' \int_0^\infty dE' \Sigma_s(\vec{r}, E \to E', \hat{\vec{\Omega}}' \cdot \hat{\vec{\Omega}}') \psi^\dagger \left(\vec{r}, \vec{\Omega}', E'\right) \end{aligned} \tag{3.8}$$

and the adjoint neutron production term $\mathcal{F}^\dagger$ is given by

$$\mathcal{F}^\dagger \psi^\dagger \left(\vec{r}, \vec{\Omega}, E\right) = \frac{\bar{\nu} \Sigma_f(\vec{r}, E)}{4\pi} \int_{4\pi} d\hat{\vec{\Omega}}' \int_0^\infty dE' \chi(\vec{r}, E') \psi^\dagger \left(\vec{r}, \vec{\Omega}', E'\right) + S^\dagger(\vec{r}, E, \vec{\Omega}), \tag{3.9}$$

Again, since we are dealing with an eigenvalue problem the source term $S^\dagger$ is zero. Further, it is known that the forward and adjoint eigenvalues corresponding to the

fundamental mode are identical[29].

The purpose of this work is to understand how a change in the system's temperature has an effect on the criticality. In order to do that, first-order perturbation theory provides an approximation of the change in criticality which is caused by a change in the core's system. Now, we introduce a differential perturbation into the steady-state system given in Eqn. (3.2) such that

$$\begin{aligned} \mathcal{F}' &= \mathcal{F} + \delta\mathcal{F} \\ \mathcal{M}' &= \mathcal{M} + \delta\mathcal{M} \\ \lambda' &= \lambda + \delta\lambda \\ \psi' &= \psi + \delta\psi \end{aligned} \tag{3.10}$$

By introducing a differential change in the absorption and production of neutrons, the population as well as the criticality eigenvalue must change leading to the following perturbed steady-state equation

$$\mathcal{M}'\psi' = \lambda'\mathcal{F}'\psi'. \tag{3.11}$$

Next, we will multiply the perturbed steady-state equation by the angular adjoint flux $\psi^\dagger$ and integrate over the whole volume, all energies and all angles yielding

$$\int_V d^3r \int_0^\infty dE \int_{4\pi} d\vec{\Omega}\ \psi^\dagger \mathcal{M}'\psi' = \int_V d^3r \int_0^\infty dE \int_{4\pi} d\vec{\Omega}\ \psi^\dagger \lambda'\mathcal{F}'\psi. \tag{3.12}$$

By definition this is the inner-product mentioned in Eqn. (3.5). In order to simplify the notation, with the assumption of spacial, energy and angular dependence, we will rewrite Eqn. (3.12) as

$$< \psi^\dagger, \mathcal{M}'\psi' > = < \psi^\dagger, \lambda'\mathcal{F}'\psi' > \tag{3.13}$$

Now by substituting back in the perturbed values given by Eqn. (3.10) we can begin to obatin an expression for a change in the criticality.

$$\begin{aligned} &< \psi^\dagger, \mathcal{M}\psi > + < \psi^\dagger, \delta\mathcal{M}\psi > + < \psi^\dagger, \mathcal{M}\delta\psi > + < \psi^\dagger, \delta\mathcal{M}\delta\psi > \\ &\quad = \; < \psi^\dagger, \lambda\mathcal{F}\psi > + < \psi^\dagger, \lambda\delta\mathcal{F}\psi > + < \psi^\dagger, \delta\lambda\mathcal{F}\psi > \\ &\qquad + < \psi^\dagger, \delta\lambda\delta\mathcal{F}\psi > + < \psi^\dagger, \lambda\mathcal{F}\delta\psi > + < \psi^\dagger, \lambda\delta\mathcal{F}\delta\psi > \\ &\qquad + < \psi^\dagger, \delta\lambda\mathcal{F}\delta\psi > + < \psi^\dagger, \delta\lambda\delta\mathcal{F}\delta\psi > \end{aligned} \tag{3.14}$$

Since we are within the realm of first-order perturbation theory, we may neglect higher-order terms. It can be shown that the terms which include $\delta\psi$ are relative to a balance in which case may be cancelled. Discarding these terms further simplifies the expression to

$$\begin{aligned} &< \psi^\dagger, \mathcal{M}\psi > + < \psi^\dagger, \delta\mathcal{M}\psi > \\ &\quad = \; < \psi^\dagger, \lambda\mathcal{F}\psi > + < \psi^\dagger, \lambda\delta\mathcal{F}\psi > + < \psi^\dagger, \delta\lambda\mathcal{F}\psi > \end{aligned} \tag{3.15}$$

By taking advantage of the property of adjointness (i.e. $< \psi^\dagger, (\mathcal{M} - \lambda\mathcal{F})\psi >=< \psi, (\mathcal{M} - \lambda\mathcal{F})\psi^\dagger >= 0$), reduces Eqn. (3.15) to

$$\delta\lambda = \frac{-\left\langle \psi^\dagger, (\delta\mathcal{M} - \lambda\delta\mathcal{F})\psi \right\rangle}{\langle \psi^\dagger, \mathcal{F}\psi \rangle} \tag{3.16}$$

This expression explicitly shows, given a change in the collision and production terms, the direct change in the eigenvalue λ given the adjoint function $\psi^\dagger$. In order to calculate this value it is necessary to calculate the integration denoted by the inner-product. Mathematically, this integration is calculated by Monte Carlo sampling, using weighted tallies. This weighting is dependent on the survivability of a neutron at a given point in phase space. This physical interpretation of the adjoint function is why it is also characterized as the importance function which represents

the neutron population, at a given interval of phase space, after an asymptotic number of generations has occured.

For completeness, recall $\lambda = 1/k$, which means $\delta\lambda = \delta k/k^2$. Also, the term $\delta\mathcal{M}$ can be written as

$$\delta\mathcal{M} = \delta\Sigma_t - \delta\mathcal{S}, \text{ where, } \quad \delta\mathcal{S} = \delta\Sigma_s\left(\vec{r}, \vec{\Omega}' \cdot \vec{\Omega}, E' \to E\right), \tag{3.17}$$

providing the following expression in terms of the eigenvalue k,

$$\delta k = \frac{-\left\langle \psi^\dagger, (\delta\Sigma_t - \delta\mathcal{S} - \frac{1}{k}\delta\mathcal{F})\psi \right\rangle}{\left\langle \psi^\dagger, \frac{1}{k^2}\mathcal{F}\psi \right\rangle} \tag{3.18}$$

3.2 Sensitivity Coefficients

It was shown how perturbation theory leads to a first-order approximation to the change in criticality with respect to a change in system parameters. When this change is normalized it is known as a sensitivity coefficient. Specifically, the sensitivity coefficient for k, $S^j_{k,x}$, to some nuclear data x^j (x is the cross section, fission ν, etc. over some energy range) is defined[32] as the ratio of the fractional change in k for a corresponding fractional change in x with respect to some isotope j, or

$$S^j_{k,x} = \left(\frac{\delta k}{k} \Big/ \frac{\delta x^j}{x^j}\right) \tag{3.19}$$

For example, consider the capture cross section Σ_c where the relative change C to the capture cross section is given by

$$C = \frac{\delta\Sigma_c}{\Sigma_c} \tag{3.20}$$

the change in the capture cross section is now fluxed. Since we are only concerned with the change in the capture cross section then all other deltas are zero

$$\delta\Sigma_t = \cancelto{0}{\delta\Sigma_s} + \cancelto{\delta\Sigma_c}{\delta\Sigma_a} = \delta\Sigma_c$$

and Eqn. (3.18) reduces to

$$\delta k = \frac{-\left\langle \psi^\dagger, \delta\Sigma_c \psi \right\rangle}{\left\langle \psi^\dagger, \frac{1}{k^2}\mathcal{F}\psi \right\rangle}, \quad \text{recall, } \delta\Sigma_c = C\Sigma_c \tag{3.21}$$

and now,

$$\delta k = \frac{-\left\langle \psi^\dagger, C\Sigma_c \psi \right\rangle}{\left\langle \psi^\dagger, \frac{1}{k^2}\mathcal{F}\psi \right\rangle}$$
$$\delta k = C\frac{-\left\langle \psi^\dagger, \Sigma_c \psi \right\rangle}{\left\langle \psi^\dagger, \frac{1}{k^2}\mathcal{F}\psi \right\rangle}$$

Now dividing both sides by Ck gives

$$\frac{\delta k}{Ck} = \frac{-\left\langle \psi^\dagger, \Sigma_c \psi \right\rangle}{\left\langle \psi^\dagger, \frac{1}{k}\mathcal{F}\psi \right\rangle}, \quad \text{recall, } C = \frac{\delta\Sigma_c}{\Sigma_c}$$

$$\left(\frac{\delta k}{k} \middle/ \frac{\delta\Sigma_c}{\Sigma_c}\right) = \frac{-\left\langle \psi^\dagger, \Sigma_c \psi \right\rangle}{\left\langle \psi^\dagger, \frac{1}{k}\mathcal{F}\psi \right\rangle} = S_{k,\Sigma_c} \tag{3.22}$$

It is clear from Eqn. (3.22) the relative change in k with respect to a relative change in the capture cross section is simply the inner product of the adjoint and the neutrons which have experienced a capture reaction divided by the total fission in the system. Using this same process, senstivity coefficients with respect to cross sections are calculated by the following inner product,

$$S_{k,x} = \frac{\left\langle \psi^\dagger, \mathcal{P}_x \psi \right\rangle}{\left\langle \psi^\dagger, \frac{1}{k}\mathcal{F}\psi \right\rangle} \tag{3.23}$$

where $\mathcal{P}_x$ is the perturbation operator defined as

$$\mathcal{P}_x = \left(-\Sigma_x + \mathcal{S}_x + \frac{1}{k}\mathcal{F}_x\right) \tag{3.24}$$

Σ_x is the cross section corresponding to x if x is a cross section, and zero otherwise. $\mathcal{S}_x$ is the scattering operator for x if x is a scattering cross section , and zero otherwise. $\mathcal{F}_x$ is the production operator for x if x is a fission cross section, fission ν, or

fission χ and zero otherwise.

Another convention defined is that the energies used to determine range g are incident for cross sections and fission ν and are outgoing for scattering or fission-χ transfer functions. For the transfer functions, sensitivities may also be further restricted to incident energy E' (with bin index g') and for scattering direction cosine change μ (with bin index n). The energy/angle-resolved sensitivities computed are actually bin-integrated. For the case of a cross-section or fission-n sensitivity,

$$S_{k,x,g,n} = \int_{E_{g-1}}^{E_g} dE \int_{\mu_{n-1}}^{\mu_n} d\mu \; S_{k,x}(E,\mu), \tag{3.25}$$

where the integrand $S_{k,x}(E,\mu)$, with explicit dependence on E and μ, is taken to be the"sensitivity density" with units of per energy per cosine. The energy/angle-integrated sensitivity is

$$S_{k,x} = \int_{0}^{\infty} dE \int_{-1}^{1} d\mu \; S_{k,x}(E,\mu). \tag{3.26}$$

While the sensitivities with respect to cross sections is given by Eqn.(3.19), the transport equation also consists of transfer functions (i.e. scattering, χ). The transfer functions themselves are probability density functions conditional on the incident energy (the standard notation for conditional probability densities is used where the variables to the left of the vertical bar are conditional on the variables to the right) and are normalized to unity. Because of this constraint, the total sensitivities over all outgoing energies and direction changes for a given incident-energy bin must sum to zero —increasing the transfer function somewhere must be offset by a corresponding decrease somewhere else.

Consider the scattering transfer function $f_s(E,\mu|E')$ which determines the probability of incoming neutron with energy E and incident cosine μ emerging with an

outgoing energy E'. Now suppose we discretize the scattering transfer function in G total energy groups such that

$$\sum_{i=1}^{G} f_{s_i} = 1 = \int_0^\infty dE f_s(E, \mu|E'), \quad \text{where, } f_{s_i} = \int_{E_{i-1}}^{E_i} dE f_s(E, \mu|E')$$

By introducing a perturbation to the g^{th} group by a factor of $(1+p)$ where p is nearly zero, the following function results for the perturbed transfer function f'_s,

$$\sum_{i=1}^{G} f'_{s_i} = C\left[f_{s_1} + f_{s_2} + \cdots + (1+p)f_{s_g} + \cdots + f_{s_{G-1}} + f_{s_G}\right] = 1 \tag{3.27}$$

where C is a renormalizing constant which maintains unity. Solving for C gives

$$\begin{aligned} C\left[f_1 + f_2 + \cdots + f_g + pf_g + \cdots + f_{G-1} + f_G\right] &= 1 \\ C\left[f_1 + f_2 + \cdots + f_g + \cdots + f_{G-1} + f_G + pf_g\right] &= 1 \\ C\left[1 + pf_g\right] &= 1 \\ C &= \frac{1}{1+pf_g} \end{aligned}$$

By expanding C in terms of a Taylor series

$$C = \frac{1}{1+pf_g} = 1 - pf_g + (pf_g)^2 - (pf_g)^3 + \ldots$$

and neglecting higher-order terms, a linear approximation for C is

$$C \approx 1 - pf_g. \tag{3.28}$$

Using this approximation for C and substituting it into Eqn. (3.27) gives

$$(1-pf_g)f_1 + (1-pf_g)f_2 + \cdots + (1-pf_g)(1+p)f_g + \cdots + (1-pf_g)f_{G-1} + (1-pf_g)f_G = 1 \tag{3.29}$$

Now consider the following definition for a general perturbation δf_s to f_{s_i} as

$$f'_{s_i} = f_{s_i} + \delta f_{s_i},$$

which gives the following definitions for each group as

$$\begin{aligned}
f'_{s_1} &= (1-pf_{s_g})f_{s_1} &&= f_{s_1} - f_{s_1}pf_{s_g} &&\implies \delta f_{s_1} &&= -f_{s_1}pf_{s_g}\\
f'_{s_2} &= (1-pf_{s_g})f_{s_2} &&= f_{s_2} - f_{s_2}pf_{s_g} &&\implies \delta f_{s_2} &&= -f_{s_2}pf_{s_g}\\
\vdots &= \vdots &&= \vdots &&\implies \vdots &&= \vdots\\
f'_{s_g} &= (1+p)f_{s_g} &&= f_{s_g} + pf_{s_g} &&\implies \delta f_{s_g} &&= pf_{s_g}\\
\vdots &= \vdots &&= \vdots &&\implies \vdots &&= \vdots\\
f'_{s_{G-1}} &= (1-pf_{s_g})f_{s_{G-1}} &&= f_{s_{G-1}} - f_{s_{G-1}}pf_{s_g} &&\implies \delta f_{s_{G-1}} &&= -f_{s_{G-1}}pf_{s_g}\\
f'_{s_G} &= (1-pf_{s_g})f_{s_1} &&= f_{s_1} - f_{s_1}pf_{s_g} &&\implies \delta f_{s_1} &&= -f_{s_1}pf_{s_g}
\end{aligned}$$

Now an expression for the sensitivity to k with respect to the change in the transfer function f_s is needed. Recall,

$$\frac{\delta k}{k} = \int_0^\infty dE \frac{\delta f_s(E)}{f_s(E)} S_{k,f_s}(E) \tag{3.30}$$

where S_{k,f_s} is unnormalized. The discretized example leads to the following sensitivity to the transfer function

$$\frac{\delta k}{k} = \sum_{i=1}^{G} \frac{\delta f_{s_i}}{f_{s_i}} S_{k,f_{s_i}}$$

By substituting in the values found for all the δf_{s_i} we get,

$$\begin{aligned}
\frac{\delta k}{k} &= -pf_{s_g}S_{k,f_{s_1}} - \cdots + \frac{pf_{s_g}}{f_{s_g}}S_{k,f_{s_g}} - pf_{s_g}S_{k,f_{s_g}} - \cdots - pf_{s_g}S_{k,f_{s_G}}\\
&= -pf_{s_g}S_{k,f_{s_1}} - \cdots + pS_{k,f_{s_g}} - pf_{s_g}S_{k,f_{s_g}} - \cdots - pf_{s_g}S_{k,f_{s_G}}\\
&= pS_{k,f_{s_g}} + \left[-pf_{s_g}S_{k,f_{s_1}} - \cdots - pf_{s_g}S_{k,f_{s_g}} - \cdots - pf_{s_g}S_{k,f_{s_G}}\right]\\
&= pS_{k,f_{s_g}} - pf_{s_g}\left[S_{k,f_{s_1}} + \cdots + S_{k,f_{s_g}} + \cdots + S_{k,f_{s_G}}\right]\\
\frac{1}{p}\frac{\delta k}{k} &= S_{k,f_{s_g}} - f_{s_g}\sum_{i=1}^{G} S_{k,f_{s_i}}
\end{aligned}$$

This expression shows a renormalized relative change in k with respect to a perturbation in group g of the transfer function f_s. By definition, this is the sensitivity coefficient of the g^{th} group of the transfer function which guarantees to constrain

the distribution to be normalized to unity. In order to denote the constrained sensitivity, the convention of $\hat{S}$ is used, therefore the normalized sensitivity to k from a perturbation in the g^{th} group is given by

$$\hat{S}_{k,f_{s_g}} = S_{k,f_{s_g}} - f_{s_g} \sum_{i=1}^{G} S_{k,f_{s_i}} \tag{3.31}$$

For this reason, MCNP6 computes the constrained sensitivity coefficient for transfer functions, $\hat{S}_{k,x}$. Note that the sensitivities for cross sections, such as fission or scattering, are not constrained, as there is no normalization condition to impose, and are therefore unaffected.

The continuous form for scattering laws,

$$\hat{S}_{k,f_s}(E,\mu|E') = S_{k,f_s}(E,\mu|E') - f_s(E,\mu|E')S^j_{k,f_s}(E'). \tag{3.32}$$

which gives the constrained sensitivity of f_s at energy E and cosine μ. This renormalization of the sensitivity coefficients for probability density distributions has been proven to be accurate[32] when calculating sensitivity with respect to moments of the transfer function.

The above definitions are used in calculating the Doppler temperature coefficient. Using these definitions, a formal definition of the Doppler temperature coefficient will be derived.

3.3 Temperature Sensitivities

The focus for this work is with respect to the sensitivity in k with respect to changes in temperature. Each of the terms in the sensitivity coefficient given by Eqn. (3.19)

are temperature dependent. Coming back to the transfer function f_s, the relative change in k from a change in the transfer function f_s is given by

$$\frac{\delta k}{k} = \int dE' \int dE \int d\vec{\Omega}\ \frac{\delta f_s(E', E, \vec{\Omega})}{f_s(E', E, \vec{\Omega})}\ \hat{S}_{k,f_s}(E', E, \vec{\Omega}) \tag{3.33}$$

where, $\hat{S}_{k,f_s}$ is the constrained sensitivity given in Eqn. (3.32). Now, suppose we take a Taylor series expansion of δf_s at some temperature T_0 in order to come up with a linear approximation for δf_s

$$\begin{aligned} f_s(T) &= f_s(T_0) + (T - T_0)\frac{\partial f_s}{\partial T} + \dots \\ &\implies \delta f_s = \delta T \frac{\partial f_s}{\partial T}. \end{aligned}$$

By moving the δT term to the left side and taking the limit, the resulting equation becomes

$$\begin{aligned} \lim_{\delta k, \delta T \to 0} \quad \frac{1}{k}\frac{\delta k}{\delta T} &= \int dE' \int dE \int d\vec{\Omega}\ \frac{\partial f_s}{\partial T}\frac{1}{f_s}\ \hat{S}_{k,f_s}(E', E, \vec{\Omega}) \\ \frac{1}{k}\frac{\partial k}{\partial T} &= \int dE' \int dE \int d\vec{\Omega}\ \frac{\partial f_s}{\partial T}\frac{1}{f_s}\ \hat{S}_{k,f_s}(E', E, \vec{\Omega}) \end{aligned} \tag{3.34}$$

By a similar derivation, it can be shown that a perturbation in temperature due to the cross sections can be given by

$$\frac{1}{k}\frac{\partial k}{\partial T} = \frac{\left\langle \psi^\dagger, \left(-\frac{\partial \Sigma_x}{\partial T} + \frac{\partial \mathcal{S}_x}{\partial T} + \frac{1}{k}\frac{\partial \mathcal{F}_x}{\partial T}\right)\psi \right\rangle}{\left\langle \psi^\dagger, \frac{1}{k}\mathcal{F}\psi \right\rangle} \tag{3.35}$$

Examining Eqn.(3.35) provides an alternate form. The reactivity ρ of a system is defined as

$$\rho = \frac{k-1}{k} \implies \frac{\partial \rho}{\partial T} = \frac{-1}{k^2}\frac{\partial k}{\partial T}, \tag{3.36}$$

therefore by dividing both sides of Eqn. (3.37) by k gives

$$\frac{\partial \rho}{\partial T} = \frac{\left\langle \psi^\dagger, \left(-\frac{\partial \Sigma_x}{\partial T} + \frac{\partial \mathcal{S}_x}{\partial T} + \frac{1}{k}\frac{\partial \mathcal{F}_x}{\partial T}\right)\psi \right\rangle}{\left\langle \psi^\dagger, \mathcal{F}\psi \right\rangle} \tag{3.37}$$

The derivative of reactivity with respect to temperature is the Doppler temperature coefficient α_T and is presented here as

$$\alpha_T = \frac{\left\langle \psi^\dagger, \left(-\frac{\partial \Sigma_x}{\partial T} + \frac{\partial \mathcal{S}_x}{\partial T} + \frac{1}{k}\frac{\partial \mathcal{F}_x}{\partial T} \right) \psi \right\rangle}{\langle \psi^\dagger, \mathcal{F}\psi \rangle} \tag{3.38}$$

It has been shown, using adjoints and linear perturbation theory how to obtain an expression of the Doppler temperature coefficient. This expression requires the ability to integrate over all phase space, to express the adjoint function and to evaluate temperature derivatives of the cross sections. MCNP currently has the capability to deal with adjoint calculations, more detail on how this is done will be discussed in the next chapter. Unfortunately, in a Monte Carlo setting, in order to analyze a system with many different materials at different temperatures would require tens of hundreds of gigabytes of memory. Therefore, the next step is to find a new way of generating temperature derivatives of the cross sections without increasing the amount of data storage. This and all other coding implementation will be discussed in detail in Chapter 4.

Chapter 4

Doppler Temperature Coefficient Code Implementation

Having shown the mathematical basis for constructing the Doppler temperature coefficient α_T, this section will focus on the implementation inside MCNP6. It was mentioned that two things were needed in order to make this calculation, the first being the adjoint flux and the second being temperature derivatives of the cross section. Adjoint capabilities are available in MCNP6[24] and a brief description of the method will be discussed.

In order to produce temperature derivatives of the cross sections without demanding more storage for cross section data a new method of obtaining temperature derivatives of the cross sections was made. This method takes advantage of an advancement made in MCNP6[33] which allows for continuous-energy cross sections to be generated on-the-fly (OTF). OTF cross section libraries are exploited in order to obtain cross section derivatives on-the-fly as well. More details are provided in the following subsections.

4.1 Adjoint-weighted Tallies In MCNP6

The code uses a physical interpretation of the adjoint flux, also known as an importance function, which describes the asymptotic population of neutrons after an infinite number of neutron generations. This interpretation begins by introducing a single neutron into an assembly at a specific position, energy and direction. Measure this neutron after an infinite amount of time has passed, then repeat this process to obtain an average which is proportional to the importance or adjoint function.

This physical interpretation of the adjoint flux takes advantage of the iterative process necessary to solve the Monte Carlo eigenvalue problem. As discussed in Chapter 2, the power iteration is used by MCNP where a block of neutrons are used to obtain a value for the eigenvalue k. Once this block is finished, the eigenvalue is updated and the process is repeated for a specific number of cycles. Within each block, neutrons are being followed for a specific number of generations (5 to 10)[3], see Figure 4.1. Events for each neutron are being recorded, progeny of those neutrons are tagged to determine original generation contribution. Once the asymptotic generation has been reached, neutron populations are assumed to be converged. The number of neutrons are then recorded using a track-length estimator. This value becomes a weighting for appropriate scores from recorded events to estimate the importance-weighted integrals by Monte Carlo.

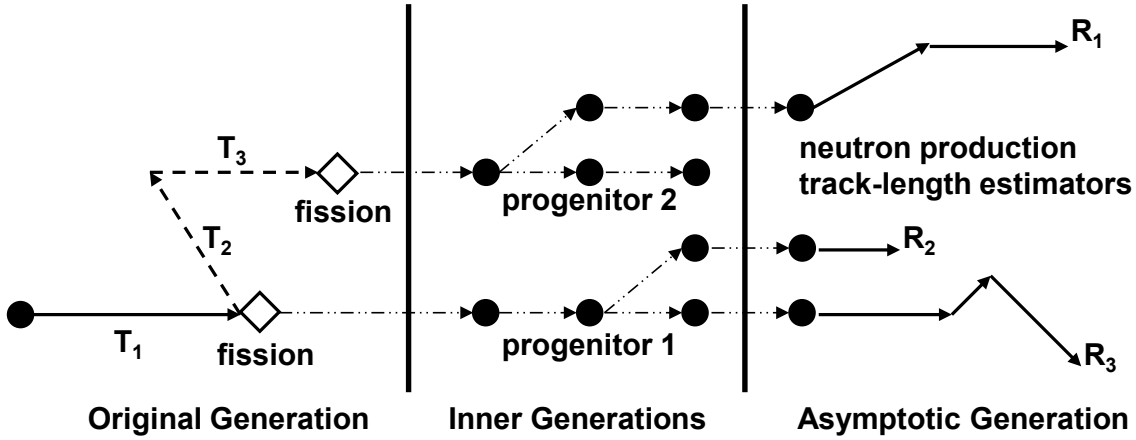

Figure 4.1: Schematic of iterative process which characterizes the adjoint function. (Source:[3])

4.2 Temperature Derivatives Using OTF Cross Sections

It is widely known that detailed reactor thermal-hydrolic calculations require vasts amount of cross section data with consistently varying temperatures. This led to the development of on-the-fly (OTF) Doppler broadened cross sections. OTF data libraries only require the storage of cross sections at $0K$ for any isotope and all other temperatures are broadened on-the-fly, significantly reducing the amount of data storage.

The methodology is based on a combination of Taylor series expansions and asymptotic series expansions. The type of series representation was determined by investigating the temperature dependence of ^{238}U resonance cross sections near the resonance peaks, midresonance and the resonance wings. The coefficients for these series expansions were determined by a regression over the energy and temperature range of interest and are based on the Adler-Adler model which results in a polynomial fitting in temperature. Due to the temperature dependence in the model, it

is possible to take a direct temperature derivative of the polynomial fitting. Reference [33] gives the following numerical result for the temperature dependent microscopic cross section $\sigma(E,T)$ for some reaction x,

$$\sigma_x(E,T) = \sum_{i=-N}^{N} c_i s(T)^i, \tag{4.1}$$

where

$$s(T) = \sqrt{\alpha T - \beta}\,.$$

The c_i's are pregenerated coefficients fit to Evaluated Nuclear Data File (ENDF) cross sections, and α and β are temperature scaling terms that are determined by the minimum and maximum temperature values used in the generation of the OTF data. $2N+1$ is the total number of coefficients needed to be within the specified fractional tolerance, as determined by the sigma1 method[34].

The temperature derivative of the cross section may be obtained by differentiating the series in Eqn. (4.1) with respect to T:

$$\frac{d\sigma(T)}{dT} \quad = \quad \sum_{i=-N}^{N} c_i \cdot \frac{i\alpha}{2} s(T)^{i-1}. \tag{4.2}$$

As a means of evaluating how well OTF generated cross sections can capture temperature derivatives, a reference solution must be produced. By using ENDF cross sections and the sigma1 method, $\sigma_{ref}(E,T)$ at some temperature T and energy E may be obtained and a central-difference derivative may be used to estimate the derivative:

$$\frac{d\sigma_{ref}(E,T)}{dT} \approx \frac{\sigma_{ref}\left(E, T+\frac{\Delta T}{2}\right) - \sigma_{ref}\left(E, T-\frac{\Delta T}{2}\right)}{\Delta T} \tag{4.3}$$

If the change in the cross section with respect to temperature is not large, Eqn. (4.3) is accurate.

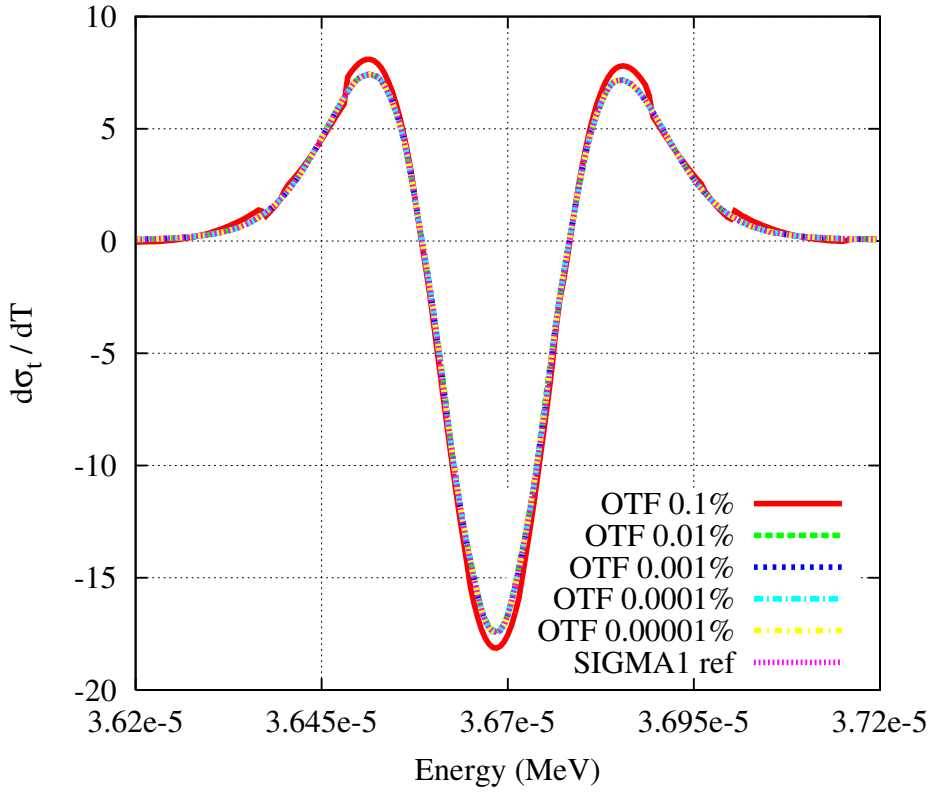

Figure 4.2: Comparison of ^{238}U total cross section with varrying tolerances.

Investigations have focused upon the resonance around 36.7 eV in ^{238}U at 298.6 K with $\Delta T = 5$ K. By default, OTF data is generated from ENDF data with a linearization tolerance of 0.1% in energy. Figure 4.2 shows increasing OTF derivative fractional tolerance data compared to a reference solution. The OTF derivatives do not agree with the reference derivatives for the default fractional tolerance. Since the default fractional tolerance of 0.1% does not accurately represent the temperature derivatives, tighter tolerances were investigated. Figure 4.3 shows a comparison of OTF cross sections with fractional tolerances of 0.1%, 0.01%, 0.001%, 0.0001% and 0.00001% with the reference solution. By increasing the fractional tolerance the temperature derivative is adequately captured at this resonance. The size of the

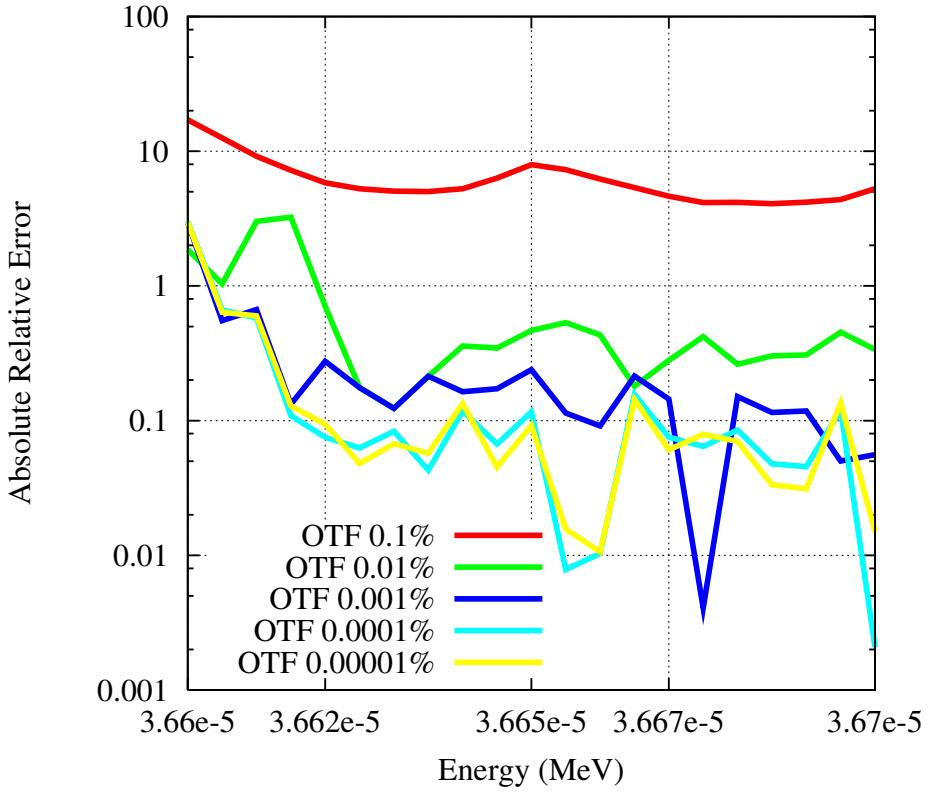

Figure 4.3: Absolute relative errors of fractional tolerances for ^{238}U total cross section.

data files going from 0.1% to 0.00001% increases the file size by about 40%. At the low energies (< 0.1 eV), the cross section derivatives should be zero, but in reality show erratic behavior indicative of numerical noise in the differentiation. Since this is unphysical and may contaminate the solution, the cross section derivatives are not evaluated below 0.1 eV, i.e., set to zero. The top energy for the temperature derivative is chosen by the same criteria in NJOY, i.e., the lowest of the start of the unresolved resonance region or the lowest energy threshold reaction.

Figure 4.3 shows the increase of the fractional tolerance from 0.001% to 0.0001%

is on average a difference of 10%. While the result of increasing the tolerance is more accurate, the amount of storage nearly doubles and therefore the storage demand severely outweighs the gain in accuracy. These results indicate the necessity of increasing the fractional tolerance from the default setting to a minimum of 0.001% in order to accurately estimate the temperature derivatives.

4.3 Doppler Temperature Coefficient Numerical Results

In order to test the Doppler coefficient using adjoint-weighted tallies and cross section derivatives, a numerical benchmark is used to test the model. The Mosteller numerical benchmark[19] was constructed and approved by the Joint Benchmark Committee of the Mathematics and Computation Division of the American Nuclear Society as a means of testing the Doppler defect within a system. This numerical benchmark will be used to test the model but is modified to only test the change in reactivity due to Doppler broadening of the cross sections, all densities are held constant as to avoid contributions from variation in the number density with respect to temperature.

4.3.1 Benchmark Specifications

The geometry of this benchmark corresponds to an infinite array of identical, infinitely long PWR fuel pin cells. Such an assembly can be modeled as a single rectangular pin cell with reflective boundaries on the top, bottom and four sides. The pin cells consist of a cylinder of fuel and cladding with a small gap separating the two, surrounded by a rectangular moderator. Table 4.1 provides the pin cell dimensions while Figure 4.4 gives a schematic of the benchmark.

Dimension (cm)	**600K**
Radius of Fuel	0.39398
Inner Radius of Clad	0.40226
Outer Radius of Clad	0.45972
Pitch	1.26678

Table 4.1: Pin cell dimensions

Doppler coefficient evaluations are done by changing the fuel temperature alone from 600K to 900K, which are respecitvely hot zero power (HZP) and hot full power (HFP) temperatures. Moderator temperature and density were kept constant at

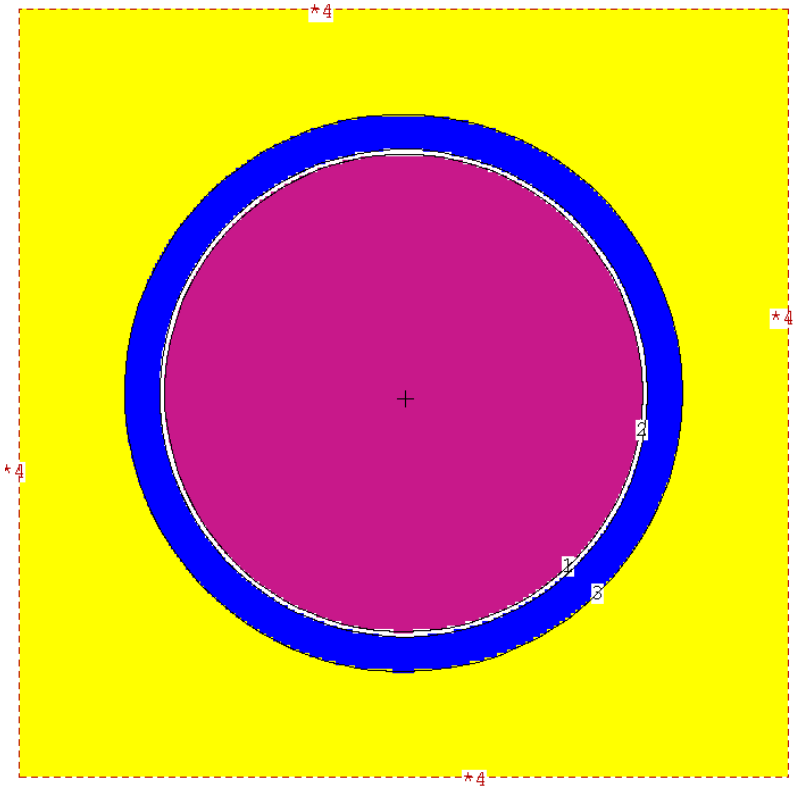

Figure 4.4: Mosteller benchmark reflecting boundary fuel pin.

600K which guarantees a change in reactivity only due to the change in the fuel temperature. The atom densities for respective fuel enrichments can be found in the Appendix in Table B.1.

4.4 Monte Carlo Model

The pin cell configuration as described above is modeled in 3-D geometry using the MCNP code. The axial direction is assumed to be infinite, while reflective boundary conditions are assumed on all other four sides of the pin cell. This geometry model is made with 500 active cycles with 50 skipped cycles each with 10000 histories per cycle. The reference solution is computed using ENDF/B-VII data, while OTF generated cross sections are used to test the adjoint-weighting calculation.

In order to calculate the change in the reactivity $\Delta\rho$, the effective multiplication factors corresponding to HZP and HFP $k_{\text{eff}}^{\text{HZP}}$ and $k_{\text{eff}}^{\text{HFP}}$ are used in Equation 4.4.

$$\Delta\rho = \frac{k_{\text{eff}}^{\text{HFP}} - k_{\text{eff}}^{\text{HZP}}}{k_{\text{eff}}^{\text{HFP}} \times k_{\text{eff}}^{\text{HZP}}} \tag{4.4}$$

Using this equation provides an estimate on the Doppler coefficient α_T describing the change in the reactivity with respect to the change in the reactor temperature ΔT,

$$\alpha_T = \frac{\Delta\rho}{\Delta T}, \qquad \text{where } \Delta T = 300K. \tag{4.5}$$

4.5 Results

4.5.1 Finite Difference Approximations

The calculated values of the multiplication factor (k_{eff}), the Doppler defect ($\Delta\rho$) and the Doppler coefficient α_T for the 7 enrichments of UO_2 mentioned in the previous section are presented. Each of these multiplication factors include the statistical uncertainty in terms of standard deviation σ. The Doppler coefficients are compared to a reference solution which uses NJOY generated cross sections at 600K and 900K. The first set of results are meant to verify MCNP's ability to accurately calculate the criticality value k using OTF cross sections.

Reference Case (NJOY + MCNP)

Enrichment (wt. %)	**HFP $k_{\text{eff}} \pm \sigma$**	**HZP $k_{\text{eff}} \pm \sigma$**	**Doppler defect $\Delta\rho$ (pcm)**	**Doppler Coefficient ($\Delta\rho/\Delta T$) (pcm/K)**
0.711	0.659742 (27)	0.665657 (27)	-1346.8 (8.7)	-4.489 (29)
1.6	0.952675 (36)	0.960809 (36)	-888.7 (5.6)	-2.962 (19)
2.4	1.090005 (39)	1.099048 (39)	-754.9 (4.7)	-2.516 (16)
3.1	1.167462 (41)	1.177192 (41)	-708.0 (4.2)	-2.360 (14)
3.9	1.229839 (42)	1.239809 (42)	-653.9 (3.9)	-2.180 (13)
4.5	1.265040 (42)	1.275161 (42)	-627.4 (3.7)	-2.091 (12)
5.0	1.289275 (42)	1.298923 (42)	-576.1 (3.6)	-1.920 (12)

Table 4.2: Results calculated with NJOY data using 24 million particles

The results show an overall agreement with Doppler coefficients calculated with OTF cross sections versus NJOY cross sections. While similar results [33] have been shown, it is important for this work to also show the difference between the data since the accuracy of the Doppler coefficient is directly correlated to the k-eigenvalue.

MCNP + OTF				
Enrichment (wt. %)	**HFP $k_{eff} \pm \sigma$**	**HZP $k_{eff} \pm \sigma$**	**Doppler defect $\Delta\rho$ (pcm)**	**Doppler Coefficient $(\Delta\rho/\Delta T)$ (pcm/K)**
0.711	0.659718 (56)	0.665643 (56)	-1349 (18)	-4.498 (60)
1.6	0.952572 (75)	0.960889 (75)	-909 (12)	-3.029 (39)
2.4	1.089921 (82)	1.099060 (83)	-762.9 (9.8)	-2.543 (33)
3.1	1.167618 (85)	1.177168 (85)	-694.8 (8.8)	-2.316 (29)
3.9	1.229932 (89)	1.239881 (87)	-652.4 (8.2)	-2.175 (27)
4.5	1.265178 (88)	1.275172 (87)	-619.5 (7.7)	-2.065 (26)
5.0	1.289420 (87)	1.299027 (88)	-573.5 (7.4)	-1.912 (25)

Table 4.3: Results calculated using OTF data.

4.5.2 Adjoint-Weighted Doppler Temperature Coefficient Approximations

Since it was shown that MCNP+OTF are correctly calculating the k-eigenvalue, a modified version of MCNP6 which directly calculates the Doppler coefficient at 600K is presented. This version of MCNP6 takes advantage of adjoint-weighted tallies and OTF cross section data in order to directly calculate the derivative of reactivity with respect to temperature using temperature derivatives of the OTF cross sections and adjoint weighting. This method requires only a single calculation to estimate the Doppler temperature coefficient without any extra storage requirements. The OTF cross section data libraries were constructed using the recommended tolerance of 0.001% mentioned in Section 4.2. Results are compared to a Monte Carlo simulation using MCNP+DBRC and two published deterministic calculations using the n-TRACER and CASMO codes[35]. The purpose of using MCNP+DBRC is use the most accurate representation of thermal scattering. Although DBRC is not currently available in the MCNP6 code, results produced by Sunny[6] used a modified version

of MCNP and is therefore used here. Figure 4.5 compares the adjoint-weighted α_T with MCNP6 with a finite difference calculation in MCNP6 using DBRC. Figure 4.6 compares results of the adjoint-weighted α_T with MCNP6 and two published deterministic results. Comparing the adjoint method with deterministic results reinforces the accuracy of this model. All of these results are within 1 standard deviation.

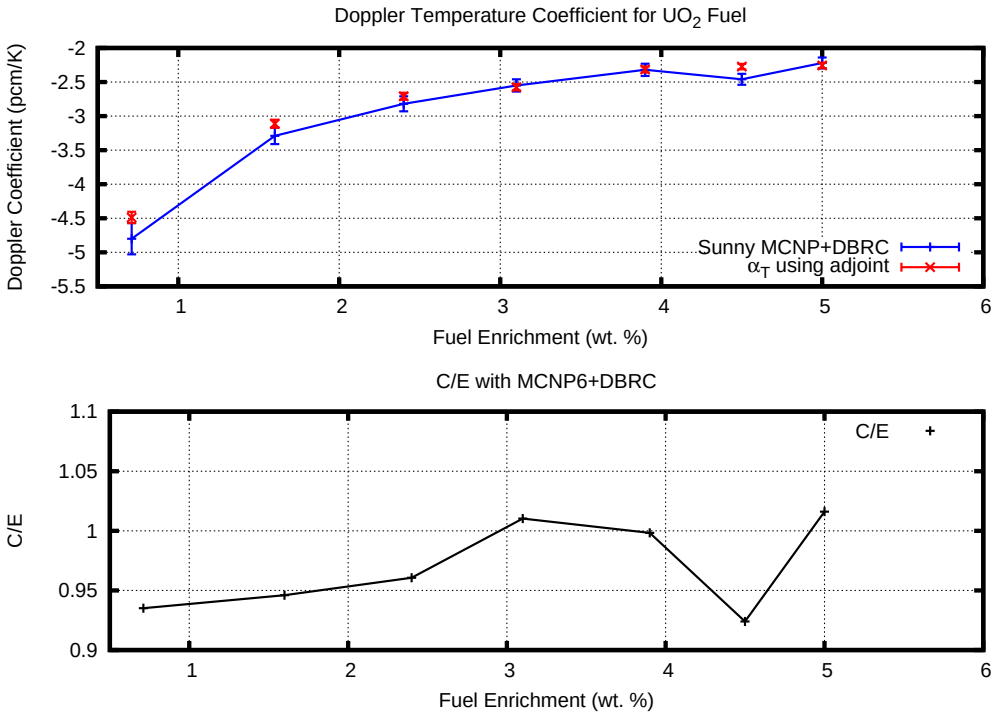

Figure 4.5: Doppler coefficient MCNP6 reference solution compared against adjoint weighted approximation.

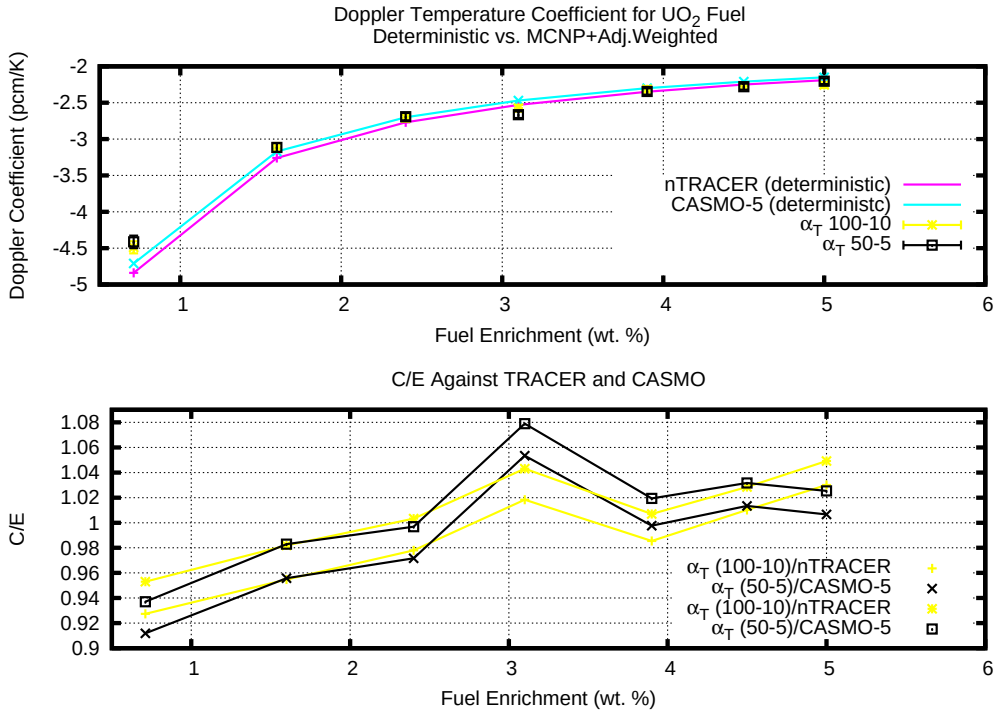

Figure 4.6: Doppler coefficient deterministic reference solution compared against adjoint weighted approximation.

4.5.3 Fuel Assembly Calculations

The Mosteller benchmark has been expanded in order to test the robustness of the adjoint model. Rather than calculating a reflective pin cell, a 15x15 PWR fuel assembly is introduced with five separate configurations. Each configuration varies the temperature distribution inside the fuel. Figure 4.7 shows a cross section of each configuration being tested. Like the Mosteller benchmark calculation, two separate calculations were made for each fuel assembly, the reference calculation will simulate the fuel at 600K and the second calculation will increase the fuel temperature to

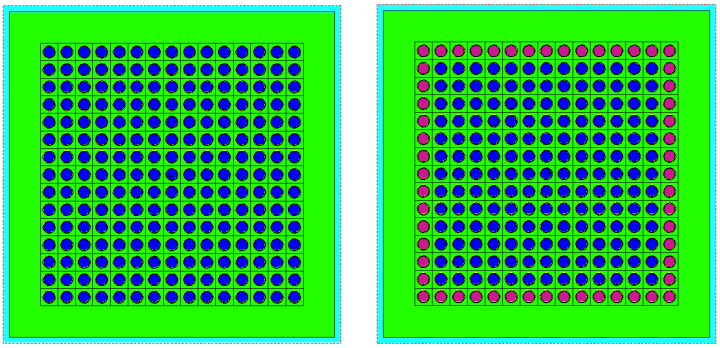

(a) Configuration 1

(b) Configuration 2

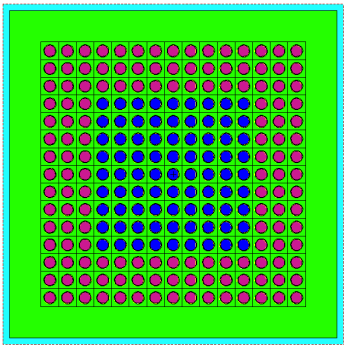

(c) Configuration 3

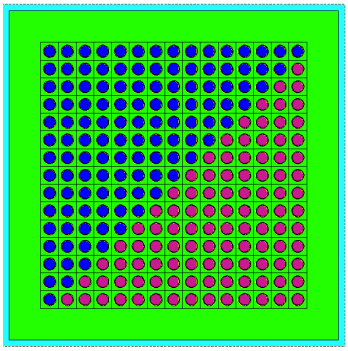

(d) Configuration 4

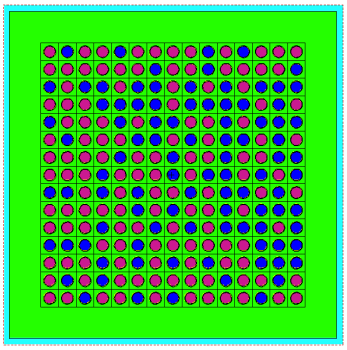

(e) Configuration 5

Figure 4.7: Fuel assembly configurations for Doppler temperature coefficient calculation.

900K and a forward difference derivative will approximate the Doppler temperature coefficient at 600K. Table 4.4 provides the dimensions of the fuel assembly. The fuel pins are infinitely long cylinders and the moderator is an infinitely long right parallelepiped with water. The iron rack surrounding the water moderator is an infinitely long right paralellepiped. The material setup is similar to the Mosteller benchmark where all atom densities are held constant and the temperature change is only inside the fuel, all other materials are held at a constant 300K. The difference in temperature distributions is shown in Fig. 4.7. Since the Doppler temperature

Dimension	**(cm)**
Radius of Fuel	0.44
Outer Radius of Clad	0.49
Outer Moderator Side (around fuel pins)	1.4
Outer Moderator Side (around fuel assembly)	26.0
Outer Iron Rack	27.0

Table 4.4: Fuel assembly dimensions for a simplified 15x15 PWR.

coefficient is on the order of percent-milli (pcm) many particles were necessary to have comparable statistics with the adjoint calculations. Each 600K configuration was simulated a total of 10 times using different random number seeds, 150000 batches of neutrons with 10000 neutrons per batch. This was repeated for 900K and errors were propagated in order to obtain the direct difference approximation of the Doppler temperature coefficient. The adjoint weighted calculations were simulated with a single calculation of 20000 batches of neutrons with 10000 neutrons per batch. OTF libraries were constructed using a tolerance of 0.001%. Table 4.5 shows the number of particles necessary to capture the Doppler temperature coefficient as well as the respective runtimes with respect to a single processor. The difference in number of particles with respect to the direct difference approximation compared to the

adjoint-weighted approximation is a factor of 150. In terms of computational time, the adjoint-weighted simulation takes 49 times less time to run on a single processor than the direct difference approximation. The main advantage comes from running a single calculation. Further, the Doppler coefficient requires such high resolution in the k-eigenvalue and the adjoint-weighting helps to amplify particle significance with respect to the importance function.

The following tables and figures show the comparison of the Doppler temperature coefficients produced by the direct difference and the adjoint method. Results were produced with fuel enrichments of 0.711%, 2.4%, 3.1%, 3.9%, 4.5%, and 5.0% in U^{235}. Two separate simulations were ran, one using uranium oxide and the second using uranium carbide. The purpose of changing the material within the fuel was to exploit the variation in resonances within the fuel as carbon has lower lying resonances than oxygen. Both oxygen and carbon contain low-energy resonances which help to increase the effect of the Doppler broadening in the cross sections. While results for the two cases only show fuel enrichment of 0.711%, all other results may be found in Appendix D. The reason for this is due to the consistent behavior between all the results. Comparisons for the adjoint method with the reference solutions show results match within statistics. While there does not seem to exist any correlation between variation in the fuel enrichment and accuracy with the method, one may be able to obtain more accurate results by reducing the temperature difference when calculating the direct difference. The reason for this is due to the linear approximation which is assumed in the perturbation theory. It may be the change in temperature is not linear and therefore the approximation of a derivative over a wide range in temperature does not make sense and a reduction in the temperature difference must be made. Overall, the adjoint method has been shown to be just as accurate as the direct difference method. The adjoint method also reduced the amount of computing power necessary to obtain the Doppler temperature coefficient.

	Direct Difference	Adjoint-Weighted
Total Particles	3.0E10	2.0E8
Total Runtime (HR)	3136	64

Table 4.5: Table of total particles along with respective runtimes.

0.711 Wgt. %		
Config.	**Direct Difference** $(\Delta\rho/\Delta T)$ **(pcm/K)**	**Adjoint-Weighted** (α_T) **(pcm/K)**
1	-5.4711e-05	-2.4864e-05
2	-1.6082e-05	-1.2625e-05
3	-4.9301e-06	-5.4991e-06
4	-4.8941e-06	-4.0595e-06
5	-5.9779e-06	-6.6279e-06

Table 4.6: Doppler temperature coefficient comparison for fuel assemblies computed with direct difference and the adjoint method.

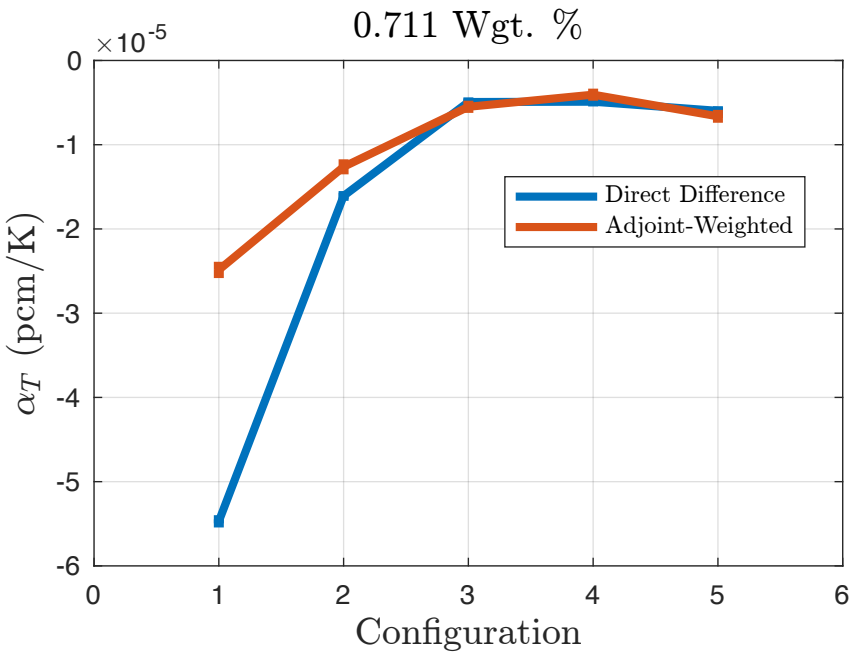

Figure 4.8: Doppler temperature coefficient comparison with uranium containing 0.711 wgt. %

0.711 Wgt. %

Config.	**Direct Difference** $(\Delta\rho/\Delta T)$ **(pcm/K)**	**Adjoint-Weighted** (α_T) **(pcm/K)**
1	-6.5660e-05	-2.5116e-05
2	-1.7636e-05	-1.3351e-05
3	-4.9010e-06	-5.6872e-06
4	-5.4068e-06	-4.5240e-06
5	-6.1763e-06	-7.2649e-06

Table 4.7: Doppler temperature coefficient comparison for fuel assemblies computed with direct difference and the adjoint method.

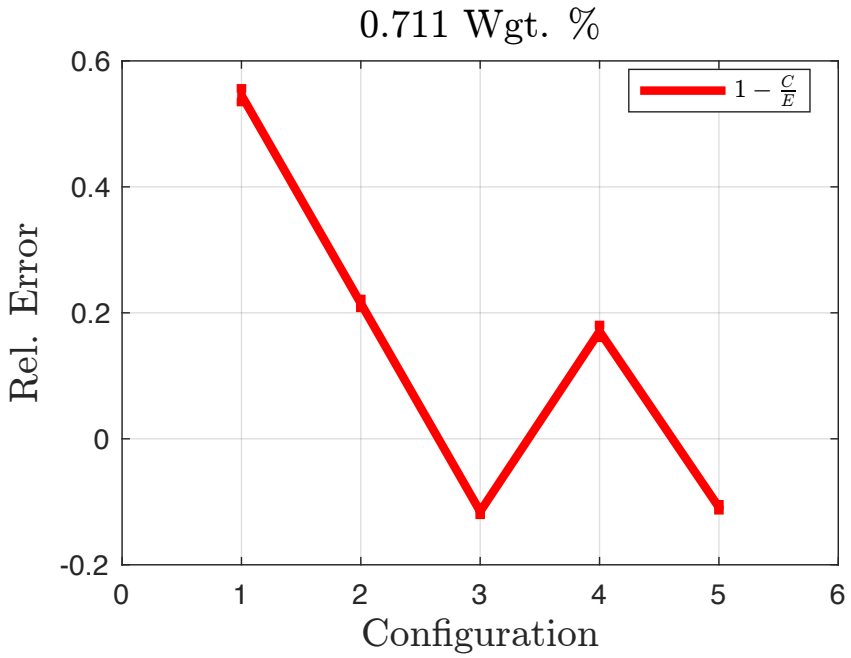

Figure 4.9: Doppler temperature coefficient comparison with uranium containing 0.711 wgt. %

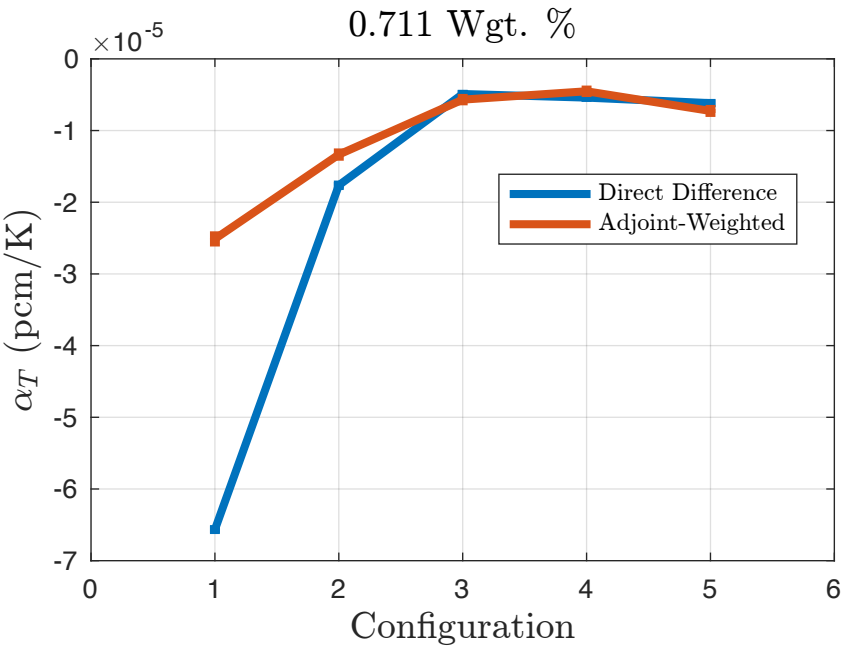

Figure 4.10: Doppler temperature coefficient comparison with uranium carbide containing 0.711 wgt. %

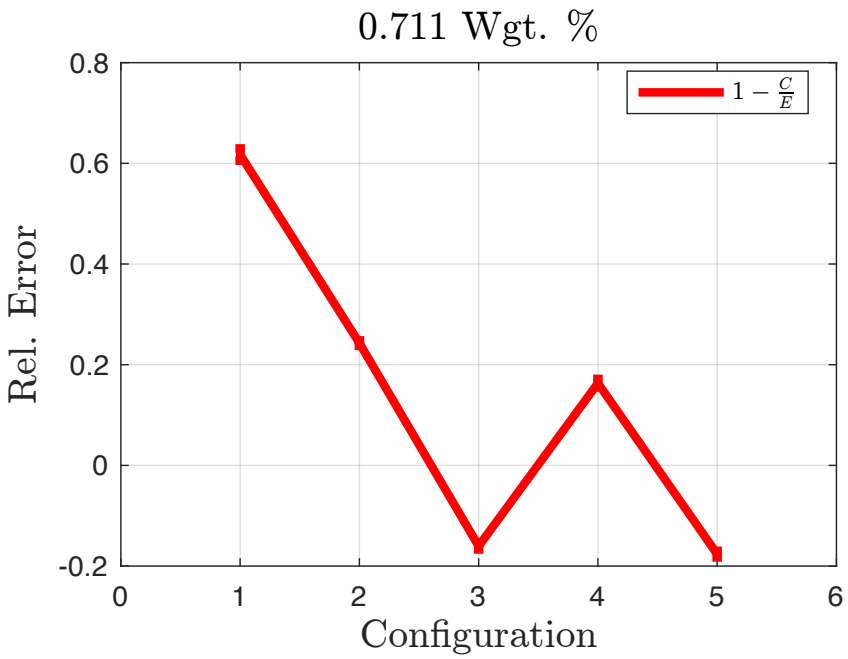

Figure 4.11: Doppler temperature coefficient comparison with uranium carbide containing 0.711 wgt. %

Chapter 5

Development of Analytic Model

The Mosteller benchmark discussed in the previous chapter is a numerical benchmark, therefore investigation into an analytic benchmark for the Doppler temperature coefficient has been made. The production of an analytic model requires simplifying the Boltzmann transport equation while still maintaining the correct scattering mechanics. As a result, research went into studying the heavy gas model. This model can be found in most nuclear reactor theory texts[36][26] but much of the details concerning the derivation have been referenced to classical texts [37][38][39]. It is the goal of this dissertation to resurrect some of the fine details in an effort to provide the reader with a thorough understanding of the approximations which result in the heavy gas model. Investigation into the heavy gas model produced an analytic benchmark of free-gas scattering mechanics in the limit as the mass ratio of the target $A >> 1$. This is the first analytic demonstration of elastic free-gas scattering mechanics inside a Monte Carlo code. The heavy gas model will be taken a step further to introduce energy dependence into the absorption cross sections which provides a pathway for producing an analytic k-eigenvalue which may then be used to approximate the Doppler temperature coefficient.

5.1 Derivation of the Heavy Gas Model

When dealing with thermal scattering of neutrons, difficulty arises in correctly treating slowing down of neutrons near thermal energies. As a result, an idealized problem where the moderator is treated as a monatomic gas whose atoms are heavy compared to the neutron is examined. This assumption ignores chemical binding effects and removes the complexity within the problem while retaining essential physics. Wigner-Wilkins[**?**] first derived and discussed an integral equation for the energy distribution of neutrons in an infinite medium with a monatomic gas. Wilkins[40] further derived a reduced form to a second order differential equation in the limit of large moderator masses strictly on mathematical grounds. A more physical basis was derived by Hurwitz[38] and most recently Larsen-Williams derived a generalized heavy gas model which may be used to derive improved Fokker-Planck approximations for other types of kinetic equations. For purposes of this research, the derivation will follow on the physical grounds similar to the classical text by Hurwitz.

The infinite homogeneous medium satisfies the following balance equation:

$$\left[\Sigma_a(E) + \Sigma_s(E)\right]\phi(E) = \int_0^\infty \Sigma_s(E' \to E)\phi(E')\mathrm{d}E' \tag{5.1}$$

where,

$$\Sigma_s(E) = \int_0^\infty \Sigma_s(E \to E')dE' \tag{5.2}$$

Recall, $\Sigma_s(E \to E')dE'/\Sigma_s(E)$ is the probability of a neutron with energy E will be scattered into the interval between E' and $E' + \mathrm{d}E'$. In the absence of absorption, thermal equilibrium will be established yielding a Maxwellian distribution in energy:

$$\phi_M(E) \equiv M(E) = \frac{E}{T^2}\, e^{\frac{-E}{T}} \tag{5.3}$$

where T is in energy units using Boltzmann's constant. Next, apply the principle of detailed balance which states the rate of neutrons with energy E moving to energy

E' is equal to the rate of neutrons of energy E' moving to energy E.

$$\Sigma_s(E \to E')M(E) = \Sigma_s(E' \to E)M(E) \tag{5.4}$$

This property of the scattering kernel is independent of absorption which allows Eqn.5.6 to be written in the following form. Consider,

$$\widehat{\phi}(E) \equiv \frac{\phi(E)}{M(E)} \tag{5.5}$$

which leads to

$$\left[\Sigma_a(E) + \Sigma_s(E)\right]\widehat{\phi}(E) = \frac{1}{M(E)}\int_0^\infty \Sigma_s(E' \to E)\phi(E')\mathrm{d}E' \tag{5.6}$$

and from the definitions in Eqn. 5.4 and Eqn. 5.5,

$$\left[\Sigma_a(E) + \Sigma_s(E)\right]\widehat{\phi}(E) = \int_0^\infty \frac{\Sigma_s(E' \to E)\widehat{\phi}(E')M(E')\Sigma_s(E \to E')}{M(E')\Sigma_s(E' \to E)}\mathrm{d}E' \tag{5.7}$$

$$\left[\Sigma_a(E) + \Sigma_s(E)\right]\widehat{\phi}(E) = \int_0^\infty \widehat{\phi}(E')\Sigma_s(E \to E')\mathrm{d}E' \tag{5.8}$$

The differential scattering operator has now been defined in terms of neutrons which have scattered into $[E', E' + \mathrm{d}E']$ and recalling Eqn. 5.2, the infinite homogeneous medium equation is written as,

$$\Sigma_a(E)\widehat{\phi}(E) = \int_0^\infty \Sigma_s(E \to E')\left[\widehat{\phi}(E') - \widehat{\phi}(E)\right]\mathrm{d}E' \tag{5.9}$$

In the absence of absorption, $\widehat{\phi}(E)$ is easily shown to be a constant and is arbitrarily chosen to be unity.

If the scattering range is small compared to the value of the flux ($\phi(E)$ or $\widehat{\phi}(E)$) over that range, than the use of a Taylor series expansion under the integral sign may be used. Take a series expansion about the point $E' = E$ for $\widehat{\phi}(E)$:

$$\widehat{\phi}(E') = \sum_{n=0}^{\infty} \frac{\widehat{\phi}^{(n)}(E)}{n!}\left(E' - E\right)^n \tag{5.10}$$

Next, substitute the Taylor series expansion into Eqn. 5.9:

$$\Sigma_a(E)\widehat{\phi}(E) = \int_0^\infty \Sigma_s(E \to E') \left[\sum_{n=0}^{\infty} \frac{\widehat{\phi}^{(n)}(E)}{n!} (E' - E)^n - \widehat{\phi}(E) \right] \mathrm{d}E'$$

$$\Sigma_a(E)\widehat{\phi}(E) = \int_0^\infty \Sigma_s(E \to E') \left[\widehat{\phi}(E) + \frac{\mathrm{d}\widehat{\phi}}{\mathrm{d}E}(E' - E) + \cdots + -\widehat{\phi}(E) \right] \mathrm{d}E'$$

$$\Sigma_a(E)\widehat{\phi}(E) = \int_0^\infty \Sigma_s(E \to E') \left[\sum_{n=1}^{\infty} \frac{\widehat{\phi}^{(n)}(E)}{n!} (E' - E)^n \right] \mathrm{d}E'$$

and finally divide by the total scattering $\Sigma_s(E)$,

$$[\Sigma_a(E)/\Sigma_s(E)]\,\widehat{\phi}(E) = \overline{\Delta E}\ \frac{\mathrm{d}\widehat{\phi}(E)}{\mathrm{d}E} + \frac{\overline{\Delta E^2}}{2}\ \frac{\mathrm{d}^2\widehat{\phi}(E)}{\mathrm{d}^2E} + \ldots \tag{5.11}$$

where,

$$\overline{\Delta E^n} \equiv \frac{1}{\Sigma_s(E)} \int_0^\infty (E' - E)^n\ \Sigma_s(E \to E')\mathrm{d}E' \tag{5.12}$$

Equation 5.11 is an expansion in the energy-change moments of the kernel. The moments were derived on a quantum-mechanical basis, where the finer details are left to Hurwitz's[38] paper. This quantum-mechanical approach first defines the cross section in terms of momentum then integrates over solid angle and over the Maxwellian velocities to produce a scattering term which is a nonsingular function of the zero temperature cross section Σ_{fr} and the nuclear-neutron mass ratio A. Carrying out the expansion to the first order in A^{-1} yields

$$\begin{aligned}\Sigma_s(E \to E') =& \Sigma_{fr}\delta(E' - E) + \\ & \left(A^{-1}\Sigma_{fr}/2\pi\right)(E' + E)(E'/E)^{1/2} \int_{-\infty}^{\infty} \mathrm{d}t[it - Tt^2] \exp[i(E' - E)t]\end{aligned} \tag{5.13}$$

In order to remove the integration, a property of the dirac delta functions is used:

$$\delta^n(x) = \frac{1}{2\pi}\int_{-\infty}^{\infty} \mathrm{d}t(it)^n \exp(itx)$$

resulting in the following definition of the scattering kernel

$$\begin{aligned}\Sigma_s(E \to E') =& \Sigma_{fr}\delta(E'-E) + \\ & (A^{-1}\Sigma_{fr})(E'+E)(E'/E)^{1/2}[\delta'(E'-E) + T\delta''(E'-E)] \end{aligned} \tag{5.14}$$

The following notation is introduced,

$$\begin{aligned}(E'-E) &= \Delta \\ (E'+E)(E'/E)^{1/2} &= f(E,\Delta) = 2E[1 + (\Delta/E) + (\Delta^2/8E^2) + \dots]\end{aligned}$$

When $E' = E$, the energy-change moments take the following form, recall Eqn. 5.12:

$$\Sigma_s = \Sigma_{fr}[1 + A^{-1}(Tf''(E,0) - f'(E,0)] \tag{5.15}$$

$$\begin{aligned}\Sigma_s\overline{\Delta E} &= \int_{-\infty}^{\infty} \mathrm{d}E\ \Sigma_{fr}[1 + A(Tf''(E,0) - f'(E,0)] \\ &= \Sigma_{fr}A^{-1}[2Tf'(E,0) - f(E,0)]\end{aligned} \tag{5.16}$$

$$\Sigma_s\overline{\Delta E^2} = \Sigma_{fr}A^{-1}[2Tf(E,0)] \tag{5.17}$$

$$\Sigma_s\overline{\Delta E^n} = \mathcal{O}(A^{-2}) \text{ for } n = 3,4; = \mathcal{O}(A^{-3}) \text{ for } n = 5,6\ \dots \tag{5.18}$$

where,

$$f^n(E,0) = \left[\frac{\partial^n f(E,\Delta)}{\partial \Delta^n}\right]_{\Delta=0} \tag{5.19}$$

Ignoring higher order terms with respect to the inverse mass ratio A^{-1} results in the following form of Eqn. 5.11:

$$\Sigma_a(E)\widehat{\phi}(E) = \Sigma_{fr}A^{-1}(-2E + 4T)\ \frac{\mathrm{d}\widehat{\phi}(E)}{\mathrm{d}E} + \Sigma_{fr}A^{-1}(2ET)\ \frac{\mathrm{d}^2\widehat{\phi}(E)}{\mathrm{d}^2E} \tag{5.20}$$

$$\Sigma_a(E)\widehat{\phi}(E) = \Sigma_{fr}\xi\left[(-E+2T)\ \frac{\mathrm{d}\widehat{\phi}(E)}{\mathrm{d}E} + (ET)\ \frac{\mathrm{d}^2\widehat{\phi}(E)}{\mathrm{d}^2E}\right] \tag{5.21}$$

Finally, recalling Eqn. 5.5 the heavy gas equation in terms of the flux $\phi(E)$ i

$$\Sigma_a(E)\phi(E) = \xi\Sigma_{fr}\left[Ek_{Boltz}T\frac{d^2\phi}{dE^2} + E\frac{d\phi}{dE} + \phi(E)\right] \tag{5.22}$$

5.2 Heavy Gas Model for Thermal Scattering

The heavy gas model for thermal scattering is the lowest nontrivial order in the asymptotic expansion of the integral scattering operator in terms of the inverse mass ratio $1/A$, and is given by the following second order differential operator[36]:

$$\int_0^\infty \Sigma_s(E'\to E)\phi(E')dE' - \Sigma_s(E)\phi(E) = \xi\Sigma_{fr}\left[Ek_{Boltz}T\frac{d^2\phi}{dE^2} + E\frac{d\phi}{dE} + \phi(E)\right] \tag{5.23}$$

The heavy gas model corresponds to a non-constant total scattering cross section given by:

$$\Sigma_s(E) = \Sigma_{fr}\left(1 + \frac{k_{Boltz}T}{2AE}\right) \tag{5.24}$$

where Σ_{fr} is the free nucleus cross section and the parameter ξ is defined by:

$$\xi = \frac{2}{A} \tag{5.25}$$

The infinite medium k-eigenvalue problem can then be written as:

$$\Sigma_a(E)\phi(E) = \xi\Sigma_{fr}\left[Ek_{Boltz}T\frac{d^2\phi}{dE^2} + E\frac{d\phi}{dE} + \phi(E)\right] + \frac{\chi(E)}{k_\infty}\int_0^\infty \nu\Sigma_f(E')\phi(E')dE' \tag{5.26}$$

Using the normalization:

$$\int_0^\infty \nu\Sigma_f(E')\phi(E')dE' = 1 \tag{5.27}$$

Eqn. (5.26) becomes

$$\Sigma_a(E)\phi(E) = \xi\Sigma_{fr}\left[Ek_{Boltz}T\frac{d^2\phi}{dE^2} + E\frac{d\phi}{dE} + \phi(E)\right] + \frac{\chi(E)}{k_\infty} \tag{5.28}$$

which, after some rearrangement, reduces to the eigenvalue problem:

$$Ek_{Boltz}T\frac{d^2\phi}{dE^2} + E\frac{d\phi}{dE} + \left[1 - \frac{\Sigma_a(E)}{\xi\Sigma_{fr}}\right]\phi(E) + \frac{\chi(E)}{k_\infty\xi\Sigma_{fr}} = 0. \tag{5.29}$$

Finally, defining a non-dimensional energy variable and transformed flux:

$$\epsilon = \frac{E}{k_{Boltz}T}, \qquad \widetilde{\phi}(\epsilon)d\epsilon = \phi(E)dE \tag{5.30}$$

Eqn. (5.29) further simplifies to:

$$\epsilon\frac{d^2\widetilde{\phi}}{d\epsilon^2} + \epsilon\frac{d\widetilde{\phi}}{d\epsilon} + \left[1 - \frac{\Sigma_a(\epsilon)}{\xi\Sigma_{fr}}\right]\widetilde{\phi}(\epsilon) + \frac{\chi(\epsilon)}{k\xi\Sigma_{fr}} = 0, \quad 0 < \epsilon < \infty. \tag{5.31}$$

Applying appropriate boundary conditions, Eqn. (5.32) is first solved for the spectrum and the normalization condition in Eqn. (5.27) is then applied to obtain the k_∞-eigenvalue. Note that the k_∞-eigenvalue is embedded in the inhomogeneous term and Eqn. (5.32) is therefore not a standard eigenvalue problem.

For energy-dependent absorption and fission cross sections, and recognizing that the fission neutron spectrum is energy dependent, direct or iterative numerical solution techniques will be necessary to solve the eigen-problem. However, an explicit solution in terms of the confluent hypergeometric function or Kummer function can be developed as a function of k_∞ when these parameters are energy independent. Again, this solution must be subjected to the normalization constraint to obtain k_∞. Although not directly applicable to the problem of interest here, the analytic

solution can serve to benchmark the solution for the energy dependent case that must be obtained numerically. Finally, since temperature is a parameter in this model (although it does not appear explicitly in the scaled equation, Eqn. (5.32) the temperature coefficient can be obtained by wrapping a numerical differentiation algorithm around the k_∞-eigenvalue calculation.

Results from the above implementation will be compared against MCNP6 using a user-defined cross section library.

5.2.1 Kummer Equation

In order to solve Eqn.(5.32), let the absorption cross section be constant in energy and assume all neutrons are produced at some energy ϵ_0.

$$\epsilon\frac{d^2\widetilde{\phi}}{d\epsilon^2}+\epsilon\frac{d\widetilde{\phi}}{d\epsilon}+\left[1-\frac{\Sigma_a(\epsilon)}{\xi\Sigma_{fr}}\right]\widetilde{\phi}(\epsilon)+\frac{\chi(\epsilon)}{k\xi\Sigma_{fr}}=0,\quad \chi(\epsilon)=\delta(\epsilon-\epsilon_0)\quad 0<\epsilon<\epsilon_0. \tag{5.32}$$

Under these conditions, Eqn.(5.32) is a homogeneous second order ODE for $\epsilon \neq \epsilon_0$. The homogeneous part can be rewritten as the Kummer equation which is given by[41]

$$z\frac{d^2w}{dz^2}+(b-z)\frac{dw}{dz}-aw=0 \tag{5.33}$$

where,

$$z=-\epsilon,\quad \frac{dz}{d\epsilon}=-1,\quad \frac{dz^2}{d\epsilon^2}=1,\quad b=0,\quad a=1-\frac{\Sigma_a}{\xi\Sigma_{fr}}$$

By using the above substitutions, we get back the homogeneous part of Eqn.(5.32):

$$\begin{aligned}-\epsilon\frac{d^2w}{dz^2}\cdot\frac{dz^2}{d\epsilon^2}-(-\epsilon)\frac{dw}{dz}\left(\frac{-dz}{d\epsilon}\right)-\left(1-\frac{\Sigma_a}{\xi\Sigma_{fr}}\right)w=0\\ -1\left[-\epsilon\frac{d^2w}{d\epsilon^2}-\epsilon\frac{dw}{d\epsilon}-\left(1-\frac{\Sigma_a}{\xi\Sigma_{fr}}\right)w\right]=0\\ \epsilon\frac{d^2w}{d\epsilon^2}+\epsilon\frac{dw}{d\epsilon}+\left(1-\frac{\Sigma_a}{\xi\Sigma_{fr}}\right)w=0 \qquad (5.34)\end{aligned}$$

(5.35)

According to Ref[41] the complete solution to Kummer's equation is the sum of two linearly-independent summations defined by

$$w = C_1\ z^{1-b}\ e^z\ K(1-a, 2-b, -z) + C_2\ z^{1-b}\ e^z\ U(1-a, 2-b, -z) \tag{5.36}$$

where C_1, C_2 are constants and K and U are the confluent hypergeometric functions of the first and second kind, also known as Kummer's equation and Tricomi's equation respectively. For a given a, b, z in Eqn.(5.33) the hypergeometric functions of the first and second kind take the following form:

$$K(a, b, z) = 1 + \frac{az}{b} + \frac{(a)_2 z^2}{(b)_2 2!} + \cdots + \frac{(a)_n z^n}{(b)_n n!} + \ldots \tag{5.37}$$

$$U(a, b, z) = \frac{\Gamma(1-b)}{\Gamma(a-b-1)} K(a, b, z) + \frac{\Gamma(b-1)}{\Gamma(a)}\ z^{1-b}\ K(a-b+1, 2-b, z) \tag{5.38}$$

where,

$$(a)_n = a(a+1)(a+2)\ldots(a+n-1), \quad (a)_0 = 1 \tag{5.39}$$

In order to obtain an explicit solution, two boundary conditions must be applied. For the heavy gas model the energy boundary $\phi(0) = 0$ forces $C_2 = 0$ since $U(a, b, 0) \neq 0$. The analytic general solution to the heavy gas model is then given by

$$\tilde{\phi}(\epsilon) = C_1 \left(\epsilon\ e^{-\epsilon}\right) K\left(\frac{\Sigma_a}{\xi\Sigma_{fr}}, 2, \epsilon\right), \quad \epsilon \neq \epsilon_0 \tag{5.40}$$

where C_1 is an arbitrary constant that must be obtained from the boundary condition defined by the source which states all neutrons are born with some energy $\epsilon = \epsilon_0$. In this evaluation, the flux approaching from the left of ϵ_0 is finite, while the flux approaching from the right is zero, leading to the following analysis. Consider a differential space 2δ over the point ϵ_0 (see Fig.5.1),
and now integrate Eqn.(5.32) over that space.

$$\int_{\epsilon-\delta}^{\epsilon+\delta} \left[\epsilon' \frac{d^2\widetilde{\phi}}{d\epsilon'^2} + \epsilon' \frac{d\widetilde{\phi}}{d\epsilon'} + \left(1 - \frac{\Sigma_a}{\xi\Sigma_{fr}}\right) \widetilde{\phi}(\epsilon')\right] d\epsilon' = \frac{-1}{k\xi\Sigma_{fr}} \tag{5.41}$$

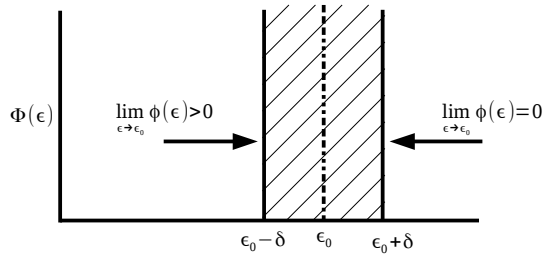

Figure 5.1: Limiting boundry condition at ϵ_0.

Integration by parts yields,

$$\epsilon' \frac{d\widetilde{\phi}}{d\epsilon'}\bigg|_{\epsilon-\delta}^{\epsilon+\delta} - \int_{\epsilon-\delta}^{\epsilon+\delta} \frac{d\widetilde{\phi}}{d\epsilon'} d\epsilon' + \epsilon' \widetilde{\phi}(\epsilon')\bigg|_{\epsilon-\delta}^{\epsilon+\delta} - \left(\frac{\Sigma_a}{\xi\Sigma_{fr}}\right) \int_{\epsilon-\delta}^{\epsilon+\delta} \widetilde{\phi}(\epsilon') d\epsilon' = \frac{-1}{k\xi\Sigma_{fr}} \tag{5.42}$$

Recall all values $\epsilon > \epsilon_0$ are zero,

$$\begin{aligned} &\cancelto{0}{(\epsilon_0+\delta)\widetilde{\phi}'(\epsilon_0+\delta)} - (\epsilon_0-\delta)\widetilde{\phi}'(\epsilon_0-\delta) - \left[\cancelto{0}{\widetilde{\phi}(\epsilon_0+\delta)} - \widetilde{\phi}(\epsilon_0-\delta)\right] \\ &+\cancelto{0}{(\epsilon_0+\delta)\widetilde{\phi}(\epsilon_0+\delta)} - (\epsilon_0-\delta)\widetilde{\phi}(\epsilon_0-\delta) - \cancelto{0}{\left(\frac{\Sigma_a}{\xi\Sigma_{fr}}\right)\int_{\epsilon-\delta}^{\epsilon+\delta} \widetilde{\phi}(\epsilon')d\epsilon'} = \frac{-1}{\xi k\Sigma_{fr}} \end{aligned} \tag{5.43}$$

And now taking the limit,

$$\lim_{\epsilon\to\epsilon_0} \quad -(\epsilon_0-\delta)\widetilde{\phi}'(\epsilon_0-\delta) + \widetilde{\phi}(\epsilon_0-\delta) - (\epsilon_0-\delta)\widetilde{\phi}(\epsilon_0-\delta) = \frac{-1}{\xi k\Sigma_{fr}} \tag{5.44}$$

$$-\epsilon_0\widetilde{\phi}'(\epsilon_0) + (1-\epsilon_0)\widetilde{\phi}(\epsilon_0) = \frac{-1}{\xi k\Sigma_{fr}} \tag{5.45}$$

Equation 5.45 leads a boundary condition which may be used to solve for the constant in Eqn.(5.40). Recall,

$$\widetilde{\phi}(\epsilon) = C_1 w(\epsilon) K\left(\frac{\Sigma_a}{\xi\Sigma_{fr}}, 2, \epsilon\right), \quad w(\epsilon) = \epsilon e^{-\epsilon} \tag{5.46}$$

$$\widetilde{\phi}'(\epsilon) = C_1\left[w(\epsilon)'K + K'w(\epsilon)\right], \quad w(\epsilon)' = e^{-\epsilon} - \epsilon\, e^{-\epsilon} = e^{-\epsilon} - w(\epsilon) \tag{5.47}$$

From Eqn.5.45 and the above substitutions,

$$-\epsilon_0 \left[C_1(w_0' K_0 + K_0' w_0)\right] + (1-\epsilon_0)\left[C_1 w_0 K_0\right] = \frac{-1}{\xi k_\infty \Sigma_{fr}} \tag{5.48}$$

where $w_0,\ K_0,\ w_0',\ K_0'$ are the respective functions evaluated at ϵ_0.

$$C_1 = \frac{-1}{\xi k_\infty \Sigma_{fr}} \cdot \left(\frac{1}{(1-\epsilon_0)[w_0 M_0] - \epsilon_0 [w_0' K_0 + K_0' w_0]} \right) \tag{5.49}$$

$$= \frac{1}{\xi k_\infty \Sigma_{fr}} \cdot \left(\frac{1}{\epsilon_0 K_0' w_0} \right) \tag{5.50}$$

and finally,

$$\widetilde{\phi}(\epsilon) = \frac{1}{\xi k_\infty \Sigma_{fr}} \cdot \left(\frac{1}{\epsilon_0^2\ e^{-\epsilon_0} K_0'} \right) \epsilon\ e^{-\epsilon} K\left(\frac{\Sigma_a}{\xi \Sigma_{fr}}, 2, \epsilon \right) \tag{5.51}$$

leads to the criticality condition

$$k_\infty = \left(\frac{\nu \Sigma_f}{\xi \Sigma_{fr}} \right) \left(\frac{1}{\epsilon_0^2\ e^{-\epsilon_0} K_0'} \right) \int_0^{\epsilon_0} \epsilon\ e^{-\epsilon} K\left(\frac{\Sigma_a}{\xi \Sigma_{fr}}, 2, \epsilon \right) d\epsilon \tag{5.52}$$

5.2.2 Verifying k_∞

In the infinite medium case the material properties dictate the criticality condition leading to the well-known result

$$k_\infty = \frac{\nu \Sigma_f}{\Sigma_a} \tag{5.53}$$

for constant cross sections. We will now show this to be true for our criticality condition given by Eqn.(5.52). Recall,

$$k_{\infty_{HG}} = \left(\frac{\nu \Sigma_f}{\xi \Sigma_{fr}} \right) \left(\frac{1}{\epsilon_0^2\ e^{-\epsilon_0} K_0'} \right) \int_0^{\epsilon_0} \epsilon\ e^{-\epsilon} K\left(\frac{\Sigma_a}{\xi \Sigma_{fr}}, 2, \epsilon \right) d\epsilon \tag{5.54}$$

Using the identity[42]

$$\int z\ e^{-z} K(a,2,z) dz = \frac{e^{-z}}{a} z^2 \frac{d}{dz} K(a,2,z) \tag{5.55}$$

to evaluate the integration inside Eqn.(5.54) results in the following

$$k_\infty = \left(\frac{\nu\Sigma_f}{\xi\Sigma_{fr}}\right)\left(\frac{1}{\epsilon_0^2\ e^{-\epsilon_0}K'\left(\frac{\Sigma_a}{\xi\Sigma_{fr}},2,\epsilon_0\right)}\right)\left(\frac{\xi\Sigma_{fr}}{\Sigma_a}\epsilon_0^2\ e^{-\epsilon_0}K'\left(\frac{\Sigma_a}{\xi\Sigma_{fr}},2,\epsilon_0\right)\right) \tag{5.56}$$

and hence,

$$k_\infty = \frac{\nu\Sigma_f}{\Sigma_a} \tag{5.57}$$

5.2.3 Weak absorption

In the absence of absorption it is known that the scattering distribution is simply the Maxwellian distribution given by

$$M_{Maxwell}(E) = E\ e^{-E/kT} \tag{5.58}$$

For the time being, consider a system which contains weak absorption where $\Sigma_a \ll 1$. Recall the flux from Eqn.(5.51),

$$\widetilde{\phi}(\epsilon) = \frac{1}{\xi k_\infty \Sigma_{fr}}\cdot\left(\frac{1}{\epsilon_0^2\ e^{-\epsilon_0}K_0'}\right)\epsilon\ e^{-\epsilon}K\left(\frac{\Sigma_a}{\xi\Sigma_{fr}},2,\epsilon\right), \quad k_\infty = \frac{\nu\Sigma_f}{\Sigma_a} \tag{5.59}$$

The exact derivative of $K(a,b,z)$ is given by

$$K'(a,b,z) = \frac{a}{b}K(a+1,b+1,z) \tag{5.60}$$

therefore, for $\Sigma_a \ll 1$ we can approximate,

$$K_0'(\frac{\Sigma_a}{\xi\Sigma_{fr}},2,\epsilon_0) \approx \frac{\frac{\xi\Sigma_{fr}}{\Sigma_a}}{2}K(1,3,\epsilon_0) \tag{5.61}$$

Substituting this expression into Eqn.(5.59) gives

$$\widetilde{\phi}(\epsilon) = \left(\frac{2}{\nu\Sigma_f}\right)\left(\frac{e^{\epsilon_0}}{\epsilon_0^2K(1,3,\epsilon_0)}\right)\left(\epsilon\ e^{-\epsilon}\right)K\left(\frac{\Sigma_a}{\xi\Sigma_{fr}},2,\epsilon\right) \tag{5.62}$$

Since, $\Sigma_a \ll 1$ the second Kummer term will go to one. Now take the first Kummer function as $\epsilon_0 \gg 1$ to give

$$\widetilde{\phi}(\epsilon) = \left(\frac{2}{\nu\Sigma_f}\right)\left[\frac{e^{\epsilon_0}}{\epsilon_0^2\left(\frac{\Gamma(3)}{\Gamma(1)}e^{\epsilon_0}\epsilon_0^{-2}\right)}\right]\epsilon\ e^{-\epsilon} \tag{5.63}$$

$$\widetilde{\phi}(\epsilon) = \left(\frac{1}{\nu\Sigma_f}\right)\epsilon\ e^{-\epsilon} \tag{5.64}$$

which is in fact the Maxwellian distribution.

5.2.4 Neutron slowing down

Now consider energies which are in the epithermal region and only elastic scattering. It is well known that the flux in this region behaves like $1/E$. In order to show the same result, recall Eqn.(5.51),

$$\widetilde{\phi}(\epsilon) = \frac{1}{\xi k_\infty \Sigma_{fr}} \cdot \left(\frac{1}{\epsilon_0^2\ e^{-\epsilon_0}K_0'}\right)\epsilon\ e^{-\epsilon}K\left(\frac{\Sigma_a}{\xi\Sigma_{fr}}, 2, \epsilon\right) \tag{5.65}$$

the case where $z \to \infty$ allows for a simplified expression of the Kummer equation given by Ref.[41],

$$K(a,b,z) = \frac{\Gamma(b)}{\Gamma(a)}e^z\ z^{a-b} \tag{5.66}$$

$$K'(a,b,z) = \frac{\Gamma(b)}{\Gamma(a)}e^z\ z^{a-b}\left[1 + (a-b)\,z^{-1}\right] \tag{5.67}$$

Using the above approximation, k_∞, in the condition where $\epsilon_0 >> 1$, is given by

$$k_\infty = \frac{\nu\Sigma_f}{\Sigma_a}\left(\frac{1}{1 + \frac{\frac{\Sigma_a}{\xi\Sigma_{fr}} - 2}{\epsilon_0}}\right) \tag{5.68}$$

therefore, in the epithermal region where $\epsilon >> 1$ Eqn.(5.68) becomes

$$\widetilde{\phi}(\epsilon) = \left(\frac{\Sigma_a}{\xi\Sigma_{fr}}\right)\left(\frac{1 + \frac{\frac{\Sigma_a}{\xi\Sigma_{fr}} - 2}{\epsilon_0}}{\nu\Sigma_f}\right)\left(\frac{e^{\epsilon_0}\left(\epsilon\ e^{-\epsilon}\right)\left(\frac{\Gamma(2)}{\Gamma(\frac{\Sigma_a}{\xi\Sigma_{fr}})}e^{\epsilon}\ \epsilon^{\frac{\Sigma_a}{\xi\Sigma_{fr}}-2}\right)}{\epsilon_0^2\left[\frac{\Gamma(2)}{\Gamma(\frac{\Sigma_a}{\xi\Sigma_{fr}})}e^{\epsilon_0}\ \epsilon_0^{\frac{\Sigma_a}{\xi\Sigma_{fr}}-2}\right]\left[1 + \frac{\frac{\Sigma_a}{\xi\Sigma_{fr}} - 2}{\epsilon_0}\right]}\right) \tag{5.69}$$

After canceling terms, the flux results in the expected slowing down distribution

$$\widetilde{\phi}(\epsilon) = \left(\frac{1}{k_\infty \xi \Sigma_{fr}}\right)\left(\frac{\epsilon}{\epsilon_0}\right)^{\frac{\Sigma_a}{\xi\Sigma_{fr}}}\left(\frac{1}{\epsilon}\right) \tag{5.70}$$

5.2.5 Infinite Medium Calculation Compared with MCNP

In order to use the continuous-energy physics in MCNP6 to simulate this analytic benchmark, it was necessary to create special continuous cross-section files (ACE files). A utility program written in *perl, simple_ace.pl*, was created to construct ACE files with either constant or piecewise-linear values of the energy grid, ν, Σ_f, Σ_c, and Σ_{fr}. Either P_0 or P_1 elastic scattering distributions are provided, with no inelastic scattering. An arbitrary delta-function source energy, problem temperature, and target mass number (A) are included. With the special ACE file data, MCNP6 will use continuous-energy collision physics, including free-gas scattering. Different ACE data files were created for different target nucleus masses. The specific infinite medium material property values used in generating numerical results are given in Table 5.1.

Parameter	Value	Parameter	Value
A	1, 2, 12, 27, 56, 238	ν	2
E_0	10 eV	Σ_f	0.01 cm^{-1}
T	294K	Σ_c	0.01 cm^{-1}
		Σ_{fr}	0.5 cm^{-1}

Table 5.1: Material properties for infinite medium free-gas scattering benchmark.

To compare the spectra obtained using the free-gas kernel in MCNP6 and the exact solution for the heavy gas model, both sets of results are normalized by the area

under the respective distribution, and the results are plotted in terms of lethargy. As the target size increases there is an increase in statistical noise in the MCNP6 results at the low-energy end of the spectrum due to small numbers of particles scattering to low energies. Since the maximum energy lost in a single collision is given by αE_{in} where $\alpha = [(A-1)/(A+1)]^2$, it is expected that larger targets would require more particle samples in order to reach energies below E_0. This noise is caused by the small energy transfers with large targets requiring a significant number of collisions for particles to slowdown; an increase of particle samples in the MCNP6 simulation will reduce the noise.

Comparisons of the MCNP and heavy gas spectra as a function of mass ratio are shown in Figure 5.2. It is observed that the heavy gas model becomes increasingly more accurate with increasing mass ratio when compared against the exact spectrum from MCNP6, with the spectra appearing very similar even for mass ratios as small as $A = 2$. Figure 5.3 shows the relative error between the heavy gas model and MCNP6 when the target size is increased from hydrogen to carbon. The heavy gas model is accurate to within %5.0 for carbon and the error reduces further with increasing mass ratio.

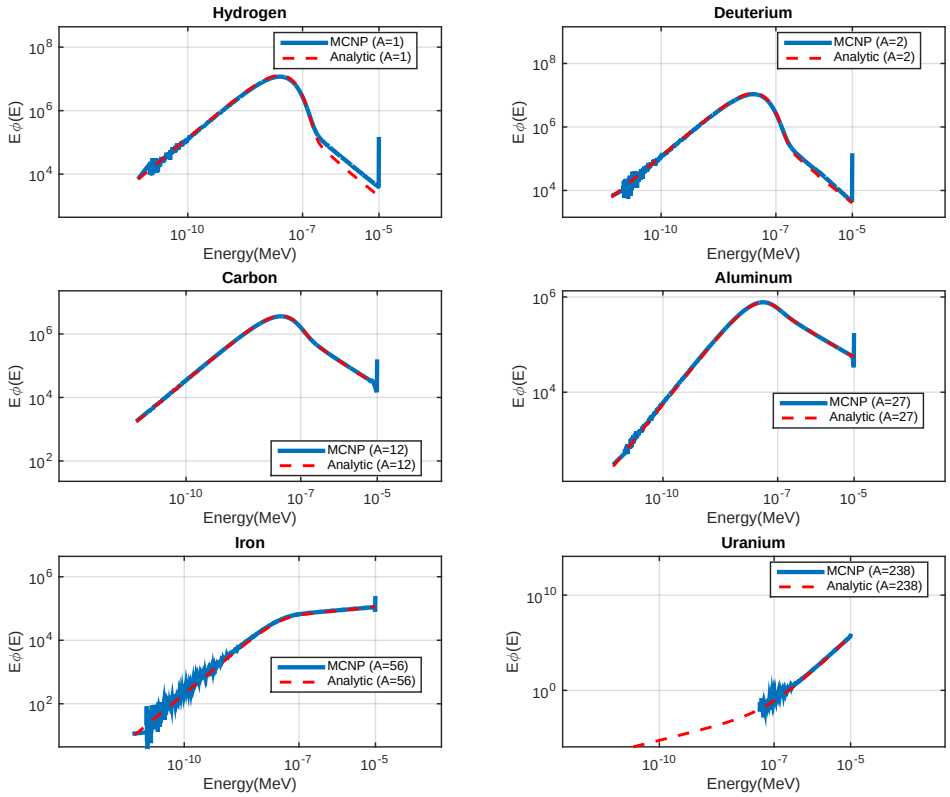

Figure 5.2: Flux comparison for infinite medium case.

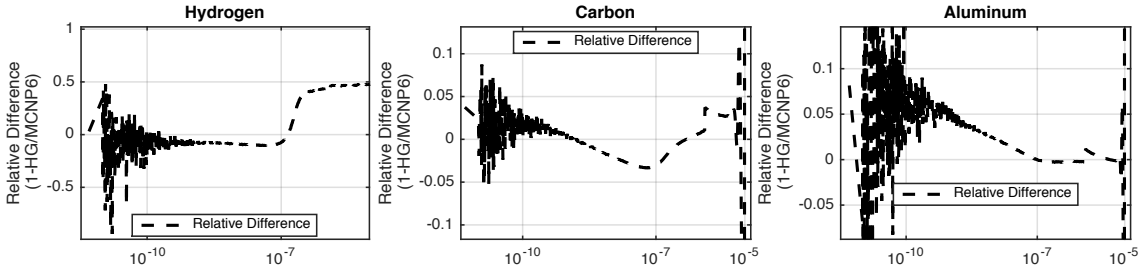

Figure 5.3: Relative difference between the heavy gas model and MCNP6 increasing target size.

5.3 Piecewise Constant Heavy Gas Model

Previous work has showed the viability of using the heavy gas model in order to produce an analytic representation of the energy flux profile within an infinite medium whose absorption cross section is energy independent. Expanding on this work, energy dependent piecewise constant absorption cross sections will be included resulting in a piecewise constant evaluation of the heavy gas model. The energy space will be discretized to separate regions in which material properties are held constant within it's respective region allowing for an analytic solution as previously shown using confluent hypergeometric functions of the first and second kind. In order to connect each region, continuity conditions must be derived connecting each region providing a continuous flux distribution.

5.3.1 Derivation

The following conventions will be used in discritizing the energy space. Energy bounds are defined with a subscript of $i \pm \frac{1}{2}$, while energy bin centers are defined with integers i. If we define the absorption cross section $\Sigma_a(E)$ with the following

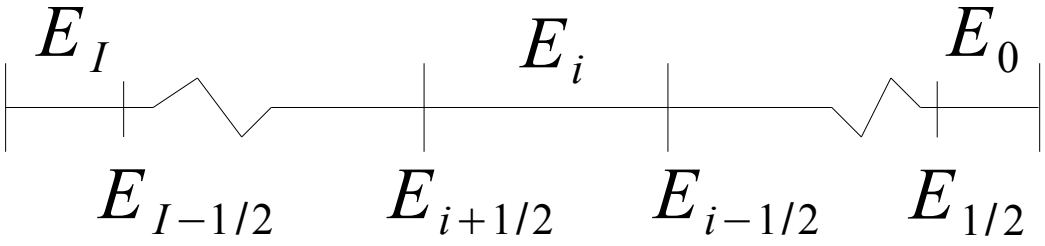

Figure 5.4: Energy discritization figure

basis function $B_i(E)$,

$$\Sigma_a(E) = \sum_{i=1}^{I} \Sigma_{a_i} B_i(E), \quad \text{where} \quad B_i(E) = \begin{cases} 1, & E \,\epsilon\, \left[E_{i+\frac{1}{2}}, E_{i-\frac{1}{2}}\right) \\ 0, & \text{otherwise} \end{cases} \tag{5.71}$$

then our flux must also be defined as

$$\phi(E) = \sum_{i=1}^{I} \phi_i B_i(E), \quad \text{where} \quad B_i(E) = \begin{cases} 1, & E \,\epsilon\, \left[E_{i+\frac{1}{2}}, E_{i-\frac{1}{2}}\right) \\ 0, & \text{otherwise} \end{cases} \tag{5.72}$$

The neutrons produced from fission are normalized to unity

$$\nu\Sigma_f \int_0^{E_0} \phi(E)\mathrm{d}E = \nu\Sigma_f \sum_{i=o}^{I} \int_{E_{i+\frac{1}{2}}}^{E_{i-\frac{1}{2}}} \phi_i(E) B_i(E)\mathrm{d}E = 1 \tag{5.73}$$

and the heavy gas equation within some energy bin $[E_{i+\frac{1}{2}}, E_{i-\frac{1}{2}})$ becomes

$$E\frac{\mathrm{d}\phi_i^2(E)}{\mathrm{d}E^2} + E\frac{\mathrm{d}\phi_i(E)}{\mathrm{d}E} + \left[1 - \frac{\Sigma_{a_i}}{\xi\Sigma_{fr}}\right]\phi_i(E) + \frac{\delta(E-E_0)}{k\xi\Sigma_{fr}} = 0, \quad E_{i+\frac{1}{2}} \leq E < E_{i-\frac{1}{2}} \tag{5.74}$$

Equation 5.74 has already been shown to have a general solution in terms of Kummer functions of the first and second kind.

In order to connect each region, continuity conditions must be derived. Consider some energy bound at $E_{i-\frac{1}{2}}$ in which the flux is given on either side of this bound by ϕ_i on the left and ϕ_{i-1} on the right and integrate over that bound symmetrically a small differential distance of 2δ (see Figure 5.5). Begin by integrating the heavy gas equation over the 2δ energy space.

$$\int_{E_{i-\frac{1}{2}}-\delta}^{E_{i-\frac{1}{2}}+\delta} \mathrm{d}E \; E\frac{\mathrm{d}\phi^2(E)}{\mathrm{d}E^2} + E\frac{\mathrm{d}\phi(E)}{\mathrm{d}E} + \left[1 - \frac{\Sigma_a(E)}{\xi\Sigma_{fr}}\right]\phi(E) = 0 \tag{5.75}$$

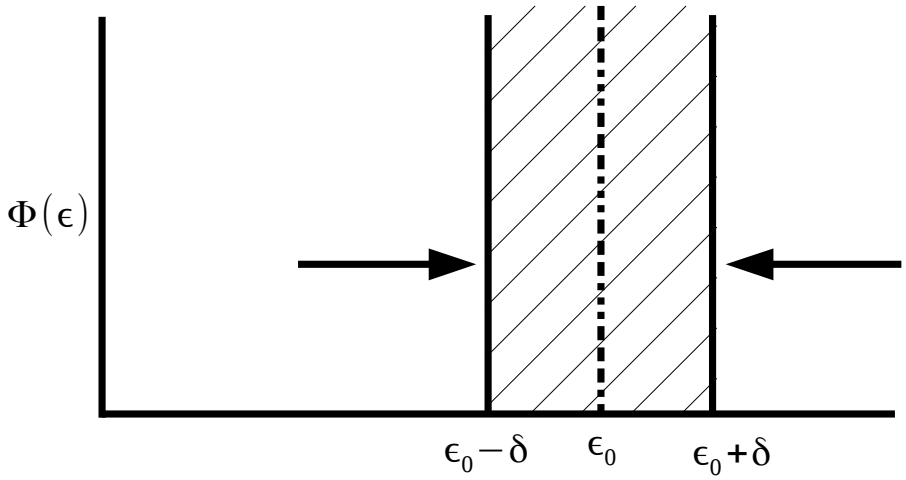

Figure 5.5: Diagram of integration of a small differential space symmetrically around an energy interface.

Integration by parts of the first two terms yields

$$\int_{E_{i-\frac{1}{2}}-\delta}^{E_{i-\frac{1}{2}}+\delta} \mathrm{d}E\ E\frac{\mathrm{d}\phi^2(E)}{\mathrm{d}E^2} = \left(E_{i-\frac{1}{2}+\delta}\right)\left.\frac{\mathrm{d}\phi}{\mathrm{d}E}\right|_{E_{i-\frac{1}{2}+\delta}} - \left(E_{i-\frac{1}{2}-\delta}\right)\left.\frac{\mathrm{d}\phi}{\mathrm{d}E}\right|_{E_{i-\frac{1}{2}-\delta}} - \left[\phi\left(E_{i-\frac{1}{2}+\delta}\right) - \phi\left(E_{i-\frac{1}{2}-\delta}\right)\right] \tag{5.76}$$

$$\int_{E_{i-\frac{1}{2}}-\delta}^{E_{i-\frac{1}{2}}+\delta} \mathrm{d}E\ E\frac{\mathrm{d}\phi(E)}{\mathrm{d}E} = \left(E_{i-\frac{1}{2}+\delta}\right)\phi\left(E_{i-\frac{1}{2}+\delta}\right) - \left(E_{i-\frac{1}{2}-\delta}\right)\phi\left(E_{i-\frac{1}{2}-\delta}\right) - \int_{E_{i-\frac{1}{2}}-\delta}^{E_{i-\frac{1}{2}}+\delta} \mathrm{d}E\ \phi(E) \tag{5.77}$$

Recall the basis function definition of the energy dependent absoprtion cross section is defined to be constant within a specific energy region. This reduces the third term

to following form

$$\int_{E_{i-\frac{1}{2}}-\delta}^{E_{i-\frac{1}{2}}+\delta} \mathrm{d}E \left[1 - \frac{\Sigma_a(E)}{\xi\Sigma_{fr}}\right] \phi(E) = \int_{E_{i-\frac{1}{2}}-\delta}^{E_{i-\frac{1}{2}}+\delta} \mathrm{d}E\ \phi(E) - \frac{\Sigma_{a_i}}{\xi\Sigma_{fr}} \int_{E_{i-\frac{1}{2}}-\delta}^{E_{i-\frac{1}{2}}} \mathrm{d}E\ \phi(E) - \frac{\Sigma_{a_{i+1}}}{\xi\Sigma_{fr}} \int_{E_{i-\frac{1}{2}}}^{E_{i-\frac{1}{2}}+\delta} \mathrm{d}E\ \phi(E) \tag{5.78}$$

Combining Eqns.[5.76-5.78] and recalling the basis function definition for the flux in Eqn.5.72, results in the following expression

$$\begin{aligned}
&(E_{i-\frac{1}{2}+\delta}) \frac{\mathrm{d}\phi_{i+1}}{\mathrm{d}E}\bigg|_{E_{i-\frac{1}{2}+\delta}} - (E_{i-\frac{1}{2}-\delta}) \frac{\mathrm{d}\phi_i}{\mathrm{d}E}\bigg|_{E_{i-\frac{1}{2}-\delta}} \\
&\quad - \left[\phi_{i-1}(E_{i+\frac{1}{2}+\delta}) - \phi_i(E_{i-\frac{1}{2}-\delta})\right] \\
&\quad + \left(E_{i-\frac{1}{2}+\delta}\right) \phi_{i-1}\left(E_{i-\frac{1}{2}+\delta}\right) - \left(E_{i-\frac{1}{2}-\delta}\right) \phi_i\left(E_{i-\frac{1}{2}-\delta}\right) \\
&\quad - \frac{\Sigma_{a_i}}{\xi\Sigma_{fr}} \int_{E_{i-\frac{1}{2}-\delta}}^{E_{i-\frac{1}{2}}} \mathrm{d}E\ \phi_i(E) - \frac{\Sigma_{a_{i-1}}}{\xi\Sigma_{fr}} \int_{E_{i-\frac{1}{2}}}^{E_{i-\frac{1}{2}}+\delta} \mathrm{d}E\ \phi_{i-1}(E) = 0
\end{aligned}$$

Taking the limit $\delta \to 0$ removes the integral terms and reduces the equation to

$$(E_{i-\frac{1}{2}}) \left[\frac{\mathrm{d}\phi_{i-1}(E_{i-\frac{1}{2}})}{\mathrm{d}E} - \frac{\mathrm{d}\phi_i(E_{i+\frac{1}{2}})}{\mathrm{d}E}\right] + (E_{i-\frac{1}{2}} - 1) \left[\phi_{i-1}(E_{i+\frac{1}{2}}) - \phi_i(E_{i-\frac{1}{2}})\right] = 0 \tag{5.79}$$

From the above equation, continuity of the flux and the gradient result in the following boundary conditions at energy interfaces

$$\phi_i(E_{i-\frac{1}{2}}) = \phi_{i-1}(E_{i-\frac{1}{2}}) \tag{5.80}$$

$$\frac{\mathrm{d}\phi_i(E_{i+\frac{1}{2}})}{\mathrm{d}E} = \frac{\mathrm{d}\phi_{i-1}(E_{i-\frac{1}{2}})}{\mathrm{d}E} \tag{5.81}$$

It has already been shown that the constant absorption cross section heavy gas equation results in the definition of the flux as a sum of two linearly independent Kummer functions. The form of this solution is in terms of a unitless parameter ε which will be reintroduced. It is assumed variables have been mapped to the

respective unitless parameter ε. The general solution of the heavy gas equation is given in the following form:

$$\phi(\varepsilon)\ \mathrm{d}\varepsilon = \phi(E)\ \mathrm{d}E, \quad \text{where, } \varepsilon = \frac{E}{kT} \tag{5.82}$$

$$\phi_i\left(\varepsilon\right) = \varepsilon \exp\left(-\varepsilon\right)\left[C_{1_i}\ K\left(\frac{\Sigma_{a_i}}{\xi\Sigma_{fr}}, 2, \varepsilon\right) + C_{2_i}\ U\left(\frac{\Sigma_{a_i}}{\xi\Sigma_{fr}}, 2, \varepsilon\right)\right] \quad \varepsilon_{i-\frac{1}{2}} \leq \varepsilon < \varepsilon_{i+\frac{1}{2}} \tag{5.83}$$

Using this general form of the constant cross section heavy gas equation will require an evaluation of boundary conditions at each energy interface of the discritized energy space given by Eqns.[5.80,5.81]. In previous work where all cross sections were constant throughout all energy space, C_2 had to be zero since Kummer's U function does not approach zero from the right for the boundary condition $\phi(0) = 0$. This condition still holds but only for the case when $i = 1$. The derivation of the upper energy boundary where integration over the upper energy bound ε_0 is taken over a small differential energy space 2δ and the flux is considered zero approaching from the right and finite approaching from the left, showed the following relationship between the flux at ε_0 and the source term

$$-\varepsilon\phi'\left(\varepsilon\right) + \left(1-\varepsilon\right)\phi\left(\varepsilon\right) = \frac{-1}{\xi\Sigma_{fr}k_\infty} \tag{5.84}$$

Taking the derivative of Eqn.5.83 yields the following:

$$\begin{aligned}\phi'(\varepsilon) = \exp(-\varepsilon)\left(1-\varepsilon\right)&\left[C_{1_i}\ K\left(\frac{\Sigma_{a_i}}{\xi\Sigma_{fr}}, 2, \varepsilon\right) + C_{2_i}\ U\left(\frac{\Sigma_{a_i}}{\xi\Sigma_{fr}}, 2, \varepsilon\right)\right] \\ &+ \varepsilon\exp(-\varepsilon)\left[C_{1_i}\ K'\left(\frac{\Sigma_{a_i}}{\xi\Sigma_{fr}}, 2, \varepsilon\right) + C_{2_i}\ U'\left(\frac{\Sigma_{a_i}}{\xi\Sigma_{fr}}, 2, \varepsilon\right)\right]\end{aligned} \tag{5.85}$$

Now reintroducing Eqn.5.83 and Eqn.5.85 for $\varepsilon = \varepsilon_0$ results in a solution in terms of

the linearly independent convergent series M' and U'.

$$\begin{aligned}
&\phi(\varepsilon_0) - \varepsilon_0\phi(\varepsilon_0) \\
&+ \varepsilon_0^2 \exp(-\varepsilon_0)\left[C_{1_I}\ K'\left(\frac{\Sigma_{a_i}}{\xi\Sigma_{fr}}, 2, \varepsilon_0\right) + C_{2_I}\ U'\left(\frac{\Sigma_{a_i}}{\xi\Sigma_{fr}}, 2, \varepsilon_0\right)\right] \\
&- \phi(\varepsilon_0) + \varepsilon_0\phi(\varepsilon_0) \qquad\qquad = \frac{-1}{\xi\Sigma_{fr}k_\infty} \\
&C_{1_I}\ K'\left(\frac{\Sigma_{a_i}}{\xi\Sigma_{fr}}, 2, \varepsilon_0\right) + C_{2_I}\ U'\left(\frac{\Sigma_{a_i}}{\xi\Sigma_{fr}}, 2, \varepsilon_0\right) = \frac{\exp(\varepsilon_0)}{\varepsilon_0^2\xi\Sigma_{fr}k_\infty}
\end{aligned} \tag{5.86}$$

This upper-energy boundary condition provides closure to a system of equations which may be obtained through standard linear algebra inversion in which the coefficients $C_{1_i},\ C_{2_i}$ are obtained for each region. When this system of equations is placed in vector matrix form:

$$\mathcal{K}c = q \tag{5.87}$$

where $\mathcal{K}$ contain the differences between flux and flux derivative values within each region, c is the vector of coefficients and q is the respective source vector. The source vector q is simply a vector of zeros (since flux and flux derivatives in adjoining cells are equal) except for the source condition given by Eqn. 5.86.

$$q = \begin{pmatrix} 0 \\ \vdots \\ \vdots \\ \frac{\exp(\varepsilon_0)}{\varepsilon_0^2\xi\Sigma_{fr}\mathbf{k}_\infty} \end{pmatrix} \tag{5.88}$$

Once the coefficients are found, the problem is easily solved in terms of the Kummer functions and interface conditions. Furthermore, the definition of the source and the source normalization which was forced to unity, produces the criticality condition

$$\int_0^{\epsilon_0} \nu\Sigma_f\phi(\varepsilon)d\varepsilon \implies k_\infty = \int_0^{\epsilon_0} \nu\Sigma_f\phi(\varepsilon)d\varepsilon \tag{5.89}$$

Mass Ratio = 27	Constant	Piecewise Constant
number of Regions	1	3
ε_0	20	20
ν	2	2, 2, 2
$\Sigma_{fr}(\varepsilon)$	.5	.5, .5, .5
$\Sigma_f(\varepsilon)$	.001	.001, .001, .001
$\Sigma_c(\varepsilon)$	.001	.001, .001, .001

Table 5.2: Table of parameters for simulation.

In order to show agreement with the constant case, a multiregion problem is compared to the original single region case using the same parameters in each region. Following this comparison, variation in the absorption cross section with respect to ε will be made. Each of these cases will also compare calculated criticality values $\mathtt{k}_\infty$.

5.3.2 Results

Reproducing Constant Model

It is important to show the multiregion case reproduces the constant cross section heavy gas model when all parameters are the same in each region. This will ensure the coding was done properly and is consistent with the derivation in the previous section. The first set of parameters is given in Tbl. 5.5 and results are shown in Fig. 5.6 As expected, the piecewise constant method reproduces the constant model when all parameters are the same in each region.

It is important to show the constant cross section case produces the correct $\mathtt{k}_\infty$. Table 5.3 shows three different values with respect to separate calculations. First, is

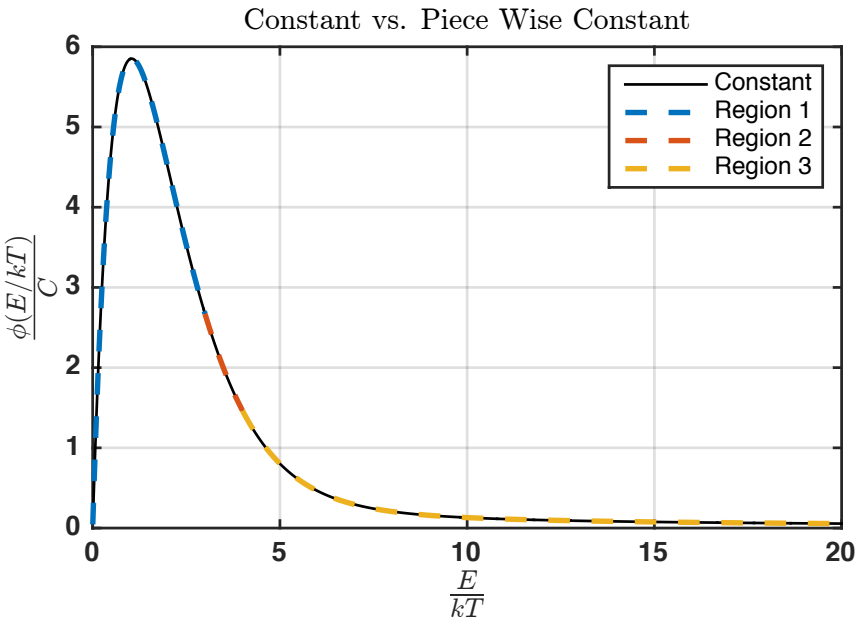

Figure 5.6: Constant heavy gas model compared to 3 region piecewise constant heavy gas model.

the expected infinite medium $\mathtt{k}_\infty$ given by diffusion theory. Second is the analytic evaluation of the constant cross section Kummer function model which has been previously shown and third is the numerical integration of the piecewise constant model using an adaptive quadrature. The use of an adaptive quadrature removes the numerical error as the tolerance for this calculation was set to machine precision.

Method	$\mathtt{k}_\infty$
Diffusion Theory $\left(\frac{\nu\Sigma_f}{\Sigma_a}\right)$	1.0000
Analytic Evaluation $\left(\int_0^{\epsilon_0} \nu\Sigma_f\phi(\varepsilon)d\varepsilon\right)$	1.0000
Numerical Evaluation (Gauss-Kronrod Adaptive)	0.9999

Table 5.3: Calculated values of infinite medium criticality for constant and piecewise constant models.

Constant Absorption With a Resonance

In order to build on the constant cross section model, a "resonance" is introduced to the capture cross section defined by a 10 region step-function and is shown in Fig. 5.7. This results in an absorption cross section which is energy dependent yet the fission cross section remains constant. By maintaining a constant fission cross section, evaluation of the criticality constant is straightforward. Specifically, while the fission cross section is energy independent, the fission cross section may be removed from the integral thus reducing the computational complexity of the eigenvalue $\mathtt{k}_\infty$. Figure 5.8 shows the total cross section in which specific features of the heavy gas model are pronounced. First, the exponential decrease in the total cross section from $\varepsilon \in (0, 2]$ is due to the scattering cross section which was shown to be nearly constant for $\varepsilon > 1$. The resonance in the absorption cross section due to the piecewise constant resonance in the capture cross section is reflected for $\varepsilon \in [2, 4]$, while the rest of the distribution remains constant as expected.

Simulations were conducted for mass ratios beginning with one on up to one thousand. Both the energy flux and criticality values are used to compare the piecewise constant model to MCNP6. Within in all energy flux profiles there are distinct features which produce the expected behavior for elastic scattering. There exists a thermal peak due to the Maxwellian distribution of the thermal neutrons in the

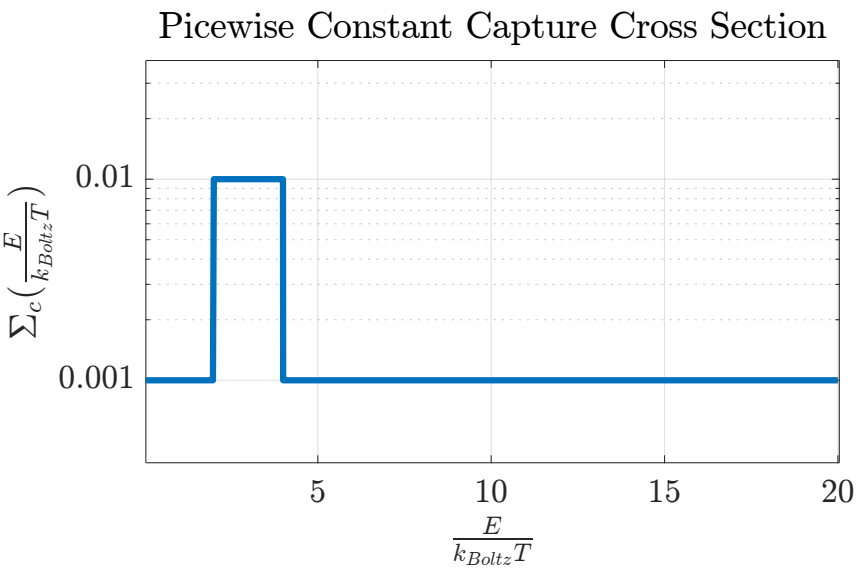

Figure 5.7: Capture cross section with resonance in the second energy bin.

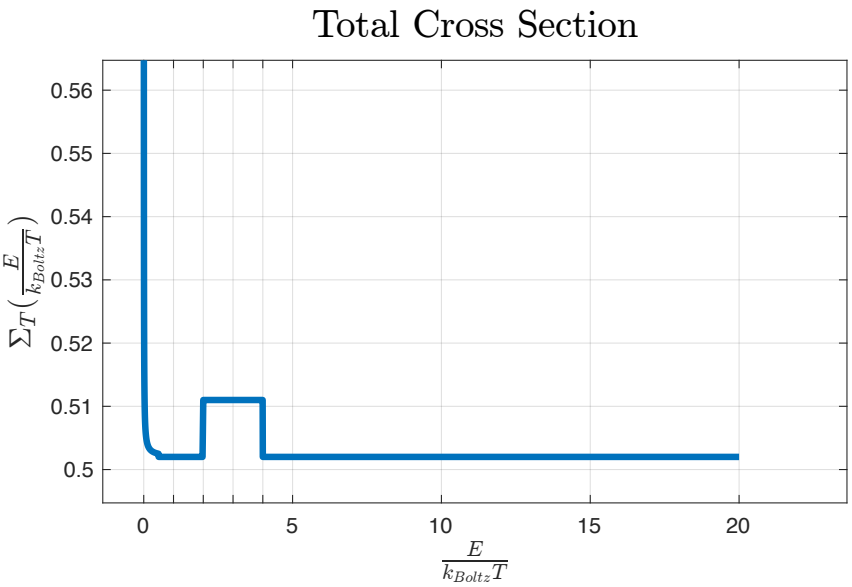

Figure 5.8: Total cross section for piecewise constant absorption.

system. Further, this peak is dependent on the target material and shifts to a higher energy with increasing mass ratio. For large mass ratios ($A > 56$), there exists a dip in the energy flux profile which is a result of the resonance in the absorption cross

section. For small mass ratios ($A < 56$) this feature does not appear within the flux since the thermal peak overlaps the area in which the resonance resides.

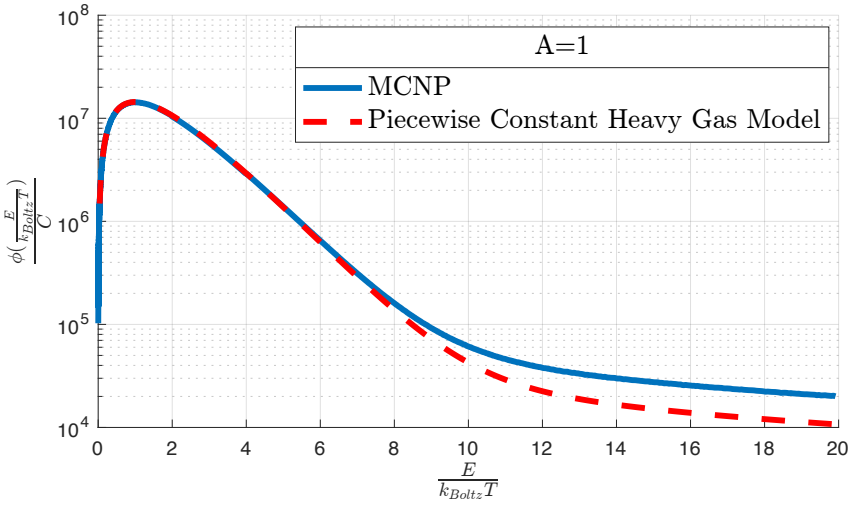

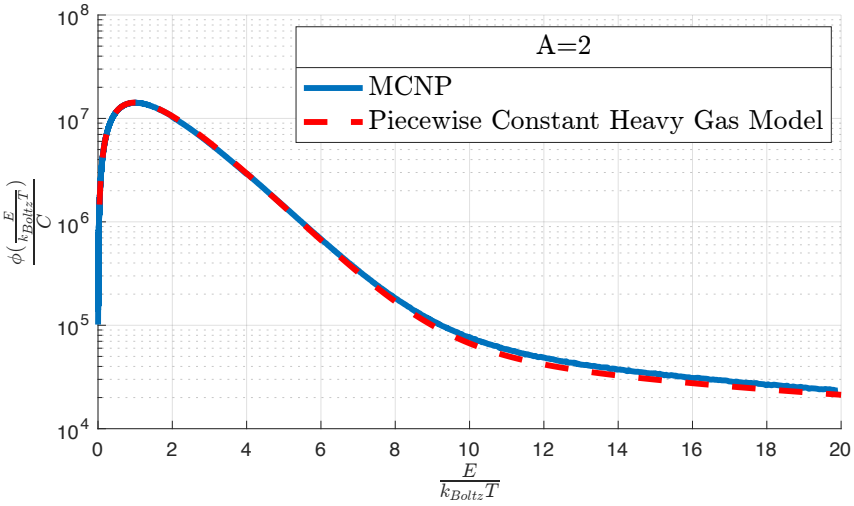

Table 5.4 shows the difference between calculated eigenvalues from MCNP6 and the heavy gas model. Values inside the parentheses for MCNP6 results are within statistical noise. The trapezoidal rule is used to calculate the heavy gas model criticality value. Both the MCNP6 and heavy gas model show eigenvalues tending

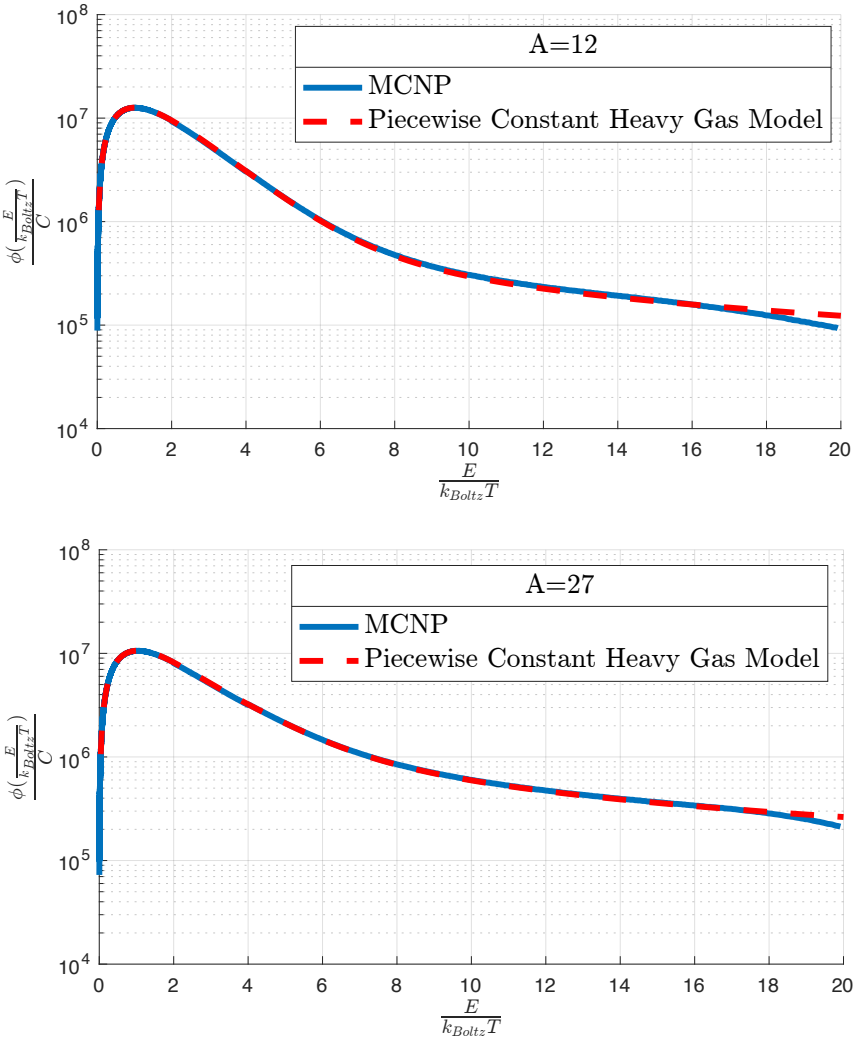

toward unity as the mass ratio increases. The tendency towards unity is caused by increasing target size since it is less likely neutrons will scatter low enough in energy to see the resonance within the absorption cross section and therefore for larger targets it is as if the absorption cross section is constant. The relative error between the two models shows with increasing target size, the heavy gas model approaches the MCNP6 value. This behavior is consistent with the heavy gas model which states the error is proportional to $\mathcal{O}\left(A^{-1}\right)$.

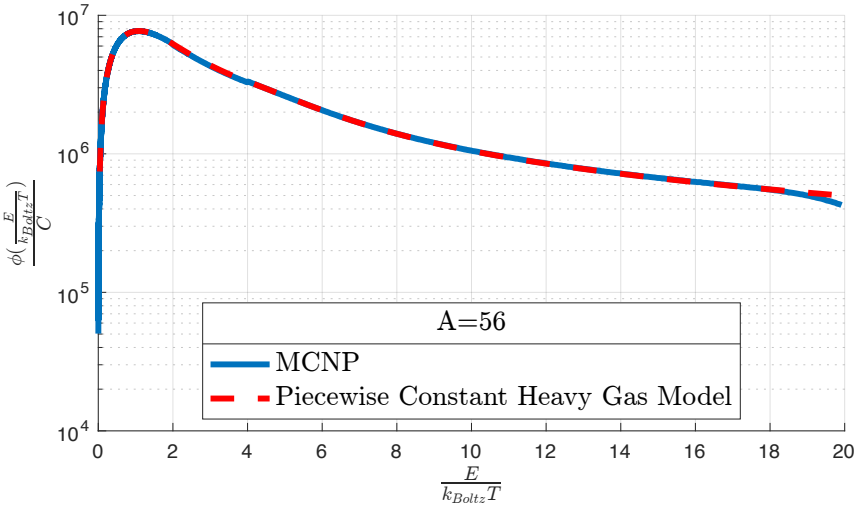
A=56
MCNP
Piecewise Constant Heavy Gas Model
$\frac{\phi(\frac{E}{k_{Boltz}T})}{C}$
$\frac{E}{k_{Boltz}T}$

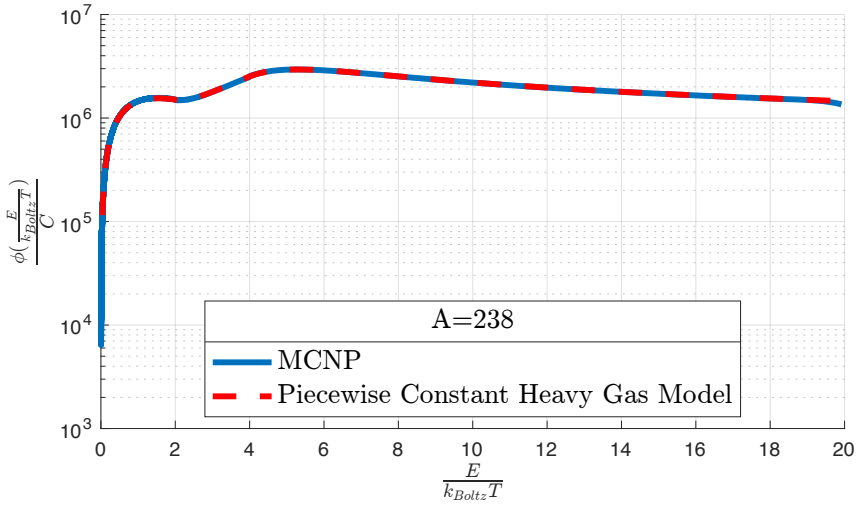
A=238
MCNP
Piecewise Constant Heavy Gas Model
$\frac{\phi(\frac{E}{k_{Boltz}T})}{C}$
$\frac{E}{k_{Boltz}T}$

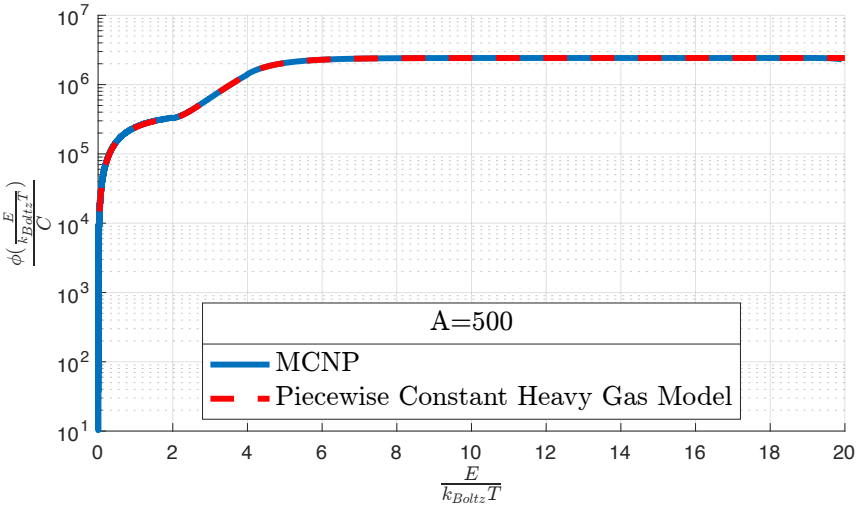
A=500
MCNP
Piecewise Constant Heavy Gas Model
$\frac{\phi(\frac{E}{k_{Boltz}T})}{C}$
$\frac{E}{k_{Boltz}T}$

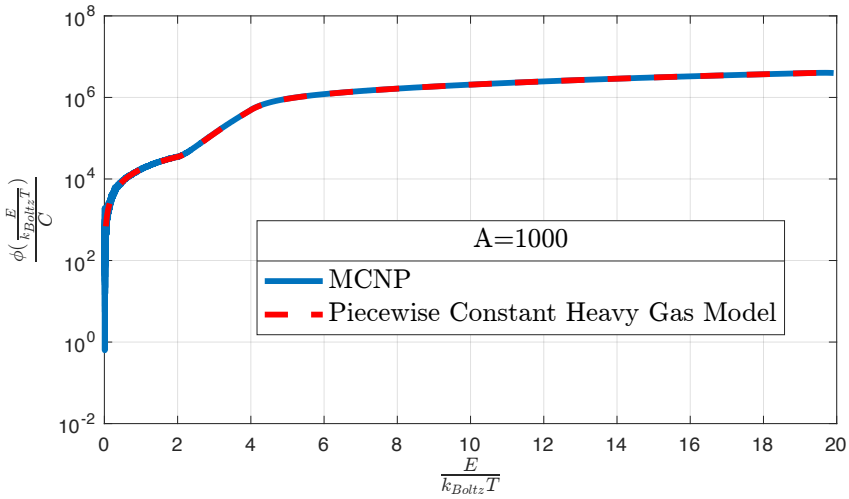

Mass Ratio	k_∞(MCNP6)	k_∞ (HG Model)	Rel. Error(%)
1	0.4194(9)	0.415	1.02
2	0.4202(9)	0.417	0.87
12	0.4349(4)	0.432	0.85
27	0.4574(9)	0.453	-0.96
56	0.5002(3)	0.495	-1.13
238	0.7114(9)	0.703	-1.26
500	0.8674(9)	0.860	0.83
1000	0.9655(3)	0.962	0.34

Table 5.4: Calculated values of infinite medium criticality for MCNP6 and heavy gas models.

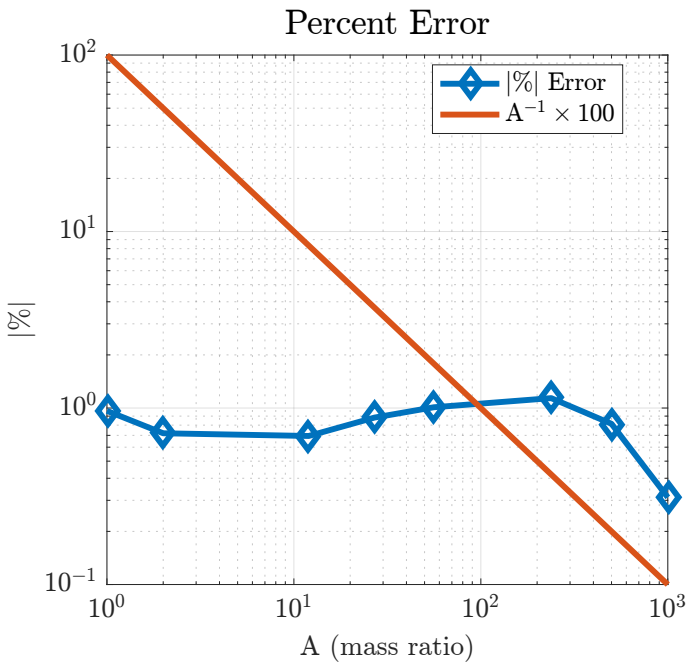

Figure 5.9: Absolute error of computed criticality values for MCNP6 and heavy gas model.

Combination of "$\frac{1}{E}$" and Resonance

In order to add further complexity to the absorption cross section, as well as to move closer to a more realistic cross section, both a "$\frac{1}{E}$" distribution and a resonance are used within the capture cross section. Again, Fig. 5.11 shows the variation in the absorption cross section as well as the contribution from scattering at energies E $\ll \frac{E}{kT}$. As expected the relative differences show with increasing target size, the flux distributions and the criticality values converge to the MCNP6 result.

Figures 5.10 & 5.11 shows the capture cross section containing a $\frac{1}{E}$ distribution from $\varepsilon \in (0, 4]$ and a resonance for $\varepsilon \in [10.12]$, while the remainder of the cross section distribution is constant.

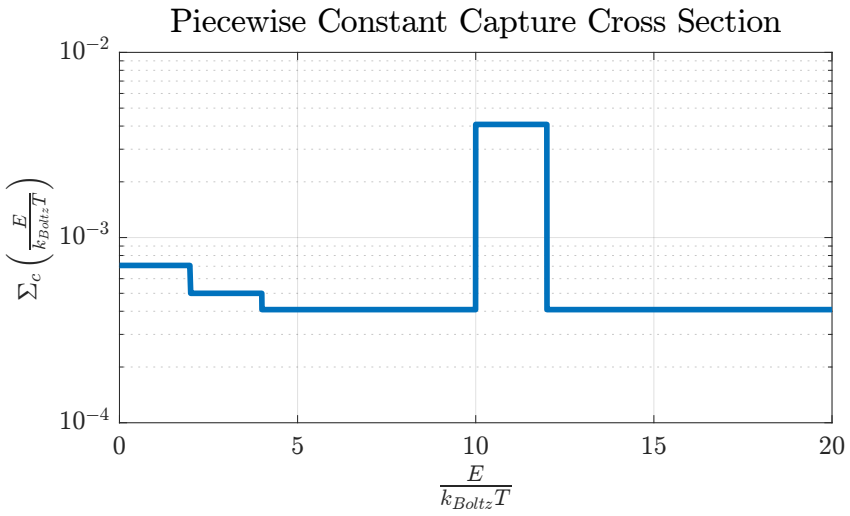

Figure 5.10: Capture cross section with $\frac{1}{E}$ and resonance.

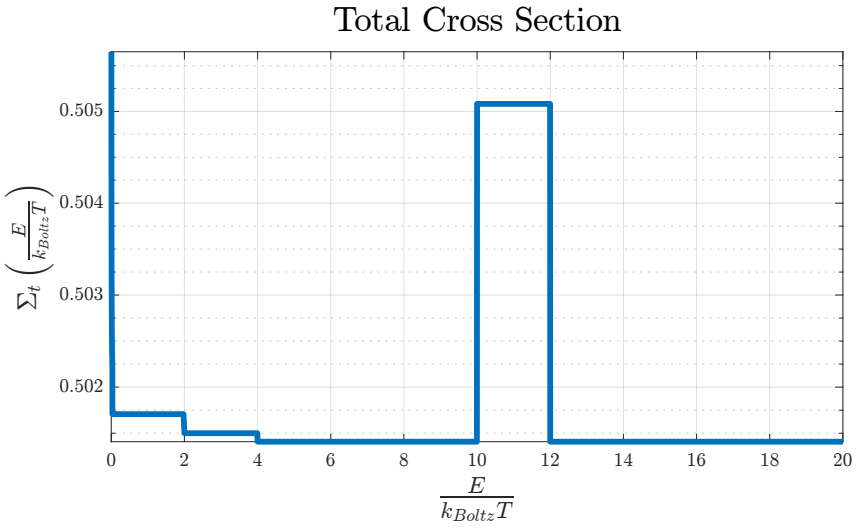

Figure 5.11: Total cross section for piecewise constant absorption.

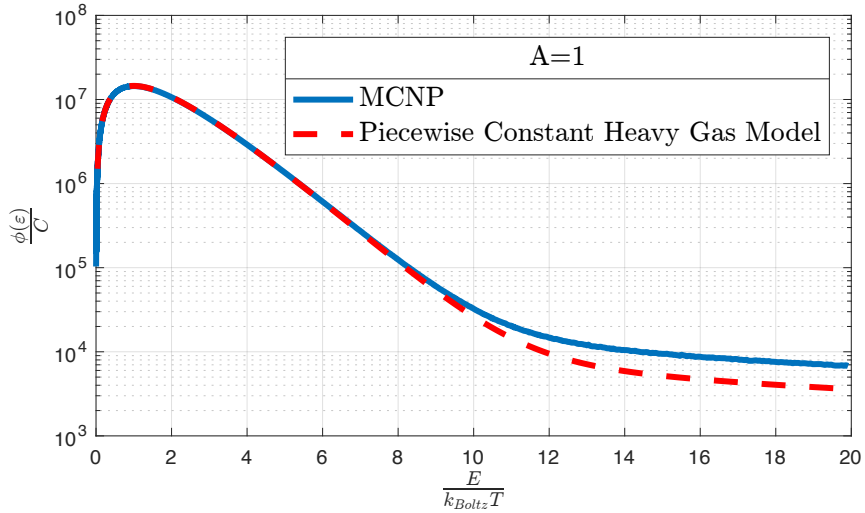

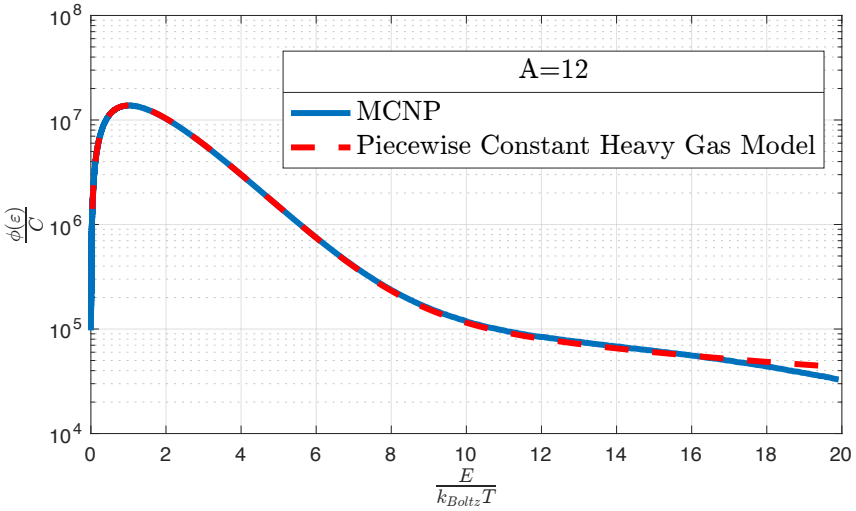
A=12
MCNP
Piecewise Constant Heavy Gas Model
$\frac{\phi(\varepsilon)}{C}$
$\frac{E}{k_{Boltz}T}$

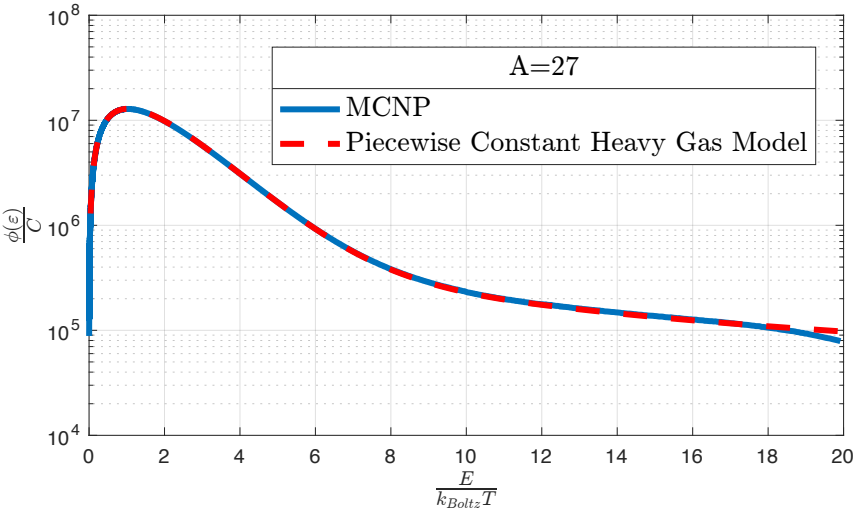
A=27
MCNP
Piecewise Constant Heavy Gas Model
$\frac{\phi(\varepsilon)}{C}$
$\frac{E}{k_{Boltz}T}$

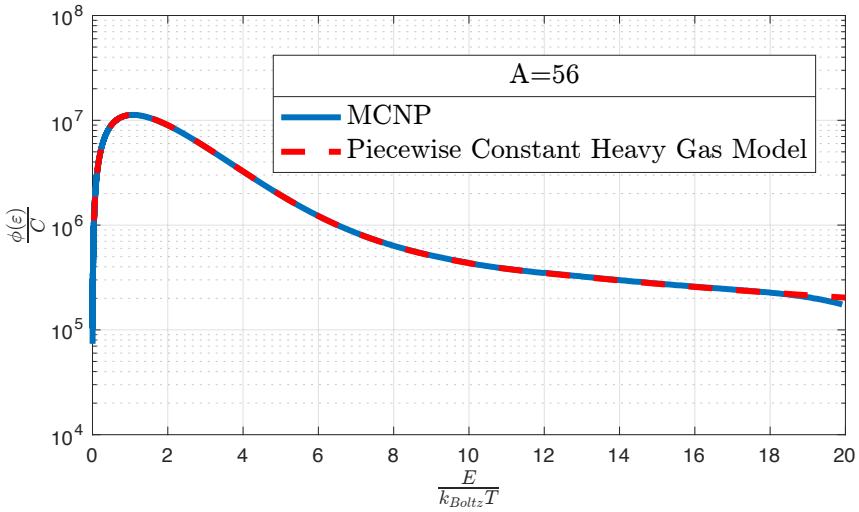
A=56
MCNP
Piecewise Constant Heavy Gas Model
$\frac{\phi(\varepsilon)}{C}$
$\frac{E}{k_{Boltz}T}$
10^8
10^7
10^6
10^5
10^4
0
2
4
6
8
10
12
14
16
18
20

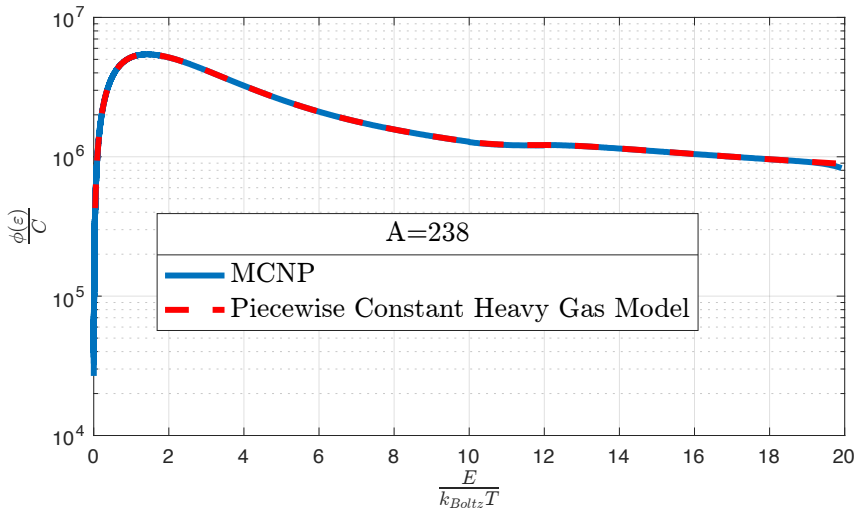
A=238
MCNP
Piecewise Constant Heavy Gas Model
$\frac{\phi(\varepsilon)}{C}$
$\frac{E}{k_{Boltz}T}$
10^7
10^6
10^5
10^4
0
2
4
6
8
10
12
14
16
18
20

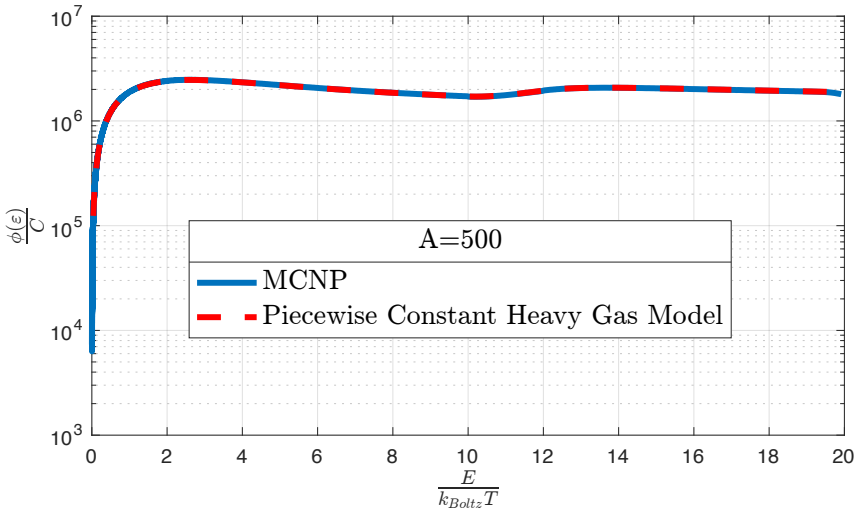
A=500
MCNP
Piecewise Constant Heavy Gas Model
$\frac{\phi(\varepsilon)}{C}$
$\frac{E}{k_{Boltz}T}$

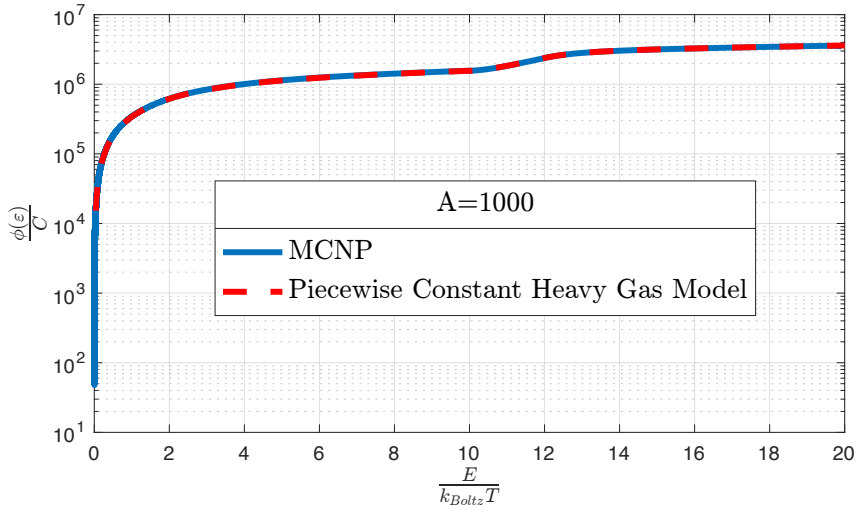
A=1000
MCNP
Piecewise Constant Heavy Gas Model
$\frac{\phi(\varepsilon)}{C}$
$\frac{E}{k_{Boltz}T}$

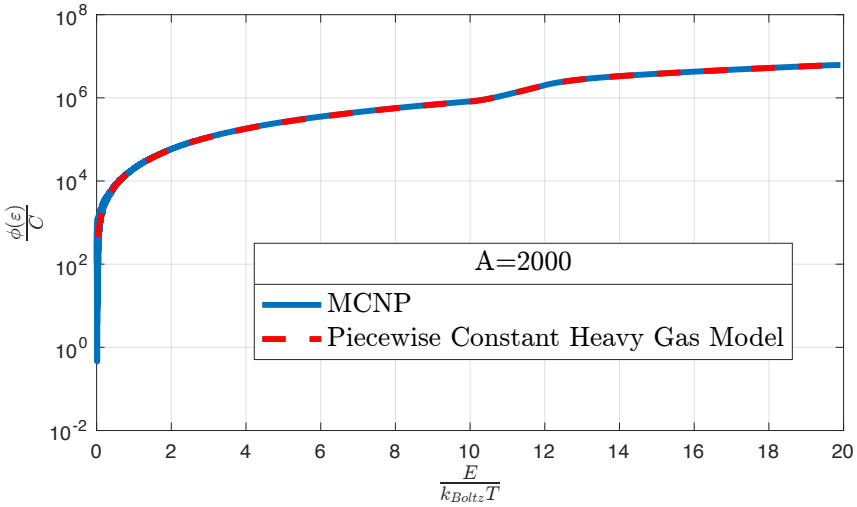
A=2000
MCNP
Piecewise Constant Heavy Gas Model
$\frac{\phi(\varepsilon)}{C}$
$\frac{E}{k_{Boltz}T}$

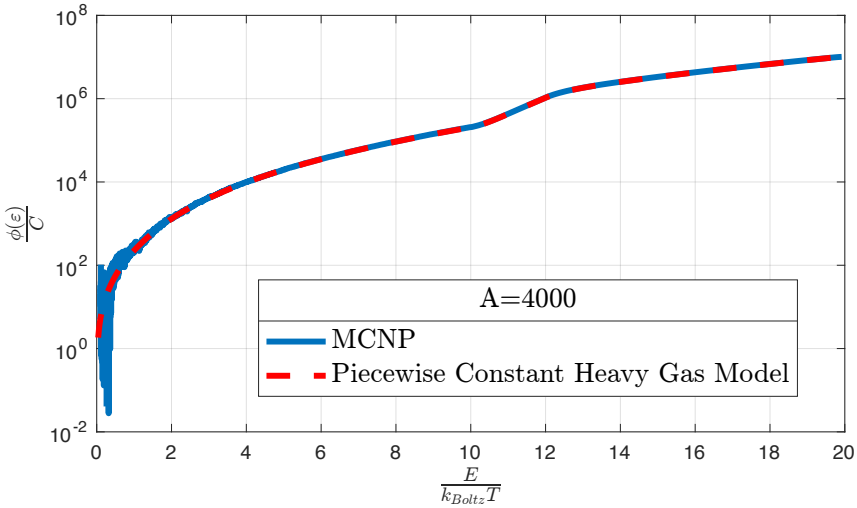
A=4000
MCNP
Piecewise Constant Heavy Gas Model
$\frac{\phi(\varepsilon)}{C}$
$\frac{E}{k_{Boltz}T}$

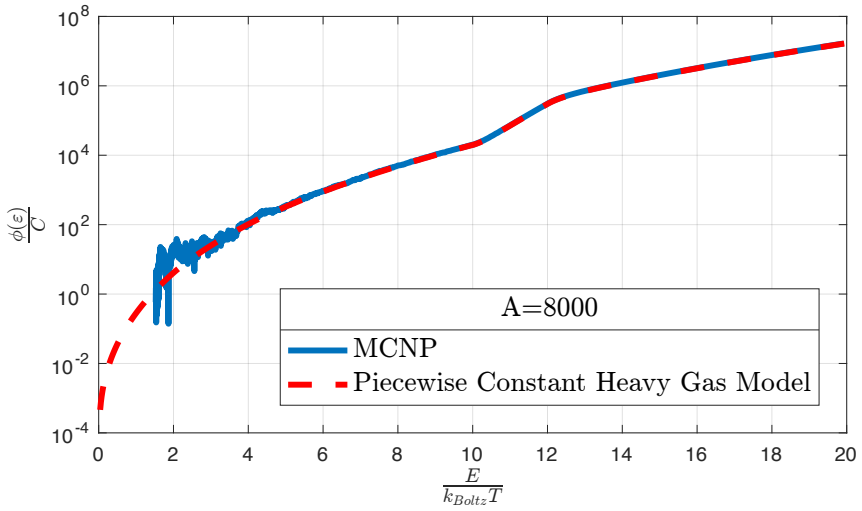

Mass Ratio	k_∞(MCNP6)	k_∞ (HG Model)	Rel. Error(%)
1	1.237(7)	1.24	-0.13
12	1.233(9)	1.23	-0.17
27	1.227(9)	1.23	-0.16
56	1.217(5)	1.22	-0.20
238	1.167(9)	1.16	-0.56
500	1.138(1)	1.13	-1.11
1000	1.152(7)	1.13	-1.79
2000	1.124(0)	1.22	-1.92
4000	1.348(3)	1.33	-1.12
8000	1.406(3)	1.40	-0.31
16000	1.419(2)	1.42	-0.03

Table 5.5: Table of parameters for simulation.

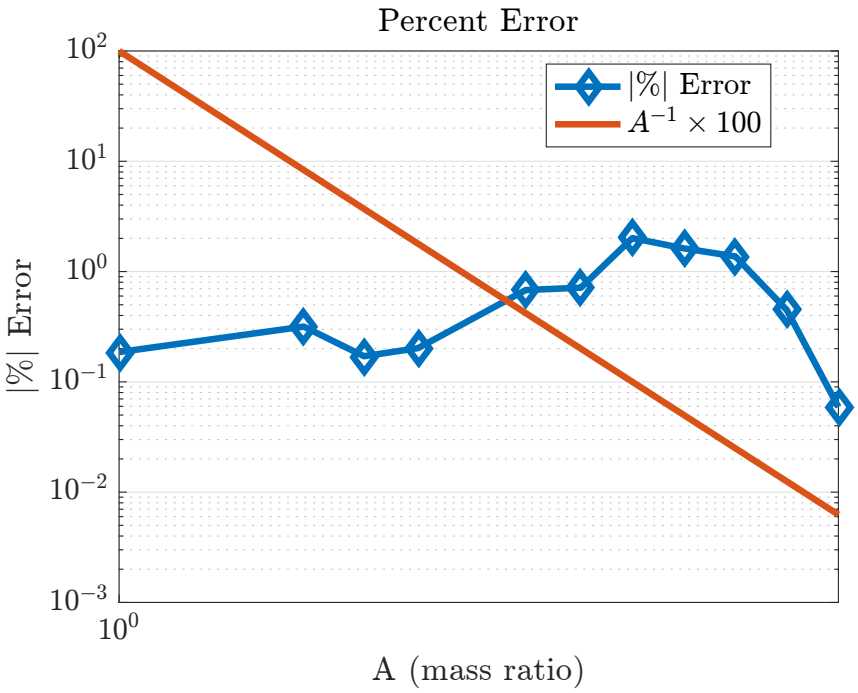

Figure 5.12: Absolute error of computed criticality values for MCNP6 and heavy gas model.

5.3.3 Conclusions

It was shown for $A \gg 1$, the energy spectrum obtained from MCNP using the free gas model agrees extremely well with the analytic solution for the heavy gas model. For small mass ratios, the spectra deviate at lower energies ($\frac{E}{k_{Boltz}T} < 1$), reflecting the inadequacy of the heavy gas model under these conditions. These results verify that the elastic scattering treatment in MCNP, including the free-gas scattering model at low energies, work correctly. This is the first demonstration of an analytic benchmark for elastic scattering inside a Monte Carlo code. Furthermore, the piecewise constant model shows the viability of the heavy gas model when dealing with energy dependent absorption cross sections. Piecewise constant distributions may be handled by the piecewise constant model within the realm of the heavy gas approximation. For this demonstration a resonance on the order of one magnitude was used, which maintained the validity of the model. For cross section distributions which begin to show extremely varying values in short energy widths, the approximation breaks down and the model is no longer valid.

5.4 Doppler Temperature Coefficient Benchmark

The previous section showed the viability of using the heavy gas model to produce k-eigenvalue calculations using piecewise linear cross sections. This model will be used to benchmark the adjoint-weighted Doppler coefficient discussed in Chapter 4. The reference solution will consist of a direct difference calculation of the Doppler temperature coefficient using the heavy gas model and compare it to the adjoint-weighted calculation in MCNP.

5.4.1 Benchmark Setup

The benchmark case will simulate a Doppler broadened capture cross section. The base temperature will be simulated at room temperature (293K) and the hot temperature will be increased 100K to 393K and the reference Doppler temperature coefficient will be given by:

$$\alpha_T = \frac{\Delta\rho}{\Delta T} = \frac{k_{\infty_{393}} - k_{\infty_{293}}}{k_{\infty_{393}} \times k_{\infty_{293}}} \cdot \frac{1}{100K} \tag{5.90}$$

The piecewise constant capture cross section will consist of 5 evenly spaced regions for $\varepsilon \in [0, 20]$ with the following parameters:

Mass Ratios = 238, 5000, 7500, 10000		
	293K	393K
ε_0	20	20
ν	2	2
$\Sigma_{fr}(\varepsilon)$	.5	.5
$\Sigma_f(\varepsilon)$	.001	.001
$\Sigma_c(\varepsilon)$	.001,.01, .001, .001, .001	.0035, .005, .0035, .001

Table 5.6: Table of parameters for benchmark simulation

Again, the cross section libraries were constructed using the *simple_ace.pl* utility program to construct ACE files. In order to create the correct OTF cross section library modifications were made to the utility program *fit_otf.F90* where careful attention was made to maintain the area under the curve when broadening the piecewise constant cross sections. This produced the correct format necessary to run the simulation using OTF data libraries and piecewise constant cross sections so the adjoint-weighted calculation could be made.

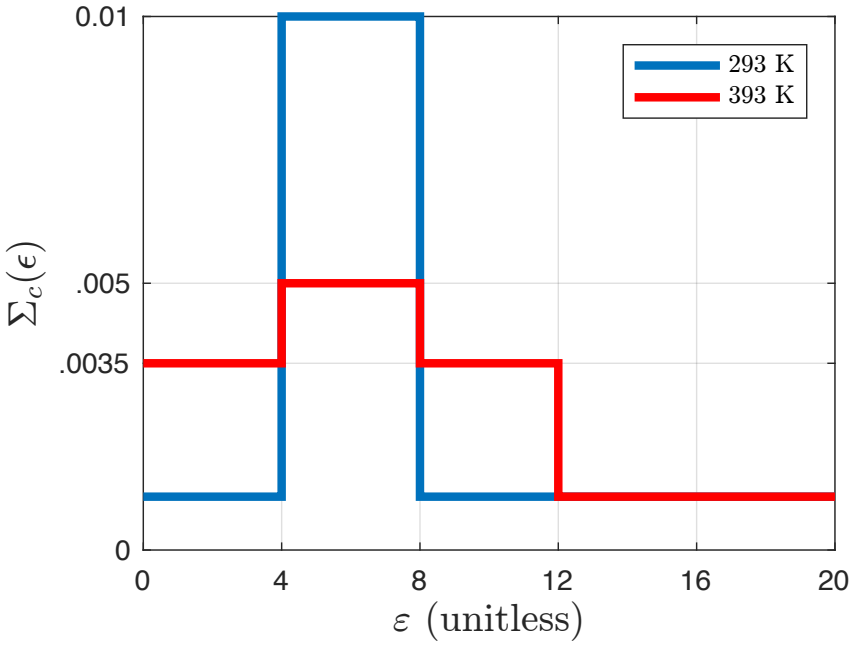

Figure 5.13: Doppler broadening of the piecewise constant capture cross section from 293K to 393K.

5.4.2 Results

Initial findings showed the heavy gas model when compared to the adjoint-weighted result required high precision k-eigenvalue calculations. In order to remove any sort of round-off error from numerical integration, a Gauss-Kronrod quadrature was used to numerically integrate the piecewise constant regions to any degree of precision. This ensured the heavy gas model was not losing any precision when solving for the criticality eigenvalue. As a result, k-eigenvalues were first compared to determine how heavy of mass ratio would be necessary to compare the heavy gas model to the adjoint-weighted calculation in MCNP6. Table 5.7 shows a comparison of criticality values for various mass ratios. Since α_T is on the order of percent-milli, k-eigenvalues must be precise to at least 3 significant figures. For a mass ratio equal to uranium, the k-eigenvalue is not precise enough and therefore when calculating the Doppler

Criticality k-eigenvalue Calculations at 293K		
Mass Ratio	**Heavy Gas**	**Adjoint-Weighted**
	Gauss-Kronrod	Monte Carlo
238	0.56837	0.580(74)
5000	0.99881	0.998(69)
7500	0.99981	0.999(80)
10000	0.99996	0.999(98)

Table 5.7: Criticality k-eigenvalue comparison for infinite medium piecewise constant cross sections.

temperature coefficient the result is not accurate. Table 5.8 shows exactly the correlation between mass ratio size and accuracy. For a mass ratio as large as 10000 results compare where for smaller size masses the comparison is no longer accurate. For a mass ratio of 238, since the k-eigenvalue is only accurate to one significant figure, the heavy gas model can not accurately calculate the Doppler coefficient.

Doppler Temperature Coefficient Calculations		
Mass Ratio	**Heavy Gas**	**Adjoint-Weighted**
	($\Delta\rho/\Delta T$) (pcm/K)	**(α_T) (pcm/K)**
238	-93.812	44.8
5000	-12.154	-17.4
7500	-3.769	-5.48
10000	-1.287	-1.28

Table 5.8: Doppler temperature coefficient comparison for infinite medium piecewise constant cross sections.

While the dependence on the mass ratio is clear, it was also important to investigate the effect of the piecewise constant data. The derivation of the heavy gas model implies that derivative of the flux exists and therefore trouble arises in the piecewise constant model where the magnitude of cross section is risen from one region to the next. In order to test this effect, a second case was simulated using a weak resonance and a weaker Doppler effect. Table 5.9 summarizes the parameters: Results for

Mass Ratios = 238, 1000, 5000, 10000, 15000		
	293K	393K
ε_0	20	20
ν	2	2
$\Sigma_{fr}(\varepsilon)$	.5	.5
$\Sigma_f(\varepsilon)$	.001	.001
$\Sigma_c(\varepsilon)$	.001,.0015, .001, .001, .001	.001125, .00125, .001125, .001

Table 5.9: Table of parameters for benchmark simulation with weak resonance.

this case show an increase in the accuracy of the k-eigenvalue due to the reduction in the cross section parameters yet a mass ratio A$\gg$ 238 is still required in order to converge the HG model and the adjoint-weighted calculation. Overall, the heavy gas model has been shown to verify the correct implementation of the adjoint-weighted Doppler temperature coefficient in the limit for large mass ratio A.

5.5 Conclusions

It has been shown in the limit as the mass ratio A $\gg 1$ that the heavy gas model may be used to benchmark the adjoint-weighted Doppler temperature coefficient calculated in MCNP6. This benchmark proves the correct implementation of the Doppler

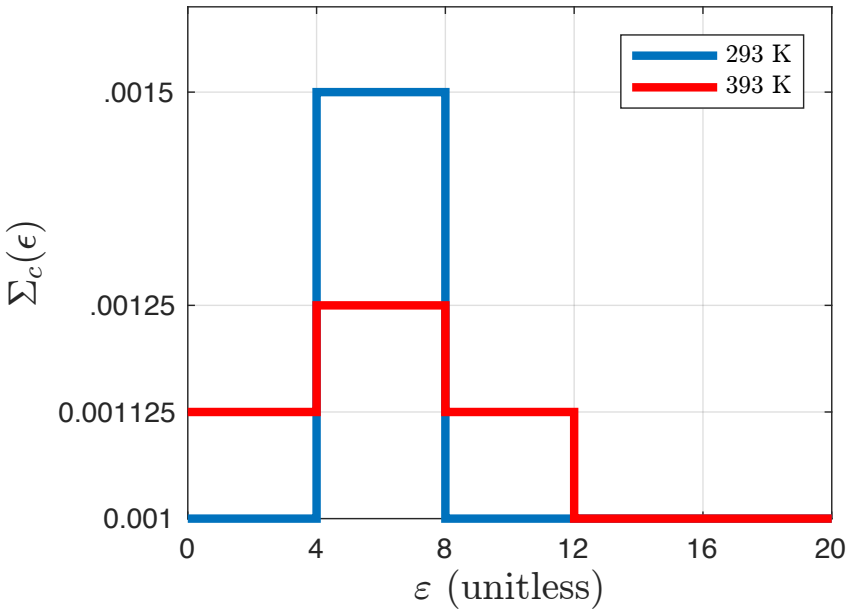

Figure 5.14: Doppler broadening of the piecewise constant capture cross section from 293K to 393K with weak resonance.

Criticality k-eigenvalue Calculations at 293K

Mass Ratio	**Heavy Gas**	**Adjoint-Weighted**
	Gauss-Kronrod	Monte Carlo
238	0.94551	0.946(78)
1000	0.97393	0.976(23)
5000	0.99968	0.999(98)
10000	0.99999	0.999(94)
15000	1.00000	1.000(31)

Table 5.10: Criticality k-eigenvalue comparison for infinite medium piecewise constant cross sections with weak resonance.

Doppler Temperature Coefficient Calculations		
Mass Ratio	**Heavy Gas** $(\Delta\rho/\Delta T)$ **(pcm/K)**	**Adjoint-Weighted** (α_T) **(pcm/K)**
238	-3.905	17.31
1000	-1.497	-1.944
5000	-1.136	-0.918
10000	-0.123	-0.088
15000	-0.019	-0.011

Table 5.11: Doppler temperature coefficient comparison for infinite medium piecewise constant cross sections with weak resonance.

temperature coefficient inside the research code. From this work, the first demonstration of an analytic benchmark of elastic free-gas scattering has been produced. Further more, extensive work was done to show the realm of validity of the heavy gas model. While the constant case showed quick convergence with increasing target size, the piecewise constant model required much larger targets for comparable results. The variation in the piecewise constant cross sections also showed the breakdown of the heavy gas model with highly varying cross section values in congruent regions. A reduction in the cross section values did show more accurate results with respect to the k-eigenvalue, yet obtaining a Doppler temperature coefficient with smaller cross section values still required larger targets. When the cross section values are reduced the effect of Doppler broadening is also reduced requiring high precision in the k-eigenvalue. This evidence reinforces the boundaries in which the heavy gas model may be applied.

Chapter 6

Future Work

6.1 Using Moments of the Scattering Kernel for Thermal Scattering

This section outlines a potential pathway for reproducing the bivariate PDF for neutron free-gas elastic scattering using moments of the probability function defined in Reference [4]. This work may provide an alternative sampling method to deal with sampling an energy-dependent scattering probability distribution functions.

The accurate and efficient computation of Legendre moments of the temperature-dependent double-differential cross section for thermal neutron scattering is essential in both Monte Carlo and deterministic computations. Under the assumption of isotropic scattering in the center of mass, Blackshaw & Murray [4, 43, 29, 44] derived explicit expressions for the zeroth and first Legendre moments of the scattering kernel, but the analytical approach is not practical for obtaining higher moments. Ouisloumen & Sanchez [5] subsequently developed an alternative expression for arbitrary order Legendre moments, which moreover accounted for anisotropy in the

center of mass. However, the numerical complexity of the formulation enabled computation of only the zeroth Legendre moment. Recent work done by Sunny [6] removed the numerical complexity by representing cross sections over the resonance regions as even powered polynomials in relative velocity. This application produced analytic forms of the double-differential resonance scattering probability distribution functions for Monte Carlo codes by solving the zeroth and first moments directly, but calculation of higher moments is too complex. In this work, the formulation of Blackshaw & Murray [4] is revisited to show that Legendre moments of arbitrary order can be obtained by applying adaptive quadrature directly with respect to the lab system scattering cosine. This approach obviates the need for variable changes widely used in the original work, yielding a significantly simpler implementation for computation of the moments. Considerations in this preliminary investigation are limited to constant cross sections and isotropic scattering in the center of mass to illustrate the technique. The ability to compute any number of moments with ease allows reconstruction of the scattering kernel and an assessment of the accuracy of the moment expansion with varying numbers of moments retained.

The Legendre moments of the scattering kernel are defined as:

$$K_n(v, v') = 2\pi \int_{-1}^{1} P_n(\mu_0) \cdot K(v, v', \mu_0) d\mu_0 \tag{6.1}$$

where $P_n(\mu_0)$ is the Legendre polynomial of degree n, and the scattering kernel can be recovered approximately from a finite number of these moments by:

$$K(v, v', \mu_0) \approx \sum_{n=0}^{N} \frac{2n+1}{4\pi} P_n(\mu_0) K_n(v, v') d\mu_0 \tag{6.2}$$

Reconstructed scattering kernels are required in deterministic codes but are also used in Monte Carlo simulations to simplify sampling of the scattering angle. Therefore, an efficient means of numerically computing an arbitrary number of Legendre moments is desired.

Evaluation Using Quadrature

Gauss quadrature rules are capable of yielding highly accurate numerical results for integrals of the type given in Eqn.(6.1). With Eqn.(6.1) approximated by the discrete sum:

$$K_n(v, v') \approx 2\pi \sum_{l=0}^{L} \omega_l P_l(\mu_0) K(v, v', \mu_0), \tag{6.3}$$

it is seen that the moment computation only requires numerical evaluation of the scattering kernel in Eqn.(6.2) and a Legendre polynomial at the quadrature nodes. The appropriate quadrature rule for this problem is Gauss-Legendre quadrature, which exactly integrates polynomials of degree $2N-1$ or less on the support $[-1, 1]$. The rapid variation of the scattering kernel as $\mu_0 \to 1$ and $v \to v'$ (in fact there is a removable singularity at $\mu_0 = 1$ and $v = v'$) can be handled using an adaptive Gauss-Kronrod quadrature scheme, which employs a low-order approximation but adaptively adds nodal points in areas where the distribution requires higher resolution. This was shown to be computationally more efficient than using a fixed quadrature order.

6.1.1 Numerical Results

Calculation of the moments was done in MATLAB using a (7,15) order pair Gauss-Kronrod quadrature. For illustration, numerical results were obtained for a 6.562 eV neutron colliding with ^{238}U . Figure 6.1 shows that quadrature results for the zeroth moment agree with the analytical solution given in Ref.[29]. Figures 6.2 and 6.3 show the value of the moments of different orders at different speeds for upscatter and down scatter. The moments rapidly decay to zero with increasing order when v and v' are sufficiently different, but the higher moments become increasingly larger in magnitude as $v \to v'$, consistent with the corresponding angular variation of the

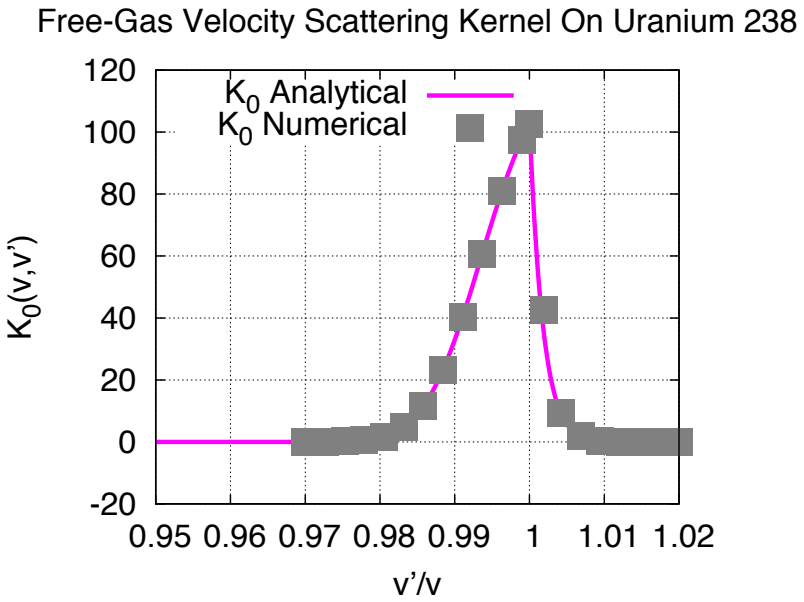

Figure 6.1: Velocity scattering kernel for 6.562 eV neutrons on ^{238}U at 300 Kelvin compared to moments produced with quadrature.

kernel.

The reconstructed scattering kernels and the corresponding error measured using a relative L_2 norm are shown in Figures 6.4 and 6.5. The results show that a large number of moments (10 or more) must be retained in order to accurately reproduce the original kernel when the incoming and outgoing speeds are similar. However, for differing speeds, when the scattering kernel varies more smoothly with angle, a few moments (2-3) generally suffice to obtain an accurate reconstruction. This behavior was consistently observed over a broad range of parameters, including low Z scatterers and high temperatures.

It is believed that moments of the non-constant cross section case may also be obtained producing the correct scattering kernel which includes the energy dependent scattering cross section. Analyzing the constant cross section case shows, the viability of Gauss-Kronrod adaptive quadrature to reproduce the zeroth Legendre moment of

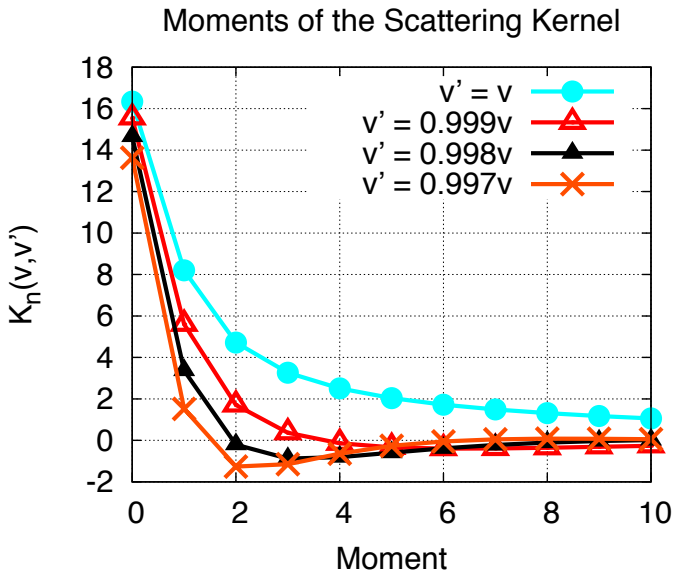

Figure 6.2: Moments of the velocity scattering kernel for 6.562 eV downscattered neutrons on ^{238}U at 300 K.

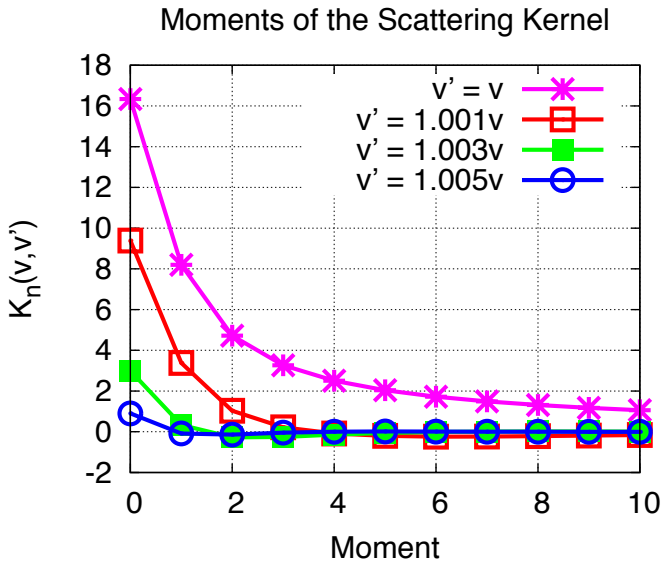

Figure 6.3: Moments of the velocity scattering kernel for 6.562 eV upscattered neutrons on ^{238}U at 300K.

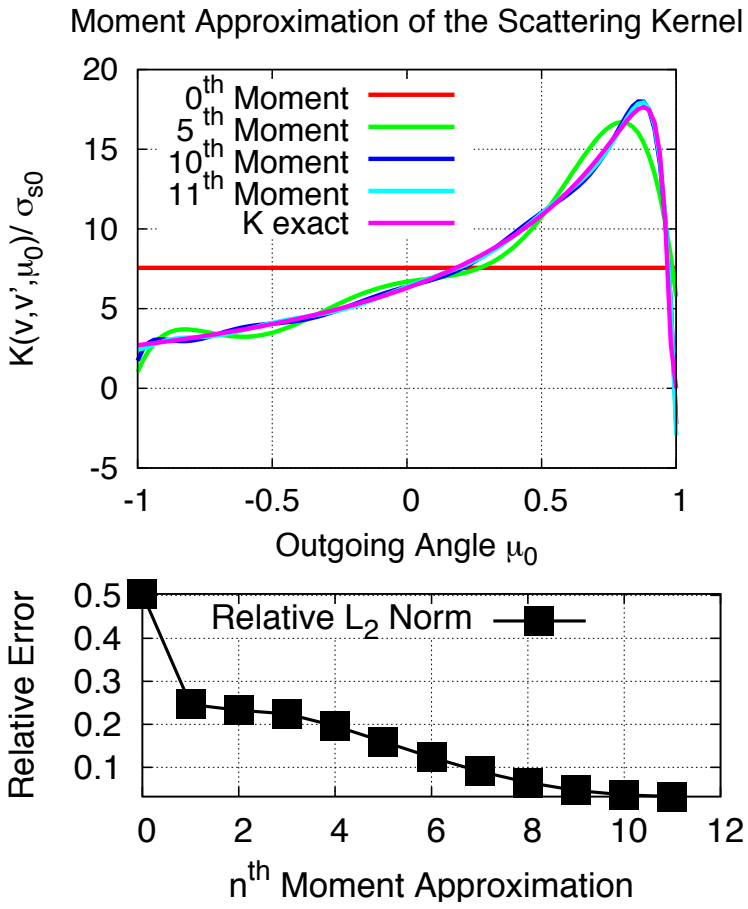

Figure 6.4: Velocity scattering kernel for 6.562 eV neutrons downscattered with $v' = 0.9985v$ on ^{238}U .

the scattering kernel. An investigation into applying the moment reconstruction of the scattering kernel using the zeroth Legendre moment including energy dependent scattering cross section could be made. This would require quadrature evaluation over energy bins with respect to energy dependent cross section data. The Gauss-Kronrod adaptive quadrature would help to streamline the integration using the energy dependent cross sections as well as provide control over numerical accuracy.

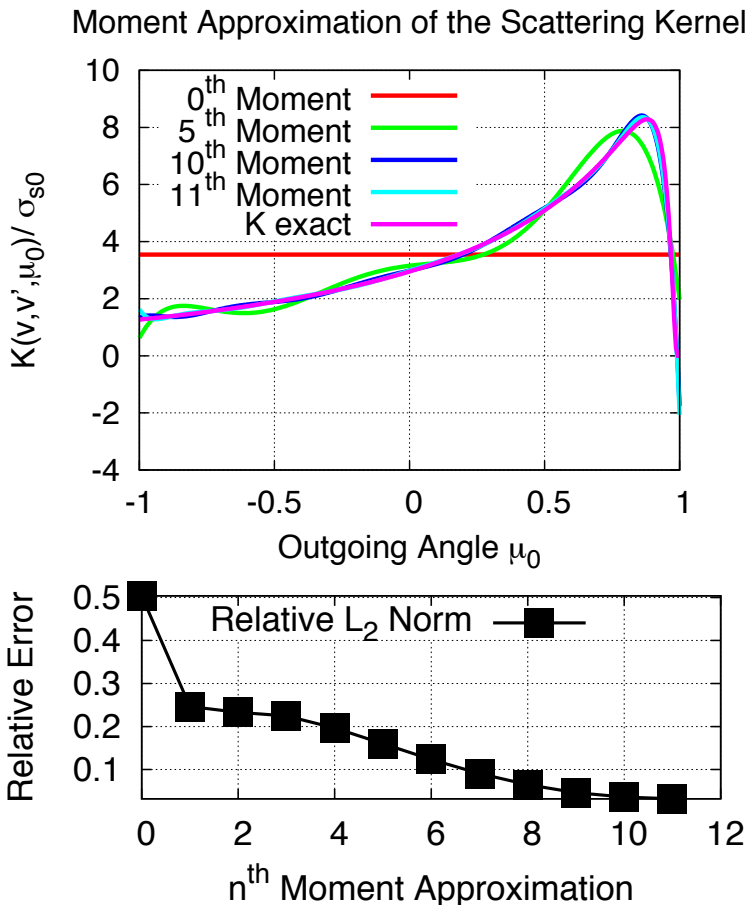

Figure 6.5: Velocity scattering kernel for 6.562 eV neutrons upscattered with $v' = 1.0015v$ on ^{238}U .

6.2 Producing Exact Temperature Derivatives

While this dissertation work showed the ability of using the OTF database to produce temperature derivatives, it was at the cost of increasing the default fractional tolerance. The temperature derivatives take an exact derivative of an approximated function. This propagates error and contributes to potential inaccuracies in the Doppler temperature coefficient. In order to remove this error from the Doppler temperature coefficient, it would be possible to first take a temperature derivative of the exact function and reproduce a separate OTF library for cross section deriva-

tives. Since the number of coefficients of the original OTF library was increased this required more data storage. Investigation into the storage cost of an OTF temperature derivative library may produce more accurate results with comparable data storage.

Appendices

Appendix A

Scattering Kernel Derivation from Blackshaw & Murray

This paper develops a new form of the scattering probability function for low-energy, neutron-nuclear interactions in a monatonic gas, fully preserving the three-dimensional aspects of the scattering process. Rather than dealing with outgoing angles and **velocities** of the neutron-nuclear collision, Blackshaw has rewritten the scattering kernel in terms of moments of the incoming and outgoing **speeds** of the neutron, weighted by it's respective spherical-harmonic moment in angle.

This formulation assumes the following:

- isotropic Maxwellian velocity distribution

- assumes classical physics

- assumes isotropic scattering at the center-of-mass

A.1 Introduction

$K(\boldsymbol{v}, \boldsymbol{v}')$ = probability per unit time that a neutron of velocity ($\boldsymbol{v}$)
will have an outgoing velocity ($\boldsymbol{v}'$)
interacting with disturbed nuclear velocities

What is K related to?

1. collision frequency $v_r \sigma_s(v_r)$
2. velocity distribution of nuclei $M(\mathbf{V})$
3. probability $P(\boldsymbol{v}, \boldsymbol{v}')$ of having an incoming neutron velocity $\boldsymbol{v}$ resulting in an outgoing neutron velocity $\boldsymbol{v}'$ after colliding with single neutron with velocity $\boldsymbol{V}$

$$K(\boldsymbol{v}, \boldsymbol{v}') = \int_{\boldsymbol{V}} v_r[\sigma_s(v_r)] \cdot [M(\boldsymbol{V})] \cdot P(\boldsymbol{v}, \boldsymbol{v}') d\boldsymbol{V} \tag{A.1}$$

A.2 Scattering Probability Function $P(\boldsymbol{v}, \boldsymbol{v}')$

Again, the scattering probability function is derived under the assumption of isotropic scattering in the center-of-mass (CMS) frame. By representing $P(\boldsymbol{v}, \boldsymbol{v}')$ in the lab-system (LS), this section will construct the scattering probabilities for speed $P(v, v')$ and direction $P(\boldsymbol{\Omega}_0, \boldsymbol{\Omega}_0')$. All values, symbols and equations are taken from Blackshaw's paper and are not defined in this summary.

Because the probability of outgoing velocity is the same in the LS and CMS,

$$P(\boldsymbol{v}, \boldsymbol{v}') dv' d\mu_0 d\phi_0 = P(\boldsymbol{v}_{mc}, \boldsymbol{v}'_{mc}) dv'_{mc} d\mu_c d\phi_c, \tag{A.2}$$

and the Jacobian between CMS and LS gives,

$$P(\boldsymbol{v}, \boldsymbol{v}') = P(\boldsymbol{v}_{mc}, \boldsymbol{v}'_{mc}) \cdot \frac{v'^2}{v'^2_{mc}}, \quad \text{where} \quad \frac{v'^2}{v'^2_{mc}} = \frac{dv'_{mc} d\mu_c d\phi_c}{dv' d\mu_0 d\phi_0}. \tag{A.3}$$

Since the CMS is assumed to be isotropic and

$$v_{mc} = \frac{A v_r}{A+1} = v'_{mc}$$

then the probability of scatter in the CMS frame can be given by the following delta function

$$P(\boldsymbol{v}_{mc}, \boldsymbol{v}'_{mc}) = \frac{\delta(v'_{mc} - v_{mc})}{4\pi} \tag{A.4}$$

which provides the following definition for the probability of scattering in the LS

$$P(\boldsymbol{v}, \boldsymbol{v}') = \frac{v'^2}{v'^2_{mc}} \cdot \frac{\delta(v'_{mc} - v_{mc})}{4\pi}. \tag{A.5}$$

This formulation isn't immediately useful, but will further the development of probabilities moving forward.

A.2.1 The $\delta(v'_{mc} - v_{mc})$ representation of $P(\boldsymbol{v}, \boldsymbol{v}')$

The purpose of this section is to rewrite the probability function $P(\boldsymbol{v}, \boldsymbol{v}')$ in terms of a delta-function with respect to azimuthal orientation of $\boldsymbol{v}_c$ and $\boldsymbol{V}$ about $\boldsymbol{v}$. This will help in the ultimate goal of deriving P in terms of its $\mathrm{P_n}$ moments.

By using two Cartesian coordinate systems, where $\boldsymbol{v}$ in the LS is coincident on the *x-axis* and $\boldsymbol{v}_c$ in the CMS is coincident with the *x′-axis*, one can express each vector in terms of both coordinate systems by the use of an orthogonal transformation. After employing this transformation, the azimuthal orientation in the LS can now be represented by

$$\phi = \cos^{-1}\left(\frac{v'^2 - v'^2_{mc} + v_c^2}{2 v' v_c k_2} - \frac{k_1}{k_2}\right) + \phi_0, \tag{A.6}$$

where

$$k_1 \equiv \mu_0 \cos\alpha \quad k_2 \equiv (1-\mu_0^2)^{\frac{1}{2}} \sin\alpha.$$

The following delta-function transform theorem is used to cast CMS outgoing speeds into functions of azimuthal orientation.

$$\delta[y(x)-y(x_0)] = \left.\frac{\partial x}{\partial y}\right|_{y=y_0} \cdot \delta[x(y)-x(y_0)] \tag{A.7}$$

Finally yielding,

$$P(\boldsymbol{v},\boldsymbol{v}') = \frac{v' v_{mc} \delta[\phi(v'_{mc})-\phi(v_{mc})]}{2\pi v'^2_{mc} v_c \left[k_2^2-(s-k_1)^2\right]^{\frac{1}{2}}}, \tag{A.8}$$

where

$$s \equiv \frac{v'^2 - v_{mc}^2 + v_c^2}{2v'v_c}$$

Important things to note about this new form:

- this function is always positive satisfying the condition $P(\boldsymbol{v},\boldsymbol{v}')$ is always real
- the absence of ϕ_0 (the azimuthal orientation of $\boldsymbol{v}$ and $\boldsymbol{v}'$) and the appearance of $(\frac{1}{2\pi})$ reveals $P(\boldsymbol{v},\boldsymbol{v}')$ is independent of azimuthal neutron scattering in the LS and shows scattering is azimuthally symmetric
- the three-dimensional aspect of scattering is retained in this formulation

A.2.2 Scattering probabilities $P(v,v')$ and $P(\boldsymbol{\Omega}_0,\boldsymbol{\Omega}'_0)$

Given the new form of $P(\boldsymbol{v},\boldsymbol{v}')$, the probability $P(v,v')$ that a neutron of speed v undergoing an elastic collision with a nucleus of initial velocity $\boldsymbol{V}$ emerging with a final speed v' is

$$P(v,v') = \int_{\phi_0}\int_{\mu_0} P(\boldsymbol{v},\boldsymbol{v}')d\mu_0 d\phi_0 \tag{A.9}$$

Using Eqn. A.6 and the theorem from Eqn. A.7 the above probability can be written like Eqn. A.9 but in terms of ϕ_0 instead of ϕ allowing for an integration over azimuthal angle yielding (k_1 and k_2 have been substituted back in),

$$P(v, v') = \frac{v'}{2\pi v_{mc} v_c} \int_{\mu_0} \frac{d\mu_0}{\left[-\mu_0^2 + (2s\cos\alpha)\mu_0 + \sin^2\alpha - s^2\right]^{\frac{1}{2}}} \tag{A.10}$$

Next, limits of integration must be analyzed. In order to maintain real solutions, the limits of μ_0 are taken to be the roots of the denominator when set equal to zero. As a result, the integration evaluates to π and the probability over a specific domain is given as (substitutions have been made with respect to Eq.(5) & Eq.(8) from Blackshaw)

$$P(v, v') = \frac{v'(A+1)}{2Av_r v_c} \tag{A.11}$$

for

$$\left| \frac{Av_r}{A+1} - v_c \right| \leq v' \leq \left(\frac{Av_r}{A+1} + v_c \right) \tag{A.12}$$

The probability $P(\mathbf{\Omega}_0, \mathbf{\Omega}_0')$ that a neutron of initial direction $\mathbf{\Omega}_0$, undergoing an elastic collision with a nucleus of initial velocity $\boldsymbol{V}$ will be scattered by $\mathbf{\Omega}_0'$ is

$$P(\mathbf{\Omega}_0, \mathbf{\Omega}_0') = \int_{v'} P(\boldsymbol{v}, \boldsymbol{v}'). \tag{A.13}$$

Blackshaw uses

$$F = \frac{v'^2 - v_{mc}'^2 + v_c^2}{2v'v_c}$$

to rewrite $P(\boldsymbol{v}, \boldsymbol{v}')$ with a delta-function in terms of $v'(v_{mc}')$ by completing the square above

$$v'(v_{mc}') = v_c F + (v_c^2 F^2 + v_{mc}^2 - v_c^2)^{\frac{1}{2}} \tag{A.14}$$

giving

$$P(\boldsymbol{v}, \boldsymbol{v}') = \frac{v'^2 v_{mc} \delta[v'(v'_{mc}) - v'(v_{mc})]}{4\pi v'^2_{mc} \left(v_c^2 F^2 + v_{mc}^2 - v_c^2\right)^{\frac{1}{2}}}. \tag{A.15}$$

Taking the above equation into Eqn. A.13 and integrating (which is a mere substitution of v'_{mc} to v_{mc}), finally yields

$$P(\boldsymbol{\Omega}_0, \boldsymbol{\Omega}'_0) = \frac{\left[v_c F + \left(v_c^2 F^2 + v_{mc}^2 - v_c^2\right)^{\frac{1}{2}}\right]^2}{4\pi v_{mc} \left(v_c^2 F^2 + v_{mc}^2 - v_c^2\right)^{\frac{1}{2}}} \tag{A.16}$$

A.3 Velocity Scattering Kernel

This section is meant to express Eqn A.1 in term of a single-integral over v_r. Using the above forms of the scattering probabilities, details concerning transformation of variables, interchange of order of integration, and evaluation of limits are given.

A.3.1 General formulation of $K(\boldsymbol{v}, \boldsymbol{v}')$

While it is assumed that scattering of the neutron is with in a monatonic medium, the distribution of velocities are therefore Maxwellian. The probability of finding a nucleus in $dVd\mu d\phi$ at $\boldsymbol{V}$ in velocity space is

$$[M(\boldsymbol{V})]d\boldsymbol{V} = [M(\boldsymbol{V})]dVd\mu d\phi \tag{A.17}$$

where

$$M(\boldsymbol{V}) = \frac{M(V)}{4\pi} = \frac{B^3}{(\pi)^{\frac{3}{2}}} V^2 \exp(-B^2V^2) \tag{A.18}$$

for

$$B^2 \equiv \frac{M}{2kT}, \quad 0 \leq V \leq \infty \tag{A.19}$$

The scattering kernel can now be expressed with the Maxwellian distribution of nuclear velocity in terms of a triple-integral over all nuclear speeds, azimuthal angle and scattering angle cosine. But the velocity scattering kernel $K(\boldsymbol{v}, \boldsymbol{v}')$ can be expressed in terms of a double-integral. The probability of scattering $P(\boldsymbol{v}, \boldsymbol{v}')$ is substituted back in, the integral over the azimuthal ϕ is then straightforward and a substitution for $v_r/v_{mc} = (A+1)/A$ is made yielding

$$K(\boldsymbol{v}, \boldsymbol{v}') = \int_{\mu} \int_{V} \frac{[\sigma_s(v_r)] \cdot [M(\boldsymbol{V})] \cdot (A+1)v' dV d\mu}{2\pi A v_c \left[k_2^2 - (s-k_1)^2\right]^{\frac{1}{2}}} \tag{A.20}$$

In order to write the above integral as a function of V and v_r Eqn. A.20 must be

- written as a function of V and μ

- μ must then be eliminated with Eqn. A.20 rearranged for integration over $\boldsymbol{V}$

By holding v and V constant

$$d\mu = -\frac{v_r dv_r}{vV} \tag{A.21}$$

and μ with Eqn.(4) from Blackshaw gives

$$K(\boldsymbol{v}, \boldsymbol{v}') = -\frac{B^3}{(\pi)^{\frac{3}{2}}} \left[\frac{(A+1)^2 v'^2}{\pi A v}\right] \int_{v_r} v_r[\sigma_s(v_r)] \int_{V(v_r)} \frac{V \exp(-B^2V^2) dV}{(a'V^4 + b'V^2 + c')^{\frac{1}{2}}} \tag{A.22}$$

where a', b', c' are defined in Blackshaw as coefficients which are a function of v, v', μ_0 and A.

The sign of a' is important for determining both the and physical characteristics of $K(\boldsymbol{v}, \boldsymbol{v}')$.

$$a' = -\frac{A^2(v^2 + v'^2 - 2vv'\mu_0)}{v^2}. \tag{A.23}$$

Since $-1 \leq \mu_0 \leq 1$ it is clear that the value in parentheses above is always positive and a' is therefore always negative. A new parameter is introduced

$$p \equiv v^2 + v'^2 - 2vv'\mu_0 \tag{A.24}$$

where it is noted that the vector $\boldsymbol{p} = \boldsymbol{v} - \boldsymbol{v}'$ is just the change in the neutron velocity. If another variable $y = B^2V^2$ is introduced the integral over $V(v_r)$ becomes

$$\frac{1}{2} \int_{y_1}^{y2} \frac{\exp(-y) dy}{(ay^2 + by + c)^{\frac{1}{2}}} \tag{A.25}$$

where $a = a'$, $b = B^2 b'$, and $c = B^4 c'$. Next the bounds on this integral must be evaluated in the same manner that was used in the previous section. The lower and

upper bounds are the roots of $ay^2 + by + c = 0$. By the quadratic equation and a transform of variables

$$y = \frac{-(b^2 - 4ac)^{\frac{1}{2}} \cos\eta}{2a} - \frac{b}{2a} \tag{A.26}$$

where the bounds of the integral become $\eta_1 = 0$ and $\eta_2 = \pi$ changing Eqn. A.25 into the following integral

$$\left[2(-a)^{\frac{1}{2}}\right]^{-1} \exp\left(\frac{b}{2a}\right) \int_0^{\pi} \exp\left[\frac{(b^2 - 4ac)^{\frac{1}{2}} \cos\eta}{2a}\right] d\eta \tag{A.27}$$

Using math tables, the integral above is of a form that yields a modified zero-order Bessel function of the first kind scaled by a factor of π. Recalling,

$$a = a' = -\frac{A^2 p^2}{v^2}$$

the velocity scattering kernel now has the following form

$$K(\boldsymbol{v}, \boldsymbol{v}') = \frac{2B^2}{(\pi)^{\frac{3}{2}}} \left(\frac{(A+1)^2}{2A}\right) \frac{v'^2}{p} \cdot \int_{v_{r_1}}^{v_{r_2}} v_r[\sigma_s(v_r)] \times \exp\left(\frac{b}{2a}\right) \cdot I_0 \left[\frac{(b^2 - 4ac)^{\frac{1}{2}}}{2a}\right] dv_r. \tag{A.28}$$

where the integration dependence over nuclear speeds has been removed.

A.4 Derivation of $K_n(v, v')$, $F(v)$ and $\gamma(v)$

In this section, the P_n moments of the velocity scattering kernel, the total scattering probability and absorption probability will be developed using results from the previous section. Again, attention is paid to representing these values as single-integral expressions over a single variable v_r.

A.4.1 The $\mathbf{P_n}$-Moments of $K(\boldsymbol{v}, \boldsymbol{v}')$

Before defining the weighted moments scattering kernel, recall, from the previous section, the following expression for the probability of an incoming neutron velocity $\boldsymbol{v}$ scattering with an outgoing velocity $\boldsymbol{v}'$:

$$K(\boldsymbol{v}, \boldsymbol{v}') = \int_{\mu} \int_{V} \frac{[\sigma_s(v_r)] \cdot [M(\boldsymbol{V})] \cdot (A+1) v' dV d\mu}{2\pi A v_c \left[k_2^2 - (s-k_1)^2\right]^{\frac{1}{2}}}, \tag{A.29}$$

where

$$M(\boldsymbol{V}) = \frac{B^3}{(\pi)^{\frac{3}{2}}} V^2 \exp(-B^2 V^2), \quad B^2 \equiv \frac{M}{2kT},$$

and

$$k_1(\mu_0, \alpha) \equiv \mu_0 \cos\alpha \quad k_2(\mu_0, \alpha) \equiv (1-\mu_0^2)^{\frac{1}{2}} \sin\alpha, \quad s \equiv \frac{v'^2 - v_{mc}^2 + v_c^2}{2v'v_c}.$$

The general expression for the nth-order spherical-harmonics weighted moment of $K(\boldsymbol{v}, \boldsymbol{v}')$ is

$$K_n(v, v') = \int_{\phi_0} \int_{\mu_0} P_n(\mu_0) \cdot K(\boldsymbol{v}, \boldsymbol{v}') d\mu_0 d\phi_0 \tag{A.30}$$

where $P_n(\mu_0)$ represents the nth-order Legendre polynomial, μ_0 is the cosine value of the scattering polar angle between $\boldsymbol{v}$ and $\boldsymbol{v}'$, and ϕ_0 is the azimuthal orientation of the outgoing neutron velocity $\boldsymbol{v}'$ about $\boldsymbol{v}$.

Blackshaw uses the quantity $\sigma_s^n(v, v')$ as a matter of "convenience", where

$$\sigma_s^n(v, v') = \int_{\phi_0} \int_{\mu_0} (\mu_0)^n K(\boldsymbol{v}, \boldsymbol{v}') d\mu_0 d\phi_0. \tag{A.31}$$

If the expression for the velocity scattering kernel from the previous expression is substituted into the above expression

$$\sigma_s^n(v, v') = \frac{B^3}{(\pi)^{\frac{3}{2}}} \frac{(A+1)v'}{2\pi A} \int_{\phi_0} \int_{\mu_0} \int_{\mu} \int_{V} \frac{(\mu_0)^n [\sigma_s(v_r)] V^2 \exp(-B^2V^2) dV d\mu d\mu_0 d\phi_0}{v_c \left[k_2^2 - (s - k_1)^2\right]^{\frac{1}{2}}} \tag{A.32}$$

then ϕ_0 is easily integrated out yielding a factor of 2π. The next step is to reintroduce the definitions of k_1, k_2, and s which will yield a similar integral equation over μ_0 as seen in Eqn. A.10 yielding a factor of π giving the following expression

$$K_n(v, v') = \frac{B^3}{(\pi)^{\frac{1}{2}}} \frac{(A+1)v'}{A} \int_{\mu} \int_{V} \frac{f_n(s, \alpha) [\sigma_s(v_r)] V^2 \exp(-B^2V^2) dV d\mu}{v_c} \tag{A.33}$$

where

$$f_0(s, \alpha) = 1$$

$$f_1(s, \alpha) = s \cos \alpha$$

$$f_2(s, \alpha) = \frac{1}{4} \left[9s^2 \cos^2 \alpha + 3 \left(\sin^2 \alpha - s^2\right) - 4\right]$$

$$f_3(s, \alpha) = \frac{1}{4} \left[5s \cos \alpha\right] \left[5s^2 \cos^2 \alpha + 3 \left(\sin^2 \alpha - s^2\right) - \frac{6}{5}\right].$$

Next, the focus will be on the zeroth and first moments of the velocity scattering kernel. The following equations

$$v_c^2 = \frac{v^2 + A^2V^2 + 2AvV\mu}{(A+1)^2} \tag{A.34}$$

$$v_r^2 = v^2 + V^2 - 2vV\mu \tag{A.35}$$

can be used to write the integrals over v_r and v_c yielding the following integral for K_0

$$K_0(v,v') = \frac{B^3}{(\pi)^{\frac{1}{2}}}\left(\frac{A+1}{A}\right)^2\left(\frac{v'}{v}\right)\exp\left(\frac{B^2v^2}{A}\right) \tag{A.36}$$
$$\times\left[\int_{v_r} v_r[\sigma_s(v_r)]\exp\left(-\frac{B^2v_r^2}{A+1}\right)dv_r\right.$$
$$\left.\times\int_{v_c}\exp\left[-B^2\left(\frac{A+1}{A}\right)v_c^2\right]dv_c\right]$$

A.5 Variable listings

$\boldsymbol{v},\boldsymbol{v}' \equiv$ initial and final velocity of the neutron in LS

$\boldsymbol{V} \equiv$ initial velocity of the nucleus in the LS

$\boldsymbol{v}_{mc},\boldsymbol{v}'_{mc} \equiv$ initial and final velocity of the neutron in the CMS

$\boldsymbol{v}_c \equiv$ invariant velocity of the center of mass

$\boldsymbol{v}_r \equiv$ relative velocity of the neutron and nucleus $\boldsymbol{v}-\boldsymbol{V}$

$\theta \equiv \angle(\boldsymbol{v},\boldsymbol{V}) = \cos^{-1}(\mu)$

$\theta_0 \equiv \angle(\boldsymbol{v},\boldsymbol{v}') = \cos^{-1}(\mu_0)$

$\theta_c \equiv \angle(\boldsymbol{v}_c,\boldsymbol{v}'_{mc}) = \cos^{-1}(\mu_c)$

$\alpha \equiv \angle(\boldsymbol{v},\boldsymbol{v}_c)$

$\gamma \equiv \angle(\boldsymbol{v}_c,\boldsymbol{v}_c)$

$A \equiv$ ratio of nuclear-to-neutron mass

A.6 Useful equations

$$\boldsymbol{v}_c = \frac{\boldsymbol{v} + A\boldsymbol{V}}{A+1}$$

$$v_c^2 = \frac{v^2 + A^2V^2 + 2AvV\mu}{(A+1)^2}$$

$$v_r^2 = v^2 + V^2 - 2vV\mu$$

$$v_{mc} = \frac{Av_r}{A+1} = v'_{mc}$$

$$v'^2 = v'^2_{mc} + v_c^2 + 2v'_{mc}v_c\mu_c$$

$$\cos\alpha = \frac{v + AV\mu}{(A+1)v_c}$$

A.7 Variable transform from Eqn. A.26

The following results verify Blackshaw's variable transform. Starting with the integral

$$I = \int \frac{dy}{(ay^2 + by + c)^{\frac{1}{2}}},$$

Blackshaw says

$$y = -\frac{(b^2 - 4ac)^{\frac{1}{2}}}{2a}\cos\eta - \frac{b}{2a}.$$

Removing a factor of $a^{-\frac{1}{2}}$, the integral becomes

$$I = \frac{1}{a^{\frac{1}{2}}} \int \frac{dy}{(y^2 + \frac{b}{a}y + \frac{c}{a})^{\frac{1}{2}}},$$

rewriting y in terms of it's factors

$$y = -\frac{b}{2a} \pm \frac{1}{2a}\sqrt{b^2 - 4ac}$$

$$y = -\left(\frac{b}{2a} + \frac{1}{2a}\sqrt{b^2 - 4ac}\right), \quad \left(-\frac{b}{2a} + \frac{1}{2a}\sqrt{b^2 - 4ac}\right).$$

Using another change of variables

$$\alpha = \frac{b}{2a}, \quad \beta = \frac{1}{2a}\sqrt{b^2 - 4ac}$$

$$y^2 + \frac{b}{a}y + \frac{c}{a} = [y + (\alpha + \beta)]\,[y + (\alpha - \beta)]\,,$$

and now

$$y = -\beta\cos\eta - \alpha \quad \Longrightarrow \quad \cos\eta = -\frac{(y+\alpha)}{\beta}$$

$$dy = \beta\sin\eta d\eta.$$

Substituting values of y in terms of $\cos\eta$ in the integral gives

$$I = \frac{1}{a^{\frac{1}{2}}}\int \frac{\beta\sin\eta}{(-\beta\cos\eta - \alpha + \alpha + \beta)^{\frac{1}{2}}\,(-\beta\cos\eta - \alpha + \alpha - \beta)^{\frac{1}{2}}}$$

$$I = \frac{1}{a^{\frac{1}{2}}}\int \frac{\beta\sin\eta}{\beta\,(-\cos\eta + 1)^{\frac{1}{2}}\,(-\cos\eta - 1)^{\frac{1}{2}}}$$

$$I = \frac{1}{-a^{\frac{1}{2}}}\int \frac{\beta\sin\eta}{[(1+\cos\eta)\,(1-\cos\eta)]^{\frac{1}{2}}} = \frac{1}{-a^{\frac{1}{2}}}\int \frac{\beta\sin\eta}{(1-\cos^2\eta)^{\frac{1}{2}}}$$

And using the trig identity $1 = \sin^2 x + \cos^2 x$ simplifies the integral to

$$I = \frac{1}{-a^{\frac{1}{2}}}\int d\eta.$$

Substituting the above integral with the variable transform gives the final result

$$\left[2(-a)^{\frac{1}{2}}\right]^{-1}\exp\left(\frac{b}{2a}\right)\int_0^{\pi}\exp\left[\frac{(b^2-4ac)^{\frac{1}{2}}\cos\eta}{2a}\right]d\eta$$

A.8 Moving integration from $dV\ d\mu$ to $dv_r\ dv_c$ from Eqn. 4.8

For purposes of examination, the beginning and end results will be shown together. The following integral is transformed as follows from

$$K_0(v,v') = \frac{B^3}{(\pi)^{\frac{1}{2}}}\frac{(A+1)v'}{A}\int_{\mu}\int_{V}\frac{f_0(s,\alpha)[\sigma_s(v_r)]V^2\exp(-B^2V^2)dV\,d\mu}{v_c} \tag{A.37}$$

to

$$\begin{aligned} K_0(v,v') = \frac{B^3}{(\pi)^{\frac{1}{2}}}\left(\frac{A+1}{A}\right)^2\left(\frac{v'}{v}\right)\exp\left(\frac{B^2v^2}{A}\right) \\ \times\left[\int_{v_r} v_r[\sigma_s(v_r)]\exp\left(-\frac{B^2v_r^2}{A+1}\right)dv_r \right. \\ \left. \times\int_{v_c}\exp\left[-B^2\left(\frac{A+1}{A}\right)v_c^2\right]dv_c\right] \end{aligned} \tag{A.38}$$

which will be transformed into an a integral of dv_r and dv_c with the help of the following equations

$$v_c^2 = \frac{v^2 + A^2V^2 + 2AvV\mu}{(A+1)^2} \tag{A.39}$$

$$v_r^2 = v^2 + V^2 - 2vV\mu \tag{A.40}$$

By first writing Eqn. A.40 in terms of $2vV\mu$,

$$2vV\mu = v^2 + V^2 - v_r^2$$

one can substitute this result into Eqn. A.39 yielding an equation for V^2 in terms of v, v_c and v_r yielding

$$v_c^2 = (A+1)^{-2}\left[v^2 + A^2V^2 + A\left(v^2 + V^2 - v_r^2\right)\right]$$

$$v_c^2 = (A+1)^{-2}\left[v^2 + A^2V^2 + Av^2 + AV^2 - Av_r^2\right]$$

$$v_c^2 = (A+1)^{-2}\left[A(A+1)V^2 + (A+1)v^2 - Av_r^2\right]$$

$$A(A+1)V^2 = (A+1)^2v_c^2 - (A+1)v^2 + Av_r^2$$

$$V^2 = \frac{A+1}{A}v_c^2 - \frac{v^2}{A} + \frac{v_r^2}{A+1} \tag{A.41}$$

Next, in order to go from $dVd\mu$ space to dv_rdv_c, a Jacobian transform must be made. The Jacobian takes on the following form

$$\begin{pmatrix} \frac{\partial V}{\partial v_c} & \frac{\partial V}{\partial v_r} \\ \frac{\partial \mu}{\partial v_c} & \frac{\partial \mu}{\partial v_r} \end{pmatrix}$$

so in terms of Eqn. A.41 the Jacobian becomes

$$\begin{pmatrix} \frac{A+1}{A}\frac{v_c}{V} & \frac{1}{A+1}\frac{v_r}{V} \\ 0 & -\frac{v_r}{vV} \end{pmatrix}$$

yielding

$$\frac{dVd\mu}{dv_cdv_r} = \det\begin{pmatrix} \frac{A+1}{A}\frac{v_c}{V} & \frac{1}{A+1}\frac{v_r}{V} \\ 0 & -\frac{v_r}{vV} \end{pmatrix} = \left(\frac{A+1}{A}\right)\frac{v_cv_r}{v}\frac{1}{V^2}. \tag{A.42}$$

Therefore in order to change from $dVd\mu$ to dv_rdv_c

$$dVd\mu = \frac{dVd\mu}{dv_cdv_r}\cdot dv_cdv_r,$$

Eqn. A.37 must be multiplied by $\frac{dVd\mu}{dv_cdv_r}$. When this is done the V^2 value in the numerator will disappear and the only V^2 term is in the exponential. Using Eqn. A.41

for V^2 gives the result for the zeroth moment

$$\frac{B^3}{(\pi)^{\frac{1}{2}}}\frac{(A+1)v'}{A}\int_{\mu}\int_{V}\frac{[\sigma_s(v_r)]\exp\left(-B^2\left(\frac{A+1}{A}v_c^2-\frac{v^2}{A}+\frac{v_r^2}{A+1}\right)\right)}{v_c}\cdot\left(\frac{A+1}{A}\right)\frac{v_c v_r}{v}\cdot dv_r dv_c \tag{A.43}$$

Simplifying terms and grouping the integrals in terms of integration over v_r and v_c gives the final result,

$$\begin{aligned}K_0(v,v') = \frac{B^3}{(\pi)^{\frac{1}{2}}}\left(\frac{A+1}{A}\right)^2\left(\frac{v'}{v}\right)\exp\left(\frac{B^2v^2}{A}\right) \\ \times\left[\int_{v_r} v_r[\sigma_s(v_r)]\exp\left(-\frac{B^2v_r^2}{A+1}\right)dv_r\right. \\ \left.\times\int_{v_c}\exp\left[-B^2\left(\frac{A+1}{A}\right)v_c^2\right]dv_c\right]\end{aligned} \tag{A.44}$$

It is important to note here that v_c is still a function of v_r but Blackshaw exploits the form of the v_c integral. While it is of the form of the error function, he is able to then express the integral over v_c in terms of the difference of two error functions, allowing for in integration over a single variable v_r.

A.9 Explicit expression for $K_0(v, v')$

The velocity scattering kernel can be written for incoming velocity v having an outgoing velocity v', in terms of the relative velocity variable v_r yielding the following expression for an energy loss ($v > v'$),

$$K_0(v,v') = \frac{h^3}{2B}\left(\frac{v'}{v}\right)\exp\left(\frac{B^2v^2}{A}\right) \tag{A.45}$$
$$\times\Bigg\{ \int_{\frac{h^2(v-v')}{2B^2}}^{\frac{h^2(v+v')}{2B^2}} v_r[\sigma_s(v_r)]\cdot\exp\left(\frac{-B^4v_r^2}{Ah^2}\right)\cdot\left[\mathrm{erf}\left(hv'+\frac{B^2v_r}{h}\right) - \mathrm{erf}\left(hv-\frac{B^2v_r}{h}\right)\right]$$
$$+\int_{\frac{h^2(v+v')}{2B^2}}^{\infty} v_r[\sigma_s(v_r)]\cdot\exp\left(\frac{-B^4v_r^2}{Ah^2}\right)\cdot\left[\mathrm{erf}\left(hv'+\frac{B^2v_r}{h}\right) - \mathrm{erf}\left(\frac{B^2v_r}{h}-hv'\right)\right]\Bigg\}$$

where,

$$h^2 \equiv \left(\frac{A+1}{A}\right)B^2, \quad B^2 \equiv \frac{M}{2kT}. \tag{A.46}$$

For the energy gain case ($v < v'$), one merely changes v and v' everywhere they appear in the integrals and the limits. If we assume that the scattering cross section $\sigma_s(v_r)$ is constant then it is convenient to break up each of these integrals into four separate equations with respect to each error function.

$$K_0(v,v') = \sigma_0\frac{h^3}{2B}\left(\frac{v'}{v}\right)\exp\left(\frac{B^2v^2}{A}\right)$$
$$\times\Bigg\{\int_{\frac{h^2(v-v')}{2B^2}}^{\frac{h^2(v+v')}{2B^2}} I_1dv_r - \int_{\frac{h^2(v-v')}{2B^2}}^{\frac{h^2(v+v')}{2B^2}} I_2dv_r + \int_{\frac{h^2(v+v')}{2B^2}}^{\infty} I_3dv_r - \int_{\frac{h^2(v+v')}{2B^2}}^{\infty} I_4dv_r\Bigg\}$$

where

$$I_1 = v_r[\sigma_s(v_r)] \cdot \exp\left(\frac{-B^4 v_r^2}{Ah^2}\right) \cdot \text{erf}\left(hv' + \frac{B^2 v_r}{h}\right)$$

$$I_2 = v_r[\sigma_s(v_r)] \cdot \exp\left(\frac{-B^4 v_r^2}{Ah^2}\right) \cdot \text{erf}\left(hv - \frac{B^2 v_r}{h}\right)$$

$$I_3 = v_r[\sigma_s(v_r)] \cdot \exp\left(\frac{-B^4 v_r^2}{Ah^2}\right) \cdot \text{erf}\left(hv' + \frac{B^2 v_r}{h}\right)$$

$$I_4 = v_r[\sigma_s(v_r)] \cdot \exp\left(\frac{-B^4 v_r^2}{Ah^2}\right) \cdot \text{erf}\left(-hv' + \frac{B^2 v_r}{h}\right)$$

When this is done, each integral has the following form,

$$I_n = \int_{A_n}^{B_n} v_r \cdot \exp\left[-a_n v_r^2\right] \cdot \text{erf}[b_n + c_n v_r] dv_r, \quad \text{for} \quad n = 1, 2, 3, 4 \tag{A.47}$$

where the coefficients a_n, b_n, and c_n are the respective coefficients of the n^{th} integral, while A_n and B_n are the respective bounds of those integrals. And the explicit solution of the velocity kernel is simply

$$K_0(v, v') = \frac{h^3}{2B}\left(\frac{v'}{v}\right) \exp\left(\frac{B^2 v^2}{A}\right) \sum_{n=1}^{4} I_n \tag{A.48}$$

For the moment the derivation will omit the n subscripts and solve for the indefinite integral I_n. Using integration by parts we get,

$$I_n = \frac{1}{-2a} \cdot \exp[-av_r^2] \cdot \text{erf}[b + cv_r] + \frac{1}{\sqrt{\pi}} \frac{c}{a} \int \exp\left[-av_r^2 - (b + cv_r)^2\right] dv_r. \tag{A.49}$$

If we focus on the exponential term in the integrand for a moment we can reconstruct

it in a manner that is easier to integrate. By completing the square we get

$$
\begin{aligned}
&-av_r^2-(b+cv_r)^2 \\
&\qquad = -av_r^2-b^2-2bcv_r-c^2v_r^2 \\
&\qquad = -\left(a+c^2\right)v_r^2-2bcv_r-b^2 \\
&\qquad = -\left(a+c^2\right)\left(v_r^2+\left(\frac{2bc}{a+c^2}\right)v_r+\frac{b^2}{a+c^2}\right) \\
&\qquad = -\left(a+c^2\right)\left(v_r^2+\left(\frac{2bc}{a+c^2}\right)v_r\pm\left(\frac{bc}{a+c^2}\right)^2+\frac{b^2}{a+c^2}\right) \\
&\qquad = -\left(a+c^2\right)\left[\left(v_r+\frac{bc}{a+c^2}\right)^2-\left(\frac{bc}{a+c^2}\right)^2+\frac{b^2}{a+c^2}\right] \\
&\qquad = -\left(a+c^2\right)\left[\left(v_r+\frac{bc}{a+c^2}\right)^2-\left(\frac{b^2c^2}{\left(a+c^2\right)^2}-\frac{b^2\left(a+c^2\right)}{\left(a+c^2\right)^2}\right)\right] \\
&\qquad = -\left(a+c^2\right)\left[\left(v_r+\frac{bc}{a+c^2}\right)^2+\frac{ab^2}{\left(a+c^2\right)^2}\right] \\
&\qquad = -\left(a+c^2\right)\left(v_r+\frac{bc}{a+c^2}\right)^2-\frac{ab^2}{a+c^2}. \qquad \text{(A.50)}
\end{aligned}
$$

If we substitute Eqn. A.50 into the exponential of the integrand,

$$\begin{aligned}
I_n =& \frac{-1}{2a} \cdot \exp[-av_r^2] \cdot \operatorname{erf}[b + cv_r] + \frac{1}{\sqrt{\pi}} \frac{c}{a} \int_B^A \exp\left[-av_r^2 - (b + cv_r)^2\right] dv_r \\
=& \frac{-1}{2a} \cdot \exp[-av_r^2] \cdot \operatorname{erf}[b + cv_r] + \\
& \frac{1}{\sqrt{\pi}} \frac{c}{a} \int_B^A \exp\left[-\left(a + c^2\right)\left(v_r + \frac{bc}{a + c^2}\right)^2 - \frac{ab^2}{a + c^2}\right] dv_r \\
=& \frac{-1}{2a} \cdot \exp[-av_r^2] \cdot \operatorname{erf}[b + cv_r] + \\
& \frac{1}{\sqrt{\pi}} \frac{c}{a} \exp\left[-\frac{ab^2}{a + c^2}\right] \cdot \int_B^A \exp\left[-\left(a + c^2\right)\left(v_r + \frac{bc}{a + c^2}\right)^2\right] dv_r,
\end{aligned} \tag{A.51}$$

and the integral expression is one that is of the form of the error function giving

$$\begin{aligned}
I_n =& \frac{-1}{2a} \cdot \exp[-av_r^2] \cdot \operatorname{erf}[b + cv_r] + \\
& \frac{1}{\sqrt{\pi}} \frac{c}{a} \exp\left[-\frac{ab^2}{a + c^2}\right] \cdot \frac{\sqrt{\pi}}{2\sqrt{(a + c^2)}} \operatorname{erf}\left[\sqrt{(a + c^2)}\left(\frac{bc}{a + c^2} + v_r\right)\right] \\
=& \frac{1}{2a}\Bigg\{ - \exp[-av_r^2] \cdot \operatorname{erf}\left[b + cv_r\right] \\
& + \frac{c}{\sqrt{(a + c^2)}} \exp\left[-\frac{ab^2}{a + c^2}\right] \cdot \operatorname{erf}\left[\sqrt{(a + c^2)}\left(\frac{bc}{a + c^2} + v_r\right)\right] \Bigg\}.
\end{aligned} \tag{A.52}$$

We can simplify this further by recognizing that a and c^2 are always the same in each I_n giving,

$$a + c^2 = \frac{B^4}{Ah^2} + \frac{B^4}{h^2} = \frac{B^4(A+1)}{Ah^2} = B^2$$

$$I_n = \left(\frac{A+1}{2B^2}\right)\left\{\frac{c}{B}\exp\left(-\frac{b^2}{A+1}\right)\cdot\operatorname{erf}\left(B\left(\frac{bc}{B^2}+v_r\right)\right)\right.$$
$$\left. -\exp\left[-\left(\frac{B^2}{A+1}\right)v_r^2\right]\cdot\operatorname{erf}\left[b+cv_r\right]\right\}$$

Now we may rewrite the velocity scattering kernel in the following form

$$\frac{K_0(v,v')}{\sigma_0} = \frac{h^3(A+1)}{4B^3}\left(\frac{v'}{v}\right)\exp\left(\frac{B^2v^2}{A}\right)\cdot\left[I_1\Big|_{B1}^{A1} - I_2\Big|_{B1}^{A1} + I_3\Big|_{B2}^{A2} - I_4\Big|_{B2}^{A2}\right]. \quad \text{(A.53)}$$

Using the definition of I_n above a factor of $(A+1)/2B^2$ has been moved out of the integral evaluation. Now, we will evaluate each n^{th} integral to it's respective bounds using the following equations

$$I_n = \frac{c_n}{B}\exp\left(-\frac{b_n^2}{A+1}\right)\cdot\operatorname{erf}\left(B\left(\frac{b_nc_n}{B^2}+v_r\right)\right)$$
$$-\exp\left(-\left(\frac{B^2}{A+1}\right)v_r^2\right)\cdot\operatorname{erf}\left[b_n+c_nv_r\right]$$

for the downscatter case $v' < v$,

n	a_n	b_n	c_n
1	$\frac{B^2}{A+1}$	hv'	$\frac{B^2}{h}$
2	$\frac{B^2}{A+1}$	hv	$-\frac{B^2}{h}$
3	$\frac{B^2}{A+1}$	hv'	$\frac{B^2}{h}$
4	$\frac{B^2}{A+1}$	$-hv'$	$\frac{B^2}{h}$

$A1 = \frac{h^2(v+v')}{2B^2} = \frac{(A+1)(v+v')}{2A}$

$B1 = \frac{h^2(v-v')}{2B^2} = \frac{(A+1)(v-v')}{2A}$

$A2 = \infty$

$B2 = A1 = \frac{h^2(v+v')}{2B^2} = \frac{(A+1)(v+v')}{2A}$

.

Appendix A. Scattering Kernel Derivation from Blackshaw & Murray

We want to evaluate

$$I_1(A1) - I_1(B1) - I_2(A1) + I_2(B1) + I_3(A2) - I_3(B2) - I_4(A2) + I_4(B2)$$

$$I_1 = I_3 \implies I_1(\infty) = I_3(\infty)$$

which reduces the integrals to

$$-I_1(B1) - I_2(A1) + I_2(B1) + I_3(A2) - I_4(A2) + I_4(B2).$$

Solving for each value in the above equations gives

$$I_1(B1) = I_1\left(\frac{h^2(v-v')}{B^2}\right) = \frac{B}{h}\exp\left(-\frac{h^2v'^2}{A+1}\right)\operatorname{erf}\left(B\left(v' + \frac{h^2(v-v')}{2B^2}\right)\right) - \exp\left(-\frac{h^2(v-v')^2}{4A}\right)\operatorname{erf}\left(hv' + \frac{h(v-v')}{2}\right)$$

$$I_2(A1) = I_2\left(\frac{h^2(v+v')}{B^2}\right) = -\frac{B}{h}\exp\left(-\frac{h^2v^2}{A+1}\right)\operatorname{erf}\left(B\left(-v + \frac{h^2(v+v')}{2B^2}\right)\right) - \exp\left(-\frac{h^2(v+v')^2}{4A}\right)\operatorname{erf}\left(hv - \frac{h(v+v')}{2}\right)$$

$$I_2(B1) = I_2\left(\frac{h^2(v-v')}{B^2}\right) = -\frac{B}{h}\exp\left(-\frac{h^2v^2}{A+1}\right)\operatorname{erf}\left(B\left(-v + \frac{h^2(v-v')}{2B^2}\right)\right) - \exp\left(-\frac{h^2(v-v')^2}{4A}\right)\operatorname{erf}\left(hv - \frac{h(v-v')}{2}\right)$$

$$I_3(A2) = I_3(\infty) = \frac{B}{h}\exp\left(-\frac{h^2v'^2}{A(A+1)}\right)$$

$$I_4(A2) = I_4(\infty) = \frac{B}{h}\exp\left(-\frac{h^2v'^2}{A(A+1)}\right)$$

$$I_4(B2) = I_4\left(\frac{h^2(v+v')}{2B^2}\right) = \frac{B}{h}\exp\left(-\frac{h^2v'^2}{A+1}\right)\operatorname{erf}\left(B\left(-v' + \frac{h^2(v+v')}{2B^2}\right)\right) - \exp\left(-\frac{h^2(v+v')^2}{4A}\right)\operatorname{erf}\left(-hv' + \frac{h(v+v')}{2}\right)$$

Clearly $I_3(A2)$ and $I_4(A2)$ will cancel each other out, also all exponential terms containing $(v \pm v')^2$ will cancel each other out when the integrals are summed together. Further simplification is made by writing all of the integrals in the following manner

$$-I_1(B1) - I_2(A1) + I_2(B1) + I_4(B2)$$

where

$$I_1(B1) = I_1\left(\frac{h^2(v-v')}{2B^2}\right) = \frac{B}{h}\exp\left(-\frac{B^2v'^2}{A}\right)\mathrm{erf}\left[B\left(\frac{A+1}{2A}v + \frac{A-1}{2A}v'\right)\right]$$

$$I_2(A1) = I_2\left(\frac{h^2(v+v')}{2B^2}\right) = \frac{-B}{h}\exp\left(-\frac{B^2v^2}{A}\right)\mathrm{erf}\left[B\left(\frac{A+1}{2A}v' - \frac{A-1}{2A}v\right)\right]$$

$$I_2(B1) = I_2\left(\frac{h^2(v-v')}{2B^2}\right) = \frac{B}{h}\exp\left(-\frac{B^2v^2}{A}\right)\mathrm{erf}\left[B\left(\frac{A+1}{2A}v' + \frac{A-1}{2A}v\right)\right]$$

$$I_4(B2) = I_4\left(\frac{h^2(v+v')}{2B^2}\right) = \frac{B}{h}\exp\left(-\frac{B^2v'^2}{A}\right)\mathrm{erf}\left[(B\left(\frac{A+1}{2A}v - \frac{A-1}{2A}v'\right)\right]$$

giving the final result for the downscattering kernel

$$\begin{aligned}\frac{K_0(v,v')}{\sigma_0} =& \frac{(A+1)^2}{4A}\left(\frac{v'}{v}\right)\left\{\exp\left(\frac{B^2v^2}{A} - \frac{B^2v'^2}{A}\right)\right.\\ &\times\left[\mathrm{erf}\left(B\left(\frac{A+1}{2A}v - \frac{A-1}{2A}v'\right)\right) - \mathrm{erf}\left(B\left(\frac{A+1}{2A}v + \frac{A-1}{2A}v'\right)\right)\right]\\ &\left.+\mathrm{erf}\left(B\left(\frac{A+1}{2A}v' - \frac{A-1}{2A}v\right)\right) + \mathrm{erf}\left(B\left(\frac{A+1}{2A}v' + \frac{A-1}{2A}v\right)\right)\right\}\end{aligned}$$

For upscatter $v' > v$ a different set of coefficients and boundaries are defined by

simply interchanging v and v' from the downscatter case giving

n	a_n	b_n	c_n
1	$\frac{B^2}{A+1}$	hv	$\frac{B^2}{h}$
2	$\frac{B^2}{A+1}$	hv'	$-\frac{B^2}{h}$
3	$\frac{B^2}{A+1}$	hv	$\frac{B^2}{h}$
4	$\frac{B^2}{A+1}$	$-hv$	$\frac{B^2}{h}$

$$A1 = \tfrac{h^2(v'+v)}{2B^2} = \tfrac{(A+1)(v'+v)}{2A}$$
$$B1 = \tfrac{h^2(v'-v)}{2B^2} = \tfrac{(A+1)(v'-v)}{2A}$$
$$A2 = \infty$$
$$B2 = A1 = \tfrac{h^2(v'+v)}{2B^2} = \tfrac{(A+1)(v'+v)}{2A}$$

.

As in the downscatter case, all the same terms will cancel giving the following left over integral solutions

$$I_1(B1) = I_1\left(\frac{h^2(v'-v)}{2B^2}\right) = \frac{B}{h}\exp\left(-\frac{B^2v^2}{A}\right)\operatorname{erf}\left[B\left(\frac{A+1}{2A}v' + \frac{A-1}{2A}v\right)\right]$$

$$I_2(A1) = I_2\left(\frac{h^2(v'+v)}{2B^2}\right) = -\frac{B}{h}\exp\left(-\frac{B^2v'^2}{A}\right)\operatorname{erf}\left[B\left(\frac{A+1}{2A}v - \frac{A-1}{2A}v'\right)\right]$$

$$I_2(B1) = I_2\left(\frac{h^2(v'-v)}{2B^2}\right) = \frac{B}{h}\exp\left(-\frac{B^2v'^2}{A}\right)\operatorname{erf}\left[B\left(\frac{A+1}{2A}v + \frac{A-1}{2A}v'\right)\right]$$

$$I_4(B2) = I_4\left(\frac{h^2(v'+v)}{2B^2}\right) = \frac{B}{h}\exp\left(-\frac{B^2v^2}{A}\right)\operatorname{erf}\left[B\left(\frac{A+1}{2A}v' - \frac{A-1}{2A}v\right)\right]$$

yielding the following scattering kernel for upscatter

$$\begin{aligned}K_0(v,v') =& \frac{(A+1)^2}{4A}\left(\frac{v'}{v}\right)\left\{\exp\left(\frac{B^2v^2}{A} - \frac{B^2v'^2}{A}\right)\right.\\ &\times\left[\operatorname{erf}\left(B\left(\frac{A+1}{2A}v - \frac{A-1}{2A}v'\right)\right) + \operatorname{erf}\left(B\left(\frac{A+1}{2A}v + \frac{A-1}{2A}v'\right)\right)\right]\\ &\left.+\operatorname{erf}\left(B\left(\frac{A+1}{2A}v' - \frac{A-1}{2A}v\right)\right) - \operatorname{erf}\left(B\left(\frac{A+1}{2A}v' + \frac{A-1}{2A}v\right)\right)\right\}\end{aligned}$$

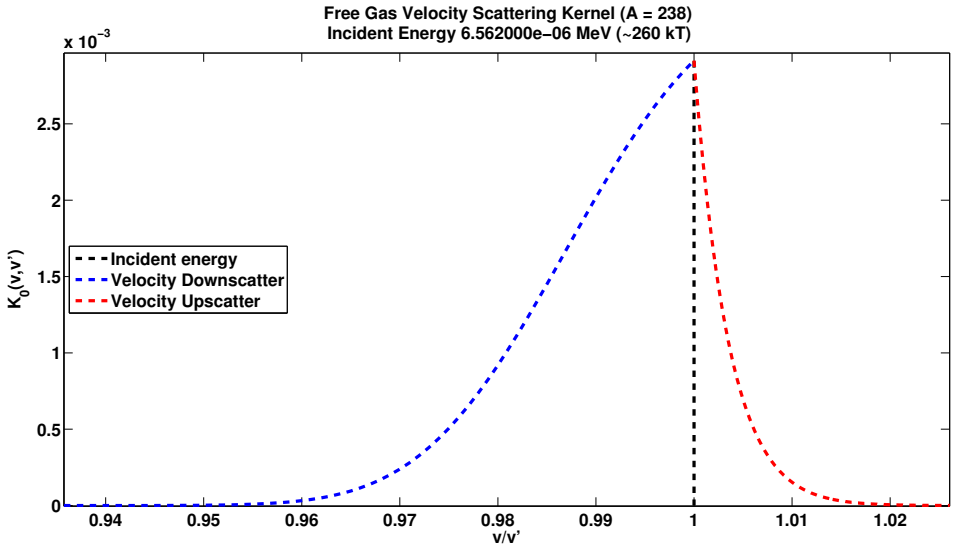

Figure A.1: Zeroth moment of the velocity scattering kernel

A.10 Relationship between $\sigma_s(E)f_{s,E}(E \rightarrow E')$ and $K_0(v, v')$

The following discussion is in relation to the scattering function for a monatomic gas, or "free gas" scattering, which implies that the scattering function is constant. According to neutron scattering theory, the probability of a neutron with an initial energy E experiencing an elastic collision and emerging with some energy $E' + dE'$ is equal to

$$\sigma_s(E)f_{s,E}(E \rightarrow E')dE',$$

where $\sigma_s(E)$ is the probability of an elastic scatter per unit distance and $f_{s,E}(E \rightarrow E')dE'$ is the probability of the neutron emerging with an energy E' within some elemental energy space dE'. Similarly, the probability per unit distance of a neutron with speed v scattering to some v' within dv' is

$$\sigma_s(v)f_{s,v}(v \rightarrow v')dv'$$

where $\sigma_s(v)$ is the probability of an elastic scatter per unit distance and $f_{s,v}(v \rightarrow v')dv'$ is the probability of the neutron emerging with a speed v' within some speed space dv'. While energy and velocity are related by

$$E' = \frac{1}{2}mv'^2 \implies \frac{dE'}{dv'} = mv'$$

where m is the mass of the neutron, it must be true that

$$\sigma_s(E)f_{s,E}(E \rightarrow E')dE' = \sigma_s(v)f_{s,v}(v \rightarrow v')dv'$$

or

$$mv' \cdot \sigma_s(E)f_{s,E}(E \rightarrow E') = \sigma_s(v)f_{s,v}(v \rightarrow v')$$

For "free gas" scattering, the energy transfer function (independent of angle) is expressed by Bell & Glasstone [29] as

$$\begin{aligned}\sigma_s(E)f_{s,E}(E \rightarrow E') = \frac{\eta^2\sigma_{s0}}{2E}\Bigg\{ &\exp\left(\frac{E}{kT} - \frac{E'}{kT}\right) \\ &\times \left[\operatorname{erf}\left(\eta\sqrt{\frac{E}{kT}} - \rho\sqrt{\frac{E'}{kT}}\right) \mp \operatorname{erf}\left(\eta\sqrt{\frac{E}{kT}} + \rho\sqrt{\frac{E'}{kT}}\right)\right] \\ &+ \operatorname{erf}\left(\eta\sqrt{\frac{E'}{kT}} - \rho\sqrt{\frac{E}{kT}}\right) \pm \operatorname{erf}\left(\eta\sqrt{\frac{E'}{kT}} + \rho\sqrt{\frac{E}{kT}}\right)\Bigg\}. \end{aligned} \tag{A.54}$$

where

$$\eta \equiv \frac{A+1}{2\sqrt{A}}, \qquad \rho \equiv \frac{A-1}{2\sqrt{A}}$$

The upper signs are to be used for $E > E'$ and the lower signs for $E < E'$. As previously discussed, Blackshaw derives the velocity scattering kernel $K(\boldsymbol{v}, \boldsymbol{v}')$, which is the probability per unit time for a neutron of initial velocity $\boldsymbol{v}$ to emerge with an outgoing velocity $\boldsymbol{v}'$, in terms of it's angular moments. More specifically, the n^{th}-order spherical-harmonics weighted moment of $K(\boldsymbol{v}, \boldsymbol{v}')$ is

$$K_n(v, v') = \int_{\phi_0}\int_{\mu_0} P_n(\mu_0) \cdot K(\boldsymbol{v}, \boldsymbol{v}')d\mu_0 d\phi_0,$$

for in incoming speed v and outgoing speed v'. The zeroth moment of the velocity scattering kernel is independent of neutron angle since $P_0 = 1$, which means it must be related to the velocity transfer function,

$$K_0(v, v') \propto \sigma_s(v) f_{s.v}(v \to v').$$

By definition, $K_0(v, v')$ is the probability per unit time of scattering from v to v', while the velocity transfer function is the probability per unit distance of scattering from v to v'. In order to change $K_0(v, v')$ from a rate of probability to a probability per unit distance, it must be divided by the the initial speed v of the neutron. Therefore it must be true that

$$\frac{1}{v} \cdot K_0(v, v') = \sigma_s(v) f_{s.v}(v \to v') = mv' \cdot \sigma_s(E) f_{s,E}(E \to E').$$

It has already been shown for downscatter that

$$\begin{aligned}\frac{K_0(v, v')}{v} = \left(\frac{1}{v}\right) \frac{\sigma_{s0}(A+1)^2}{4A} \left(\frac{v'}{v}\right) \Bigg\{ & \exp\left(\frac{B^2 v^2}{A} - \frac{B^2 v'^2}{A}\right) \\ & \times \left[\operatorname{erf}\left(B\left(\frac{A+1}{2A}v - \frac{A-1}{2A}v'\right)\right) - \operatorname{erf}\left(B\left(\frac{A+1}{2A}v + \frac{A-1}{2A}v'\right)\right)\right] \\ & + \operatorname{erf}\left(B\left(\frac{A+1}{2A}v' - \frac{A-1}{2A}v\right)\right) + \operatorname{erf}\left(B\left(\frac{A+1}{2A}v' + \frac{A-1}{2A}v\right)\right) \Bigg\}\end{aligned}$$

What we would like to show is that the zeroth moment velocity scattering kernel above is in fact the same as the energy transfer function described by Eqn.A.54. By only focussing on the downscatter or energy loss equation, begin by writing terms in

energy in terms of speeds to get the following values from Eqn.A.54,

$$\begin{aligned}
\frac{\eta^2}{2E} =& \frac{(A+1)^2}{4A} \cdot \frac{1}{2} \cdot \frac{2}{mv^2} = \frac{(A+1)^2}{4A \cdot mv^2} \\
\frac{E}{kT} =& \frac{mv^2}{2kT} \cdot \frac{\frac{M}{m}}{A} = \frac{Mv^2}{2kTA} \\
\eta\sqrt{\frac{E}{kT}} =& \frac{A+1}{2\sqrt{A}} \cdot \sqrt{\frac{mv^2}{2kT}} = \frac{A+1}{2\sqrt{A}} \cdot \frac{\sqrt{\frac{M}{m}}}{\sqrt{A}} \sqrt{\frac{mv^2}{2kT}} = \frac{A+1}{2A} \cdot \sqrt{\frac{M}{2kT}} \cdot v \\
\rho\sqrt{\frac{E'}{kT}} =& \frac{A-1}{2\sqrt{A}} \cdot \sqrt{\frac{mv'^2}{2kT}} = \frac{A-1}{2\sqrt{A}} \cdot \frac{\sqrt{\frac{M}{m}}}{\sqrt{A}} \sqrt{\frac{mv'^2}{2kT}} = \frac{A-1}{2A} \cdot \sqrt{\frac{M}{2kT}} \cdot v'
\end{aligned}$$

which means that

$$\begin{aligned}
&\sigma_s(E) f_{s,E}\Big(E(v) \to E'(v')\Big) \\
&= \frac{\sigma_{s0}(A+1)^2}{4A \cdot mv^2} \Bigg\{ \exp\left(\frac{Mv^2}{2kTA} - \frac{Mv'^2}{2kTA}\right) \\
&\times \Bigg[\operatorname{erf}\left(\frac{A+1}{2A} \cdot \sqrt{\frac{M}{2kT}} \cdot v - \frac{A-1}{2A} \cdot \sqrt{\frac{M}{2kT}} \cdot v'\right) \\
&- \operatorname{erf}\left(\frac{A+1}{2A} \cdot \sqrt{\frac{M}{2kT}} \cdot v + \frac{A-1}{2A} \cdot \sqrt{\frac{M}{2kT}} \cdot v'\right) \Bigg] \\
&+ \operatorname{erf}\left(\frac{A+1}{2A} \cdot \sqrt{\frac{M}{2kT}} \cdot v' - \frac{A-1}{2A} \cdot \sqrt{\frac{M}{2kT}} \cdot v\right) \\
&+ \operatorname{erf}\left(\frac{A+1}{2A} \cdot \sqrt{\frac{M}{2kT}} \cdot v' + \frac{A-1}{2A} \cdot \sqrt{\frac{M}{2kT}} \cdot v\right) \Bigg\}.
\end{aligned}$$

Recall,

$$B^2 \equiv \frac{M}{2kT}$$

giving the energy transfer function in terms of speed to be written as

$$\sigma_s(E) f_{s,E}\Big(E(v) \to E'(v')\Big) = \frac{\sigma_{s0}(A+1)^2}{4A}\frac{1}{mv^2}\Bigg\{ \exp\left(\frac{B^2v^2}{A} - \frac{B^2v'^2}{A}\right) \times \left[\operatorname{erf}\left(B\left(\frac{A+1}{2A}v - \frac{A-1}{2A}v'\right)\right) - \operatorname{erf}\left(B\left(\frac{A+1}{2A}v + \frac{A-1}{2A}v'\right)\right)\right] + \operatorname{erf}\left(B\left(\frac{A+1}{2A}v' - \frac{A-1}{2A}v\right)\right) + \operatorname{erf}\left(B\left(\frac{A+1}{2A}v' + \frac{A-1}{2A}v\right)\right)\Bigg\}.$$

Now multiplying this result by the Jacobian it follows

$$mv' \cdot \sigma_s(E) f_{s,E}\Big(E(v) \to E'(v')\Big) = \frac{\sigma_{s0}(A+1)^2}{4A}\frac{v'}{v^2}\Bigg\{ \exp\left(\frac{B^2v^2}{A} - \frac{B^2v'^2}{A}\right) \times \left[\operatorname{erf}\left(B\left(\frac{A+1}{2A}v - \frac{A-1}{2A}v'\right)\right) - \operatorname{erf}\left(B\left(\frac{A+1}{2A}v + \frac{A-1}{2A}v'\right)\right)\right] + \operatorname{erf}\left(B\left(\frac{A+1}{2A}v' - \frac{A-1}{2A}v\right)\right) - \operatorname{erf}\left(B\left(\frac{A+1}{2A}v' - \frac{A-1}{2A}v\right)\right)\Bigg\},$$

which is in fact equal to

$$\frac{K_0(v,v')}{v} = \left(\frac{1}{v}\right)\frac{\sigma_{s0}(A+1)^2}{4A}\left(\frac{v'}{v}\right)\Bigg\{ \exp\left(\frac{B^2v^2}{A} - \frac{B^2v'^2}{A}\right) \times \left[\operatorname{erf}\left(B\left(\frac{A+1}{2A}v - \frac{A-1}{2A}v'\right)\right) - \operatorname{erf}\left(B\left(\frac{A+1}{2A}v + \frac{A-1}{2A}v'\right)\right)\right] + \operatorname{erf}\left(B\left(\frac{A+1}{2A}v' - \frac{A-1}{2A}v\right)\right) + \operatorname{erf}\left(B\left(\frac{A+1}{2A}v' + \frac{A-1}{2A}v\right)\right)\Bigg\}$$

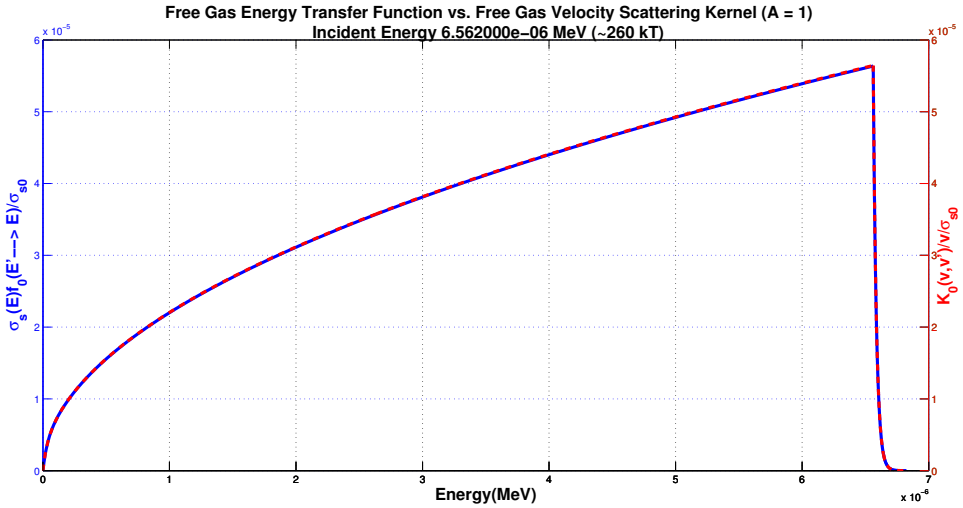

Figure A.2: Plot comparison of the energy transfer function and velocity scattering kernel

A.11 Numerically evaluating $K(\boldsymbol{v}, \boldsymbol{v}')$

The following evaluation will be using an expression from Blackshaw's paper describing the velocity scattering kernel in terms of a constant cross section. Using equation 70 from this paper we get the following:

$$K(\boldsymbol{v}, \boldsymbol{v}') = \frac{B\sigma_0}{(\pi)^{3/2}} \left(\frac{A+1}{2A}\right)^2 \frac{v'^2}{p} \times \exp\left[-\frac{B^2}{4p^2}\left(v'^2 - v^2 + \frac{p^2}{A}\right)^2\right] \tag{A.55}$$

where,

$$p^2 \equiv v^2 + v'^2 - 2vv'\mu_0, \quad B^2 \equiv \frac{M}{2kT}.$$

A simple unit analysis shows that K is $[\#/s]$ or probability per unit time. The goal of this section is to numerically compare the integral over all angles of the above equation to the constant cross section zeroth moment of the velocity scattering kernel K_0. Before the numerical evaluation is done, it was necessary to get an idea of what K looks like. The plot below is a surface plot of the $K(\boldsymbol{v}, \boldsymbol{v}')$ for the case specified in the figure.

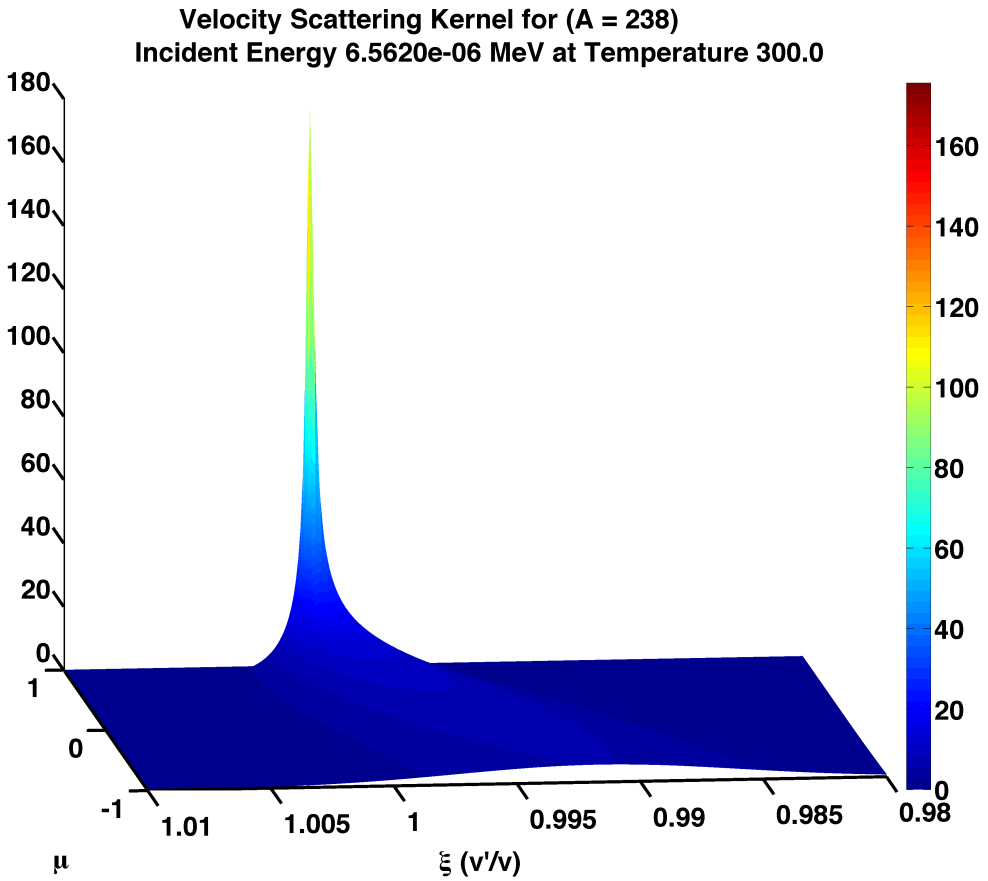

Figure A.3: Examination of singularity around $\xi = 1$ for the velocity scattering kernel $K(\boldsymbol{v}, \boldsymbol{v}')$

Clearly, there exists a strong singularity when the outgoing velocity of the neutron is equal to the incoming velocity causing a highly peaked distribution. Due to this dependence on the relative velocity a change of variable will be made on Eqn.G.1. If we say that

$$\xi = \frac{v'}{v} \tag{A.56}$$

(A.57)

then we can rewrite p in the following manner

$$p^2 = v^2 + v'^2 - 2vv'\mu_0$$

$$p^2 = v^2\left(1 + \frac{v'^2}{v^2} - 2\left(\frac{v'}{v}\right)\mu_0\right)$$

$$p^2 = v^2\left(1 + \xi^2 - 2\xi\mu_0\right)$$

And for further simplification we will redefine

$$p^2 \equiv v^2\widetilde{p}^2, \quad \text{where} \quad \widetilde{p} = \sqrt{|1 + \xi^2 - 2\xi\mu_0|}$$

Substituting the new definition of p into the original equation gives

$$\begin{aligned} K(\boldsymbol{v}, \boldsymbol{v}') &= \frac{B\sigma_0}{(\pi)^{3/2}}\left(\frac{A+1}{2A}\right)^2 \frac{v'^2}{v\widetilde{p}} \times \exp\left[-\frac{B^2}{4v^2\widetilde{p}^2}\left(v'^2 - v^2 + \frac{v^2\widetilde{p}^2}{A}\right)^2\right] \\ &= \frac{B\sigma_0}{(\pi)^{3/2}}\left(\frac{A+1}{2A}\right)^2 \frac{v'^2}{v\widetilde{p}}\frac{v}{v} \times \exp\left[-\frac{B^2}{4v^2\widetilde{p}^2}\left(v^2\left(\frac{v'^2}{v^2} - 1 + \frac{\widetilde{p}^2}{A}\right)\right)^2\right] \\ &= \frac{B\sigma_0}{(\pi)^{3/2}}\left(\frac{A+1}{2A}\right)^2 \xi^2\frac{v}{\widetilde{p}} \times \exp\left[-\frac{B^2v^2}{4\widetilde{p}^2}\left(\xi^2 - 1 + \frac{\widetilde{p}^2}{A}\right)^2\right] \end{aligned}$$

$$K(\boldsymbol{v}, \boldsymbol{v}') = \frac{\xi^2 B\sigma_0}{(\pi)^{3/2}}\left(\frac{A+1}{2A}\right)^2 \left(\frac{v}{\widetilde{p}}\right) \times \exp\left[-\frac{B^2}{4}\left(\frac{v}{\widetilde{p}}\right)^2\left(\xi^2 - 1 + \frac{\widetilde{p}^2}{A}\right)^2\right] \quad \text{(A.58)}$$

Now that we have an equation for the scattering kernel in terms of the relative velocity ξ, we will attempt to numerically integrate out all angles. By definition, this should result in the zeroth moment of the velocity scattering kernel derived by Blackshaw, where the scattering kernel is a function of incoming and outgoing speeds, independent of angle. The following equation will be evaluated using Gauss-Kronrod quadrature:

$$K(v, v') = 2\pi \int \frac{\xi^2 B\sigma_0}{(\pi)^{3/2}}\left(\frac{A+1}{2A}\right)^2 \left(\frac{v}{\widetilde{p}}\right) \times \exp\left[-\frac{B^2}{4}\left(\frac{v}{\widetilde{p}}\right)^2\left(\xi^2 - 1 + \frac{\widetilde{p}^2}{A}\right)^2\right] d\mu_0$$

(A.59)

The variable being integrated is buried in $\widetilde{p}$, so for the simple case of scattering off hydrogen we get

$$
\begin{aligned}
K(v, v', A = 1) &= 2\pi \int \frac{\xi^2 B \sigma_0}{(\pi)^{3/2}} \left(\frac{v}{\widetilde{p}}\right) \times \exp\left[-\frac{B^2}{v^2 \widetilde{p}^2}\left(v'^2 - v' v \mu_0\right)^2\right] d\mu_0 \\
&= 2\pi \int \frac{\xi^2 B \sigma_0}{(\pi)^{3/2}} \left(\frac{v}{\widetilde{p}}\right) \times \exp\left[-\frac{B^2}{v^2 \widetilde{p}^2}\left(v^2\left(\frac{v'^2}{v^2} - \frac{v'}{v}\mu_0\right)\right)^2\right] d\mu_0 \\
&= 2\pi \int \frac{\xi^2 B \sigma_0}{(\pi)^{3/2}} \left(\frac{v}{\widetilde{p}}\right) \times \exp\left[-\frac{B^2 v^2}{\widetilde{p}^2}\left(\xi^2 - \xi\mu_0\right)^2\right] d\mu_0 \\
&= 2\pi \int \frac{\xi^2 B \sigma_0}{(\pi)^{3/2}} \left(\frac{v}{\widetilde{p}}\right) \times \exp\left[-\frac{B^2 v^2 \xi^2}{\widetilde{p}^2}\left(\xi - \mu_0\right)^2\right] d\mu_0
\end{aligned}
$$

While the integrand does contain a singularity when $\widetilde{p} = 0$, it is easily removed since $\widetilde{p} \approx \sqrt{\mu_0}$. As a result the numerical evaluation does a great job when compared to the zeroth moment. Figure A.6 shows the comparison of the numerical integral with the zeroth moment which is taken as the analytic solution.

As a sanity check, we wanted to see what the value of the peak should be when the incoming and outgoing velocities are the same. The following derivation will

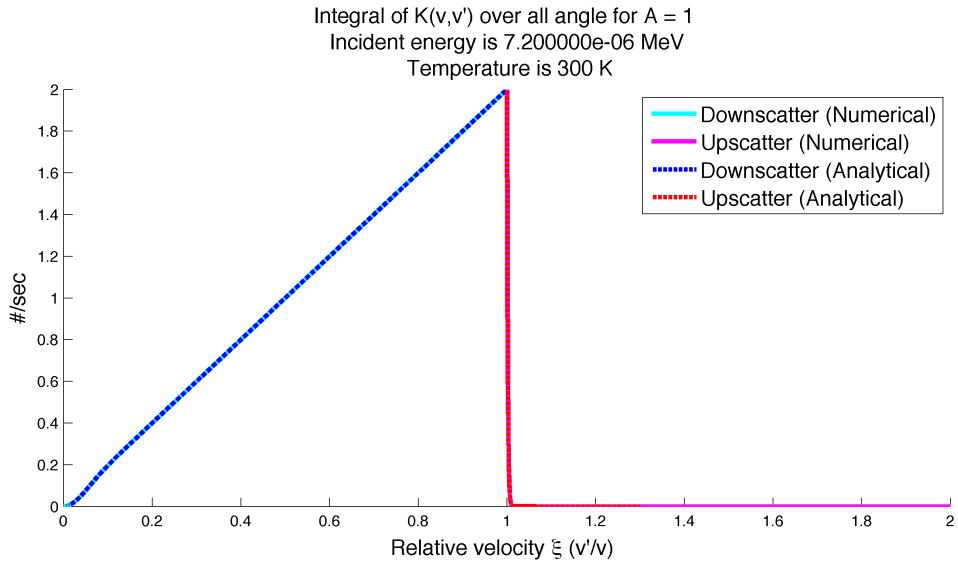

Figure A.4: Numerical evaluation of the integral over all angles of the velocity scattering kernel $K(\boldsymbol{v}, \boldsymbol{v}')$

evaluate the above integral over μ_0 when $\xi = 1$:

$$K(\xi = 1, \mu_0) = \frac{2\pi B \sigma_0}{(\pi)^{3/2}} \left(\frac{A+1}{2A}\right)^2 \int_{-1}^{1} \left(\frac{v}{\widetilde{p}}\right) \times \exp\left[-\frac{B^2}{4}\left(\frac{v}{\widetilde{p}}\right)^2 \left(\frac{\widetilde{p}^2}{A}\right)^2\right] d\mu_0$$

$$\widetilde{p}^2 = 1 + \xi^2 - 2\mu_0 \quad \Longrightarrow \quad \widetilde{p}^2 = 2(1-\mu_0)$$

$$K(\xi = 1, \mu_0) = \frac{2\pi B \sigma_0}{(\pi)^{3/2}} \left(\frac{A+1}{2A}\right)^2 \int_{-1}^{1} \left(\frac{v}{\sqrt{2}(1-\mu_0)^{1/2}}\right) \times \exp\left[-\frac{B^2}{4}\frac{v^2}{2(1-\mu_0)}\left(\frac{4(1-\mu_0)^2}{A^2}\right)\right] d\mu_0$$

$$K(\xi = 1, \mu_0) = \frac{B\sigma_0}{\sqrt{\pi}} \left(\frac{(A+1)^2}{2A^2} \right) \int_{-1}^{1} \left(\frac{v}{\sqrt{2}(1-\mu_0)^{1/2}} \right) \times \exp\left[-\frac{B^2 v^2}{2A^2} (1-\mu_0) \right] d\mu_0$$

Using the following variable transform:

$$x = (1-\mu_0)^{1/2} \quad \Longrightarrow \quad x^2 = (1-\mu_0)$$

$$dx = -\frac{1}{2}(1-\mu_0)^{-1/2} d\mu_0$$

$$x(-1) = 0, \quad x(1) = \sqrt{2}$$

gives

$$K(\xi = 1, \mu_0) = \frac{B\sigma_0}{\sqrt{\pi}} \left(\frac{(A+1)^2}{2A^2} \right) \left(\frac{v}{\sqrt{2}} \right) \int_{0}^{\sqrt{2}} 2 \exp\left[-\frac{B^2 v^2 x^2}{2A^2} \right] dx.$$

Applying another variable transform:

$$y = \frac{Bv}{\sqrt{2}A} x \quad \Longrightarrow \quad dx = \frac{\sqrt{2}A}{Bv} dy$$

$$y(0) = 0, \quad y(\sqrt{2}) = \frac{Bv}{A}$$

$$K(\xi = 1, \mu_0) = \frac{\sigma_0}{\sqrt{\pi}} \left(\frac{(A+1)^2}{A} \right) \int_{0}^{Bv/A} \exp\left[-y^2 \right] dy$$

$$= \frac{\sigma_0}{\sqrt{\pi}} \left(\frac{(A+1)^2}{A} \right) \left(\frac{\sqrt{\pi}}{2} \right) \left[\mathrm{erf}\left(\frac{Bv}{A} \right) - \mathrm{erf}0 \right]$$

$$K(\xi = 1) = K_{peak} = \sigma_0 \left(\frac{(A+1)^2}{2A} \right) \operatorname{erf}\left(\frac{Bv}{A} \right) \tag{A.60}$$

Figure A.6 shows that for targets from $A = [1, 10]$ the peaks of the numerical integrals are identical to the analytic peak value but also the distribution of the numerical evaluation matches the zeroth moments of the scattering kernel.

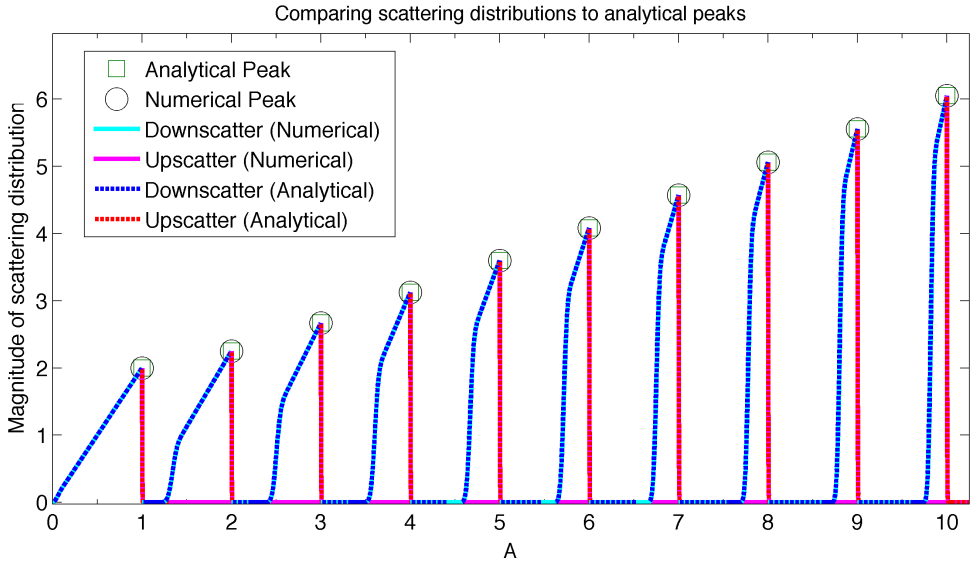

Figure A.5: Numerical evaluation of the integral over all angles of the velocity scattering kernel $K(\boldsymbol{v}, \boldsymbol{v}')$ when $v = v'$.

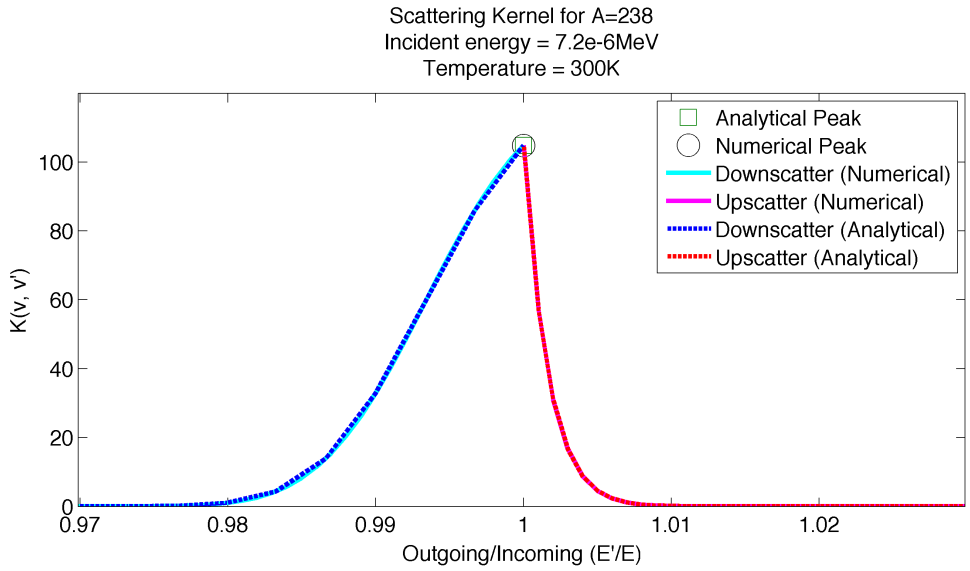

Figure A.6: Scattering kernel distribution for uranium 238 at 300K with a neutron of incident energy 7.2 eV.

A.12 Analytical P_1 Moment Proof

The following section compares the analytical solution obtained for the P_1 moment obtained by Conkie. In this problem the analytical solution is derived assuming hydrogenous material and the speeds of the neutron are in units of thermal speed. Conkie defines the first moment of the scattering kernel as

$$K_1^{(Conkie)}(v,v') = \begin{array}{ll} \frac{2}{v'}\left\{\exp\left[-\left(v^2-v'^2\right)\right]\frac{\left(v'^2-1\right)}{v'}\cdot\operatorname{erf}\left[v'\right]+\frac{2}{\sqrt{pi}}\exp\left[-v^2\right]\right\}, & v>v' \\ \frac{2v}{v'^2}\left\{\frac{\left(v^2-1\right)}{v}\cdot\operatorname{erf}\left[v\right]+\frac{2}{\sqrt{pi}}\exp\left[-v^2\right]\right\}, & v<v' \end{array} \tag{A.61}$$

In order to show the numerical evaluation of the P_1 moment of the scattering kernel is being calculated correctly, the value of $K_1(v, v' = v)$ is derived and compared to Conkie's. Begin with

$$v = v', \quad p^2 \equiv v^2 + v'^2 - 2vv'\mu_0 \implies p^2 = 2v^2(1-\mu_0), \quad B^2 \equiv \frac{M}{2kT}, \quad A = 1$$

$$K(v,v') = \frac{B\sigma_0}{(\pi)^{3/2}} \frac{v^2}{\sqrt{2}v\sqrt{1-\mu}} \times \exp\left[-\frac{B^2}{4(2v^2(1-\mu_0))} \frac{\left(2v^2(1-\mu_0)\right)^2}{1}\right]$$

$$= \frac{\sigma_0 B}{\sqrt{2}\,(\pi)^{3/2}} \frac{v}{\sqrt{1-\mu}} \times \exp\left[-\frac{B^2}{2}v^2(1-\mu_0)\right]$$

The P_1 moment of K is defined as

$$K_1(v, v'=v) \equiv 2\pi \int_1^{-1} \mu_0[\cdots] d\mu_0 \tag{A.62}$$

so then,

$$K_1 = \sqrt{\frac{2}{\pi}}\, Bv \int_1^{-1} \frac{\mu_0}{\sqrt{1-\mu_0}} \exp\left[-\frac{B^2}{2}v^2(1-\mu_0)\right] d\mu_0$$

using the following variable transforms

$$y = \sqrt{1-\mu_0} \implies dy = \frac{-1}{2}\sqrt{1-\mu_0}\, d\mu_0$$

$$C = \sqrt{\frac{2}{\pi}}\, Bv \quad D^2 = \frac{B^2 v^2}{2}$$

gives

$$K_1 = C \int_0^{\sqrt{2}} 2(1-y^2) \exp\left[-D^2 y^2\right] dy$$

$$= 2C \int_0^{\sqrt{2}} (K_{11} - K_{12}) dy$$

Focusing on K_{11} and K_{12} individually

$$K_{11} = \int_0^{\sqrt{2}} \exp\left[-D^2 y^2\right] dy, \quad K_{12} = \int_0^{\sqrt{2}} y^2 \exp\left[-D^2 y^2\right] dy$$

using the following variable transform

$$u = Dy \implies du = D dy$$

and now,

$$K_{11} = \frac{1}{D} \int_0^{D\sqrt{2}} \exp\left[-u^2\right] du, \quad K_{12} = \frac{1}{D^3} \int_0^{D\sqrt{2}} u^2 \exp\left[-u^2\right] du$$

Clearly, K_{11} is the error function, so we will look at K_{12}, making a variable transform on the limits on integration

$$\alpha = D\sqrt{2} \implies \alpha^2 = 2D^2$$

which gives

$$\begin{aligned}
K_{12} &= \frac{1}{D^3} \left[\int_0^{\alpha} u^2 \exp\left[-u^2\right] du \right] \\
&= \frac{1}{D^3} \left[\int_0^{\alpha} d\left(-\frac{1}{2} \exp[-u^2] \right) u \right] \\
&= \frac{1}{D^3} \left[\left[\frac{-u}{2} \exp\left[-u^2\right] \right] \Bigg|_0^{\alpha} + \frac{1}{2} \int_0^{\alpha} \exp[-u^2] du \right] \\
&= \frac{1}{D^3} \left[\frac{-D\sqrt{2}}{2} \exp\left[-2\gamma^2\right] + \frac{1}{2} \int_0^{D\sqrt{2}} \exp[-u^2] du \right] \\
&= \frac{-1}{D^2\sqrt{2}} \exp\left[-2D^2\right] + \frac{1}{2D^2} K_{11}.
\end{aligned}$$

Now putting this value for K_{12} into K_1 gives

$$\begin{aligned}
K_1 &= 2C \left[K_{11} + \frac{1}{D^2\sqrt{2}} \exp\left[-2D^2\right] - \frac{1}{2D^2} K_{11} \right] \\
&= 2C \left[\frac{1}{D^2\sqrt{2}} \exp\left[-2D^2\right] + \left(1 - \frac{1}{2D^2} \right) K_{11} \right].
\end{aligned}$$

Now at this point we need to solve for K_{11}, so looking at it

$$K_{11} = \frac{1}{D}\int_0^{D\sqrt{2}} \exp[-u^2]du$$

$$= \frac{1}{D}\frac{\pi^{1/2}}{2}\mathrm{erf}\left(D\sqrt{2}\right), \quad \text{recall } D^2 = \frac{B^2v^2}{2}$$

$$= \frac{\sqrt{2\pi}}{2Bv}\mathrm{erf}\left(Bv\right)$$

Finally,

$$K_1 = 2C\left[\frac{1}{D^2\sqrt{2}}\exp\left[-2D^2\right] + \left(1 - \frac{1}{2D^2}\right)\frac{1}{Bv}\sqrt{\frac{\pi}{2}}\mathrm{erf}\left(Bv\right)\right] \tag{A.63}$$

and substituting back in values for C and D

$$K_1 = 2\sigma_0\left(\sqrt{\frac{2}{\pi}}Bv\right)\left[\frac{1}{\left(\frac{B^2v^2}{2}\right)\sqrt{2}}\exp\left[-2\left(\frac{B^2v^2}{2}\right)\right] + \left(1 - \frac{1}{2\left(\frac{B^2v^2}{2}\right)}\right)\frac{1}{Bv}\sqrt{\frac{\pi}{2}}\mathrm{erf}\left(Bv\right)\right] \tag{A.64}$$

$$= \frac{2}{Bv}\sigma_0\left[\frac{2}{\sqrt{\pi}}\exp\left[-B^2v^2\right] + \left(\frac{B^2v^2-1}{Bv}\right)\mathrm{erf}\left(Bv\right)\right] \tag{A.65}$$

Conkie normalized the velocity term by the thermal velocity, therefore if we assume that

$$v \to \frac{v}{V_{thermal}} \implies B = 1$$

If we set the cross section equal to unity

$$K_1(v,v) = \frac{2}{v}\left[\frac{2}{\sqrt{\pi}}\exp\left[-v^2\right] + \left(\frac{v^2-1}{v}\right)\mathrm{erf}\left(v\right)\right] \tag{A.66}$$

which is the exact equation given by Conkie

$$K_1^{(Conkie)}(v,v) = \frac{2}{v}\left[\frac{2}{\sqrt{\pi}}\exp\left[-v^2\right] + \left(\frac{v^2-1}{v}\right)\mathrm{erf}\left(v\right)\right] \tag{A.67}$$

A.13 Normalization of the Scattering Kernel

In order to produce the probability density function (PDF), it is necessary to integrate out all outgoing angles and speeds. The zeroth moment is the angular independent scattering kernel, which provides an analytic expression of the scattering in terms of incoming and outgoing speeds. Therefore, in order to get the desired normalization one must simply integrate over all outgoing speeds.

$$P(v, v', \mu_0) = \frac{K(v, v', \mu_0)}{\int_{v'} \int_{\mu_0} K(v, v', \mu_0) d\mu_0' dv'} \tag{A.68}$$

As previously shown, the angular independent velocity scattering kernel is given by:

$$\begin{aligned} K_0(v,v') &= \int_{\mu_0} K(v, v', \mu_0) d\mu_0 \\ &= \frac{\sigma_0 (A+1)^2}{4A} \left(\frac{v'}{v}\right) \Bigg\{ \exp\left(\frac{B^2 v^2}{A} - \frac{B^2 v'^2}{A}\right) \\ &\quad \times \left[\operatorname{erf}\left(B\left(\frac{A+1}{2A} v - \frac{A-1}{2A} v'\right)\right) \mp \operatorname{erf}\left(B\left(\frac{A+1}{2A} v + \frac{A-1}{2A} v'\right)\right)\right] \\ &\quad + \operatorname{erf}\left(B\left(\frac{A+1}{2A} v' - \frac{A-1}{2A} v\right)\right) \pm \operatorname{erf}\left(B\left(\frac{A+1}{2A} v' + \frac{A-1}{2A} v\right)\right) \Bigg\} \end{aligned}$$

where the upper signs represent down scatter and the lower signs are down scatter. The scattering kernel will be written in the following form in order to simplify the integration:

$$\begin{aligned} \int_0^\infty K_0(v, v') dv' = a \int_0^\infty v' \Bigg\{ & \exp\left(\Delta - b v'^2\right) \times \left[\operatorname{erf}\left(c_v - d v'\right) \mp \operatorname{erf}\left(c_v + d v'\right)\right] \\ & + \operatorname{erf}\left(c v' - d_v\right) \pm \operatorname{erf}\left(c v' + d_v\right) \Bigg\} dv' \end{aligned}$$

where,

$$a = \frac{\sigma_0(A+1)^2}{4Av}, \qquad \Delta = \frac{B^2v^2}{A}, \qquad , b = \frac{B^2}{A}$$
$$c = B\frac{A+1}{2A}, \qquad c_v = B\frac{A+1}{2A}(v), \qquad , d = B\frac{A-1}{2A}, \qquad , d_v = B\frac{A-1}{2A}(v)$$

Recall, the integral must be split due to bounds of the minimum and maximum speeds in the center of mass frame. The integration over all speeds then becomes:

$$\int_0^\infty K_0(v,v')dv' = \int_0^v K_{0_{down}}(v,v')dv' + \int_v^\infty K_{0_{up}}(v,v')dv' \tag{A.69}$$

Inspection of this integral shows that four separate integrals may be integrated individually, specifically:

$$\int_0^\infty K_0(v,v')dv' = a\Big(I_1 - I_2 + I_3 + I_4\Big) + a\Big(I_1 + I_2 + I_3 - I_4\Big)$$

where,

$$I_1 = \exp(\Delta)\int v'\exp(-bv'^2)\mathrm{erf}(c_v - dv')dv'$$
$$I_2 = \exp(\Delta)\int v'\exp(-bv'^2)\mathrm{erf}(c_v + dv')dv'$$
$$I_3 = \int v'\mathrm{erf}(cv' - d_v)dv'$$
$$I_4 = \int v'\mathrm{erf}(cv' + d_v)dv'$$

These integrals were evaluated using *Wolfram Alpha*'s symbolic integrator.

$$I_1\Big|_{v_{min}}^{v_{max}} = \frac{-1}{2b\sqrt{b+d^2}}\Bigg[d\cdot\exp\left(\Delta-\frac{bc_v^2}{b+d^2}\right)\operatorname{erf}\left(\frac{bv'-c_vd+d^2v'}{\sqrt{b+d^2}}\right) + \sqrt{b+d^2}\cdot\exp\left(\Delta-bv'^2\right)\operatorname{erf}\left(c_v-dv'\right)\Bigg]\Bigg|_{v_{min}}^{v_{max}}$$

$$I_2\Big|_{v_{min}}^{v_{max}} = \frac{1}{2b\sqrt{b+d^2}}\Bigg[d\cdot\exp\left(\Delta-\frac{bc_v^2}{b+d^2}\right)\operatorname{erf}\left(\frac{bv'+c_vd+d^2v'}{\sqrt{b+d^2}}\right) - \sqrt{b+d^2}\cdot\exp\left(\Delta-bv'^2\right)\operatorname{erf}\left(c_v+dv'\right)\Bigg]\Bigg|_{v_{min}}^{v_{max}}$$

$$I_3\Big|_{v_{min}}^{v_{max}} = \frac{1}{4c^2}\Bigg[-(2c^2v'^2-2d_v^2-1)\operatorname{erf}(-cv'+d_v) + \frac{2}{\sqrt{\pi}}\exp\left(-(d_v-cv')^2\right)(cv'+d_v)\Bigg]\Bigg|_{v_{min}}^{v_{max}}$$

$$I_4\Big|_{v_{min}}^{v_{max}} = \frac{1}{4c^2}\Bigg[(2c^2v'^2-2d_v^2-1)\operatorname{erf}(cv'+d_v) + \frac{2}{\sqrt{\pi}}\exp\left(-(d_v+cv')^2\right)(cv'-d_v)\Bigg]\Bigg|_{v_{min}}^{v_{max}}$$

Using the respective bounds on these integrals for the down scatter and up scatter case will cause some integrals to cancel giving,

$$\int_0^\infty K_0(v,v')dv' = a\Big(I_1(\infty)-I_1(0)+I_2(\infty)+I_2(0) + I_3(\infty)-I_3(0)-I_4(0)-I_4(\infty)+2I_4(v)-2I_2(v)\Big)$$

$$I_2(0) - I_1(0) = 0$$

$$I_1(\infty) + I_2(\infty) = 0$$

$$-I_3(0) - I_4(0) = 0$$

$$I_3(\infty) - I_4(\infty) = 0$$

$$\int_0^\infty K_0(v, v')dv' = 2a\Big(I_4(v) - I_2(v)\Big) \tag{A.70}$$

$$2\Big(I_4(v) - I_2(v)\Big) =$$

$$\frac{1}{2c^2}\left[(2c^2v^2 - 2d^2v^2 - 1)\cancelto{1}{\mathrm{erf}(cv + dv)} + \frac{2}{\sqrt{\pi}}\cancelto{0}{\exp\left(-(dv + cv)^2\right)}(cv - dv)\right]$$

$$-\frac{1}{b\sqrt{b + d^2}}\left[d \cdot \cancelto{1}{\exp\left(\Delta - \frac{bc_v^2}{b + d^2}\right)}\mathrm{erf}\left(\cancelto{1}{\frac{bv + cvd + d^2v}{\sqrt{b + d^2}}}\right)\right]^1$$

$$- \sqrt{b + d^2} \cdot \cancelto{1}{\exp\left(\Delta - bv^2\right)}\cancelto{1}{\mathrm{erf}\left(c_v + dv\right)}\Bigg]^1$$

$$= \frac{1}{2c^2}\left[(2c^2v^2 - 2d^2v^2 - 1)\right] - \left[\frac{d}{b\sqrt{b + d^2}} - \frac{1}{b}\right]$$

$$= \left[v^2\left(1 - \frac{d^2}{c^2}\right) - \frac{1}{2c^2}\right] - \left[\frac{d}{b\sqrt{b + d^2}} - \frac{1}{b}\right]$$

When we reintroduce the variables from the original equation, we get

$$2a\Bigg(I_4(v) - I_2(v)\Bigg) = \left(\frac{\sigma_0(A+1)^2}{4Av}\right)\Bigg\{v^2\left[1 - \frac{(A-1)^2}{(A+1)^2}\right] - \frac{2A^2}{(A+1)^2B^2} - \frac{(A-1)}{2B}\cdot\frac{1}{\sqrt{\frac{B^2}{A} + \frac{B^2(A-1)^2}{4A^2}}} + \frac{A}{B^2}\Bigg\}$$

$$= \left(\frac{\sigma_0(A+1)^2}{4Av}\right)\Bigg\{v^2\left[1 - \frac{(A-1)^2}{(A+1)^2}\right] - \frac{A}{(A+1)^2B^2}\Bigg\}$$

Finally, the normalization is given simply by

$$\int_0^\infty K_0(v, v')dv' = \sigma_0\left(v - \frac{1}{4vB^2}\right) \tag{A.71}$$

Now that we have integrated out both outgoing angle and outgoing velocity, the normalized scattering kernel is given by:

$$P(v, v', \mu_0) = \frac{K(v, v', \mu)}{\int_{v'}\int_{\mu_0} K(v, v', \mu)d\mu_0'dv'} = \frac{K(v, v', \mu_0)}{\sigma_0\left(v - \frac{1}{4vB^2}\right)} \tag{A.72}$$

The figures below are the respective PDF's for angular independent distributions.

A.14 Calculating $\frac{dP}{dT}$

In order to calculate the change in the probability density function with respect to temperature, one must calculate the following:

$$\frac{dP}{dT} = \frac{d}{dT}\left[\frac{K(v,v',\mu_0,T)}{\widehat{K}(T)}\right], \quad \text{where,} \quad \widehat{K} = \int_{v'}\int_{\mu_0} K(v,v',\mu_0)d\mu_0 dv' \tag{A.73}$$

which gives,

$$\frac{dP}{dT} = \frac{1}{\widehat{K}}\left(\frac{dK}{dT} - \frac{d\widehat{K}}{dT}\frac{K}{\widehat{K}}\right) \tag{A.74}$$

As seen in the previous section $\widehat{K}$ is given by:

$$\widehat{K} = \sigma_0\left(v - \frac{1}{4vB^2}\right) \tag{A.75}$$

Since both the scattering kernel and the normalization both contain the scattering cross section, all derivatives are taken with this cancellation.

$$\begin{aligned}
\frac{d\widehat{K}}{dT} &= \frac{d}{dT}\left[v - \frac{1}{4vB^2}\right] \\
&= \frac{dB}{dT}\left[\frac{1}{2vB^3}\right], \quad \text{recall,} \quad \frac{dB}{dT} = -\frac{B}{2T} \\
&= -\frac{1}{4TvB^2}, \quad \text{recall } B^2 = \frac{M}{2kT} \\
&= -\frac{k}{2Mv}
\end{aligned}$$

It is clear from the form of $d\widehat{K}/dT$ that the change in the normalization factor with respect to temperature is independent to temperature itself.

A.14.1 Evaluating the Temperature Derivative of the Scattering Kernel $\frac{dK(v,v',\mu_0,T)}{dT}$

$$K(v,v',\mu_0,T) = \frac{B\sigma_0}{(\pi)^{3/2}}\left(\frac{A+1}{2A}\right)^2\frac{v'^2}{p}\times\exp\left[-\frac{B^2}{4p^2}\left(v'^2-v^2+\frac{p^2}{A}\right)^2\right] \quad \text{(A.76)}$$

where,

$$p^2 \equiv v^2+v'^2-2vv'\mu_0, \quad B^2 \equiv \frac{M}{2kT}.$$

For simplicity, use the following variable substitutions

$$\gamma = \frac{\sigma_0}{(\pi)^{3/2}}\left(\frac{A+1}{2A}\right)^2\frac{v'^2}{p} \quad \text{and} \quad \Omega = \frac{\left(v'^2-v^2+\frac{p^2}{A}\right)^2}{4p^2}$$

which gives a more simple equation

$$K(v,v',\mu_0,T) = \gamma B(T)\exp\left(-\Omega B(T)^2\right) \quad \text{(A.77)}$$

so then

$$\frac{dK(v,v',\mu_0,T)}{dT} = \frac{dK}{dB(T)}\cdot\frac{dB(T)}{dT}$$

$$= \left[\gamma\exp\left[-\Omega B(T)^2\right]-(2\Omega B(T)\exp\left[-\Omega B(T)^2\right])\gamma B(T)\right]\frac{dB(T)}{dT}$$

where

$$\frac{dB(T)}{dT} = \frac{d}{dT}\left(\sqrt{\frac{M}{2kT}}\right) = \sqrt{\frac{M}{2k}}\cdot\frac{-1}{2}\cdot\frac{1}{T^{3/2}} = -\frac{B(T)}{2T}$$

and now,

$$\frac{dK(v,v',\mu_0,T)}{dT} = \left[\exp\left[-\Omega B(T)^2\right]-(2\Omega B(T)^2\exp\left[-\Omega B(T)^2\right])\gamma\right]\frac{-B(T)}{2T}$$

$$= 2\Omega B(T)\gamma B(T)\exp\left[-\Omega B(T)^2\right]\frac{B(T)}{2T}-\gamma B(T)\exp\left[-\Omega B(T)^2\right]\frac{1}{2T}$$

using, the definition of K above

$$\frac{dK(v,v',\mu_0,T)}{dT} = \frac{\Omega B(T)^2}{T} K(v,v',\mu_0,T) - \frac{1}{2T} K(v,v',\mu_0,T) \tag{A.78}$$

$$\frac{dK(v,v',\mu_0,T)}{dT} = \left(\frac{2\Omega B(T)^2 - 1}{2T}\right) \cdot K(v,v',\mu_0,T) \tag{A.79}$$

Now substituting Ω back into our solution gives

$$\frac{dK(v,v',\mu_0,T)}{dT} = K(v,v',\mu_0,T) \left(\frac{B(T)^2}{T} \left(\frac{\left(v'^2 - v^2 + \frac{p^2}{A}\right)^2}{4p^2} \right) - \frac{1}{2T} \right) \tag{A.80}$$

$v' = v \quad \mu_0 = .98$		Central Difference/Analytic			
A, E, T	Analytic	$\Delta T = 50$	$\Delta T = 25$	$\Delta T = 10$	$\Delta T = 5$
238, 6.67eV, 300K	-9.042E-2	1.017	1.004	1.001	1.000
238, 6.67eV, 1500K	-8.302E-3	1.001	1.000	1.000	1.000
238, 36.67eV, 300K	-1.818E-1	1.013	1.003	1.001	1.000
238, 36.67eV, 1500K	-1.890E-2	1.001	1.000	1.000	1.000
12, 6.67eV, 300K	-1.124E-2	0.996	0.999	1.000	1.000
12, 6.67eV, 1500K	-1.912E-3	1.001	1.000	1.000	1.000
12, 36.67eV, 300K	2.393E-2	1.018	1.004	1.001	1.000
12, 36.67eV, 1500K	-2.134E-3	0.998	1.000	1.000	1.000

Table A.1: Central difference derivative comparison to exact analytic values.

Table A.1 was made as a sanity check in order to ensure that the derivative of the scattering kernel was calculated correctly.

A.14.2 Results for PDF

Now all the pieces of the normalized scattering kernel have been calculated. Results below show the normalized scattering distribution for an incident neutron with 6.67 eV on uranium 238.

$v' = 0.98v \quad \mu_0 = .98$		Central Difference/Analytic			
dP/dT	Analytic	$\Delta T = 50$	$\Delta T = 25$	$\Delta T = 10$	$\Delta T = 5$
238, 6.67eV, 300K	-2.531E-6	1.017	1.004	1.001	1.000
238, 6.67eV, 1500K	-2.324E-6	1.001	1.000	1.000	1.000
238, 36.67eV, 300K	-2.171E-6	1.013	1.003	1.001	1.000
238,36.67eV, 1500K	-2.257E-7	1.001	1.000	1.000	1.000
12, 6.67eV, 300K	-3.146E-7	0.996	0.999	1.000	1.000
12, 6.67eV, 1500K	-5.351E-8	1.001	1.000	1.000	1.000
12, 36.67eV, 300K	2.857E-7	1.018	1.004	1.001	1.000
12, 36.67eV, 1500K	-2.548E-8	0.998	1.000	1.000	1.000

Table A.2: Central difference derivative comparison to exact analytic values.

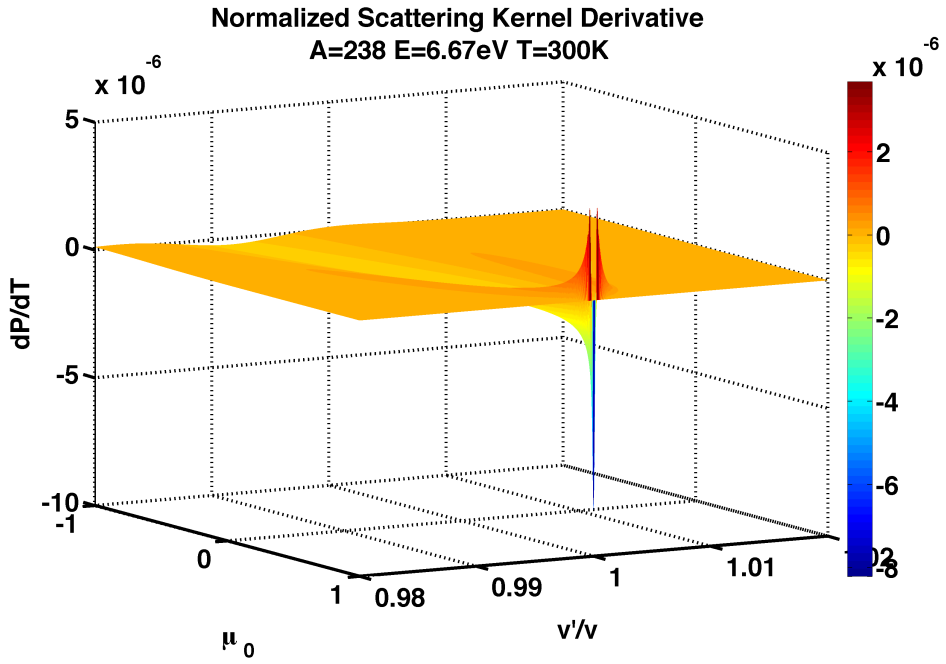

Figure A.7: Derivative of the normalized scattering kernel distribution for uranium 238 at 300K with a neutron of incident energy 6.67 eV.

Appendix B

Material Number Densities

Fuel Enrichment (wt.%)	^{16}**O**	^{234}**U**	^{235}**U**	^{238}**U**
0.711	4.61171 x 10^{-2}	0	1.66029 x 10^{-4}	2.28925 x 10^{-2}
1.6	4.61218 x 10^{-2}	3.00175 x 10^{-6}	3.73618 x 10^{-4}	2.26843 x 10^{-2}
2.4	4.61260 x 10^{-2}	4.50257 x 10^{-6}	5.60420 x 10^{-4}	2.24981 x 10^{-2}
3.1	4.61297 x 10^{-2}	5.51576 x 10^{-6}	7.23867 x 10^{-4}	2.23352 x 10^{-2}
3.9	4.61339 x 10^{-2}	7.31651 x 10^{-6}	9.10661 x 10^{-4}	2.21490 x 10^{-2}
4.5	4.61317 x 10^{-2}	8.44205 x 10^{-6}	1.05075 x 10^{-4}	2.20093 x 10^{-2}
5.0	4.61397 x 10^{-2}	9.37995 x 10^{-6}	1.16749 x 10^{-4}	2.18930 x 10^{-2}

Table B.1: Number Density of UO_2 Fuel at 600K/900K for Different Enrichments (atoms/barn-cm)

Material	**Isotope**	**Number density in atoms/barn-cm**	
		600K	**900K**
Cladding	^{90}Zr	2.17036 x 10^{-}2	2.17036 x 10^{-}2
	^{91}Zr	4.7330 x 10−3	4.7330 x 10−3
	^{92}Zr	7.2345 x 10−3	7.2345 x 10−3
	^{94}Zr	7.3315 x 10−3	7.3315 x 10−3
	^{96}Zr	1.1811 x 10−3	1.1811 x 10−3
Moderator	^{1}H	4.21838 x 10^{-2}	4.21838 x 10^{-2}
	^{10}B	4.42326 x 10^{-2}	4.42326 x 10^{-2}
	^{11}B	1.02133 x 10^{-5}	1.02133 x 10^{-5}
	^{16}O	2.21163 x 10^{-2}	2.21163 x 10^{-2}

Table B.2: Number Density of Clad & Moderator for Different Temperatures

Appendix C

Reference Data

Reference Case (NJOY + MCNP)			
Enrichment (wt. %)	**HFP $k_{eff} \pm \sigma$**	**HZP $k_{eff} \pm \sigma$**	**Doppler Coefficient ($\Delta\rho/\Delta T$) (pcm/K)**
0.711	0.65979 (19)	0.66556 (18)	-4.38 (.20)
1.6	0.95293 (25)	0.96094 (26)	-2.92 (.13)
2.4	1.08997 (26)	1.09912 (27)	-2.55 (.10)
3.1	1.16744 (27)	1.17718 (27)	-2.36 (.09)
3.9	1.22920 (30)	1.23967 (27)	-2.29 (.09)
4.5	1.26526 (27)	1.27501 (30)	-2.01 (.09)
5.0	1.28920 (29)	1.29901 (31)	-1.95 (.08)

Table C.1: Results taken from Brown et al. ANS Transaction Summer 2012 with 5 million particles

Reference Case (NJOY + MCNP)

Enrichment (wt. %)	**HFP $k_{eff} \pm \sigma$**	**HZP $k_{eff} \pm \sigma$**	**Doppler defect $\Delta\rho$ (pcm)**	**Doppler Coefficient $(\Delta\rho/\Delta T)$ (pcm/K)**
0.711	0.659742 (27)	0.665657 (27)	-1346.8 (8.7)	-4.489 (29)
1.6	0.952675 (36)	0.960809 (36)	-888.7 (5.6)	-2.962 (19)
2.4	1.090005 (39)	1.099048 (39)	-754.9 (4.7)	-2.516 (16)
3.1	1.167462 (41)	1.177192 (41)	-708.0 (4.2)	-2.360 (14)
3.9	1.229839 (42)	1.239809 (42)	-653.9 (3.9)	-2.180 (13)
4.5	1.265040 (42)	1.275161 (42)	-627.4 (3.7)	-2.091 (12)
5.0	1.289275 (42)	1.298923 (42)	-576.1 (3.6)	-1.920 (12)

Table C.2: Results calculated with MCNP6.1 using 24 million particles

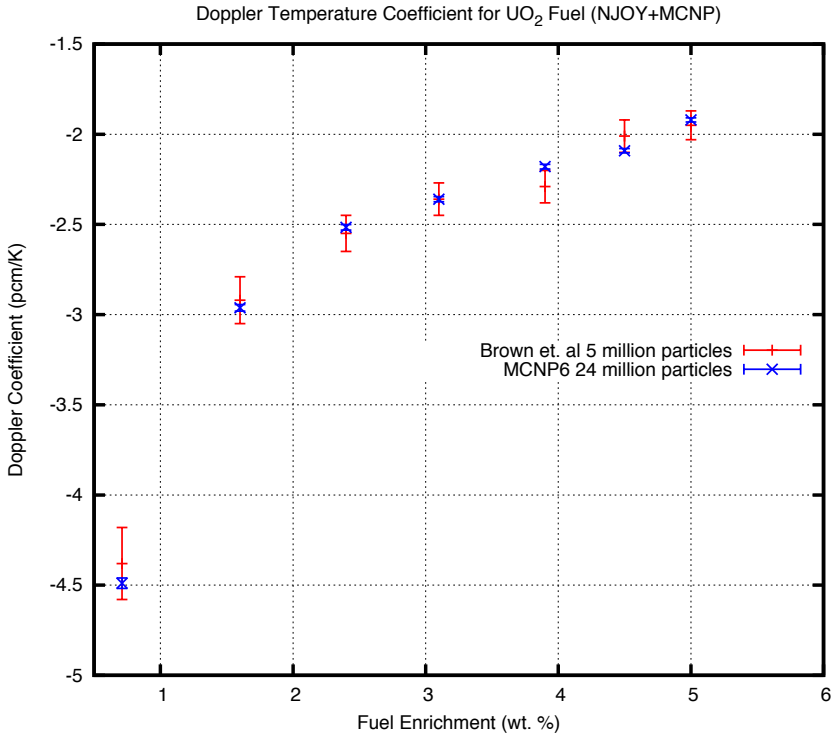

Figure C.1: Comparison of reference solution with an increase of particle samples

Case I

Enrichment (wt. %)	**HFP $k_{eff} \pm \sigma$**	**HZP $k_{eff} \pm \sigma$**	**Doppler defect $\Delta\rho$ (pcm)**	**Doppler Coefficient $(\Delta\rho/\Delta T)$ (pcm/K)**
0.711	0.659780 (57)	0.665722 (56)	-1353 (18)	-4.510 (61)
1.6	0.952570 (75)	0.960893 (76)	-909 (12)	-3.030 (39)
2.4	1.089900 (82)	1.099162 (81)	-773.1 (9.6)	-2.577 (32)
3.1	1.167477 (85)	1.177080 (85)	-698.8 (8.7)	-2.329 (29)
3.9	1.229887 (88)	1.239723 (87)	-645.1 (8.7)	-2.150 (27)
4.5	1.265047 (88)	1.275237 (88)	-631.6 (7.7)	-2.105 (26)
5.0	1.289294 (88)	1.299120 (89)	-586.7 (7.6)	-1.956 (25)

Case II

Enrichment (wt. %)	**HFP $k_{eff} \pm \sigma$**	**HZP $k_{eff} \pm \sigma$**	**Doppler defect $\Delta\rho$ (pcm)**	**Doppler Coefficient $(\Delta\rho/\Delta T)$ (pcm/K)**
0.711	0.659716 (56)	0.665617 (57)	-1343 (18)	-4.479 (60)
1.6	0.952598 (77)	0.960885 (75)	-905 (12)	-3.018 (39)
2.4	1.090034 (82)	1.099021 (82)	-750.2 (9.7)	-2.501 (32)
3.1	1.167541 (86)	1.177194 (85)	-702.3 (8.8)	-2.341 (29)
3.9	1.230054 (86)	1.239785 (86)	-638.1 (8.1)	-2.127 (27)
4.5	1.265054 (88)	1.275071 (89)	-621.0 (7.7)	-2.070 (26)
5.0	1.289265 (88)	1.298870 (90)	-573.5 (7.5)	-1.912 (25)

Case III

Enrichment (wt. %)	**HFP $k_{eff} \pm \sigma$**	**HZP $k_{eff} \pm \sigma$**	**Doppler defect $\Delta\rho$ (pcm)**	**Doppler Coefficient $(\Delta\rho/\Delta T)$ (pcm/K)**
0.711	0.659676 (56)	0.665708 (57)	-1373 (18)	-4.578 (60)
1.6	0.952649 (74)	0.960884 (77)	-900 (12)	-2.999 (39)
2.4	1.089863 (82)	1.099225 (82)	-781.5 (9.7)	-2.605 (32)
3.1	1.167550 (87)	1.177037 (86)	-690.4 (8.9)	-2.301 (30)
3.9	1.229905 (87)	1.239640 (88)	-638.5 (8.1)	-2.128 (27)
4.5	1.265048 (87)	1.275091 (89)	-622.6 (7.7)	-2.075 (26)
5.0	1.289188 (88)	1.299002 (88)	-586.0 (7.5)	-1.953 (25)

Case VI

Enrichment (wt. %)	**HFP $k_{eff} \pm \sigma$**	**HZP $k_{eff} \pm \sigma$**	**Doppler defect $\Delta\rho$ (pcm)**	**Doppler Coefficient $(\Delta\rho/\Delta T)$ (pcm/K)**
0.711	0.659718 (56)	0.665643 (56)	-1349 (18)	-4.498 (60)
1.6	0.952572 (75)	0.960889 (75)	-909 (12)	-3.029 (39)
2.4	1.089921 (82)	1.099060 (83)	-762.9 (9.8)	-2.543 (33)
3.1	1.167618 (85)	1.177168 (85)	-694.8 (8.8)	-2.316 (29)
3.9	1.229932 (89)	1.239881 (87)	-652.4 (8.2)	-2.175 (27)
4.5	1.265178 (88)	1.275172 (87)	-619.5 (7.7)	-2.065 (26)
5.0	1.289420 (87)	1.299027 (88)	-573.5 (7.4)	-1.912 (25)

Table C.3: Doppler coefficient results for varying OTF data sets

Appendix D

Assembly Data

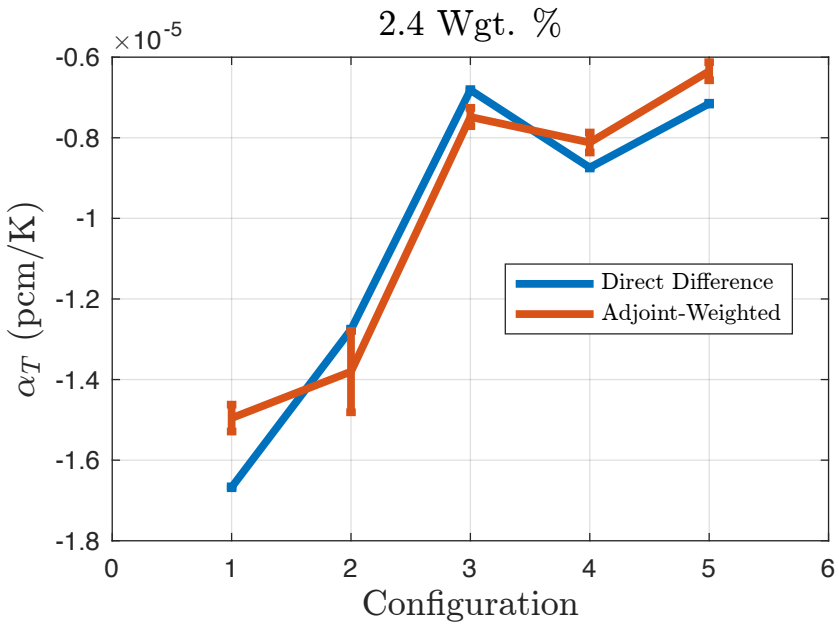

Figure D.1: Doppler temperature coefficient comparison with uranium containing 2.4 wgt. %

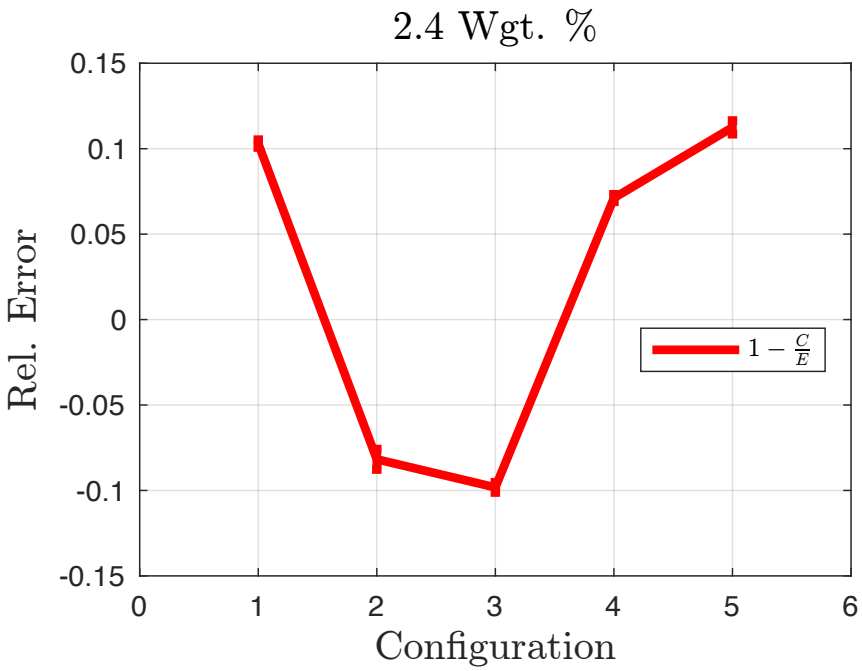

Figure D.2: Doppler temperature coefficient comparison with uranium containing 2.4 wgt. %

2.4 Wgt. %

Config.	**Direct Difference** $(\Delta\rho/\Delta T)$ **(1/K)**	**Adjoint-Weighted** (α_T) **(1/K)**
1	-1.6673e-05	-1.4956e-05
2	-1.2760e-05	-1.3803e-05
3	-6.8150e-06	-7.4843e-06
4	-8.7391e-06	-8.1175e-06
5	-7.1531e-06	-6.3485e-06

Table D.1: Doppler temperature coefficient comparison for fuel assemblies computed with direct difference and the adjoint method.

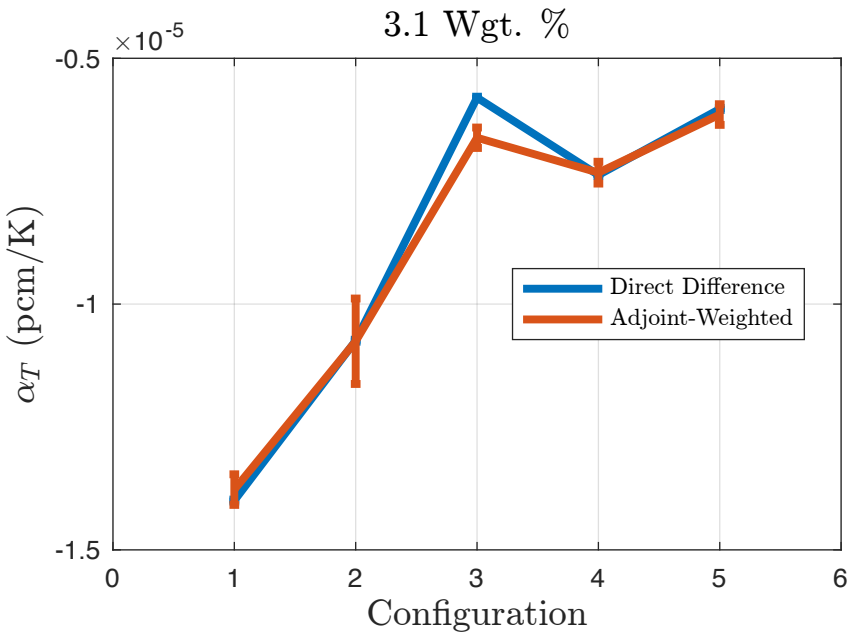

Figure D.3: Doppler temperature coefficient comparison with uranium containing 3.1 wgt. %

3.1 Wgt. %

Config.	**Direct Difference** $(\Delta\rho/\Delta T)$ **(1/K)**	**Adjoint-Weighted** (α_T) **(1/K)**
1	-1.3997e-05	-1.3774e-05
2	-1.0745e-05	-1.0756e-05
3	-5.8005e-06	-6.6161e-06
4	-7.3755e-06	-7.3264e-06
5	-6.0308e-06	-6.1440e-06

Table D.2: Doppler temperature coefficient comparison for fuel assemblies computed with direct difference and the adjoint method.

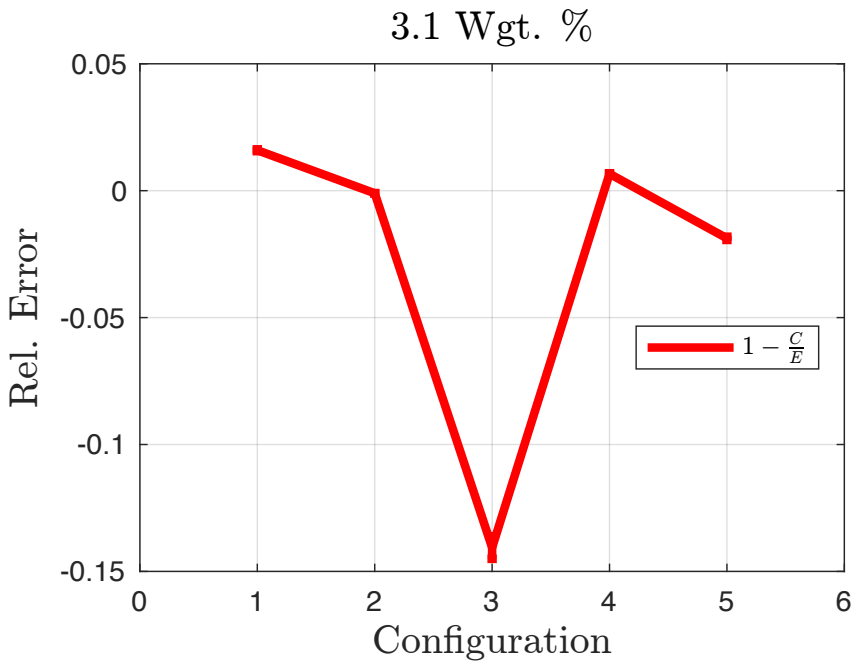

Figure D.4: Doppler temperature coefficient comparison with uranium containing 3.1 wgt. %

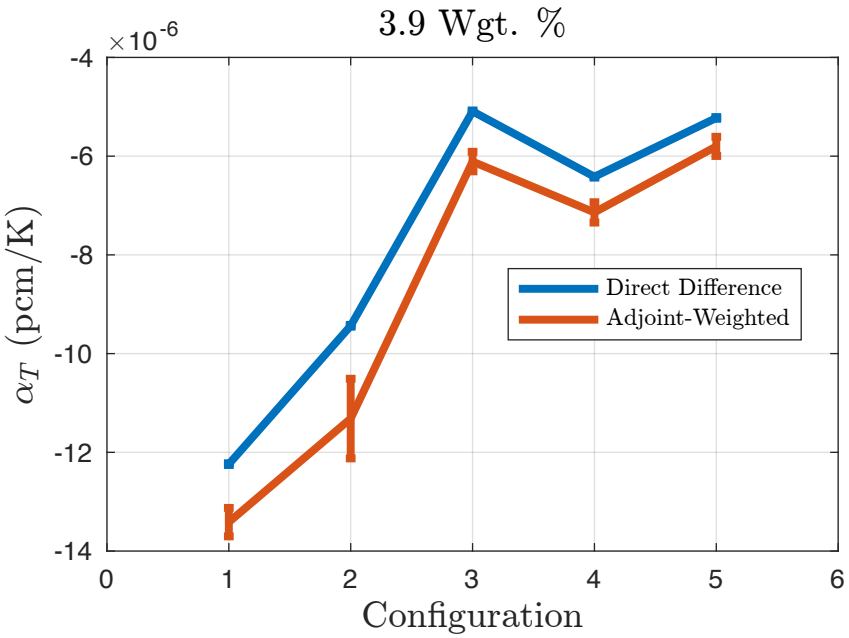

Figure D.5: Doppler temperature coefficient comparison with uranium containing 3.9 wgt. %

3.9 Wgt. %

Config.	**Direct Difference** $(\Delta\rho/\Delta T)$ **(1/K)**	**Adjoint-Weighted** (α_T) **(1/K)**
1	-1.2239e-05	-1.3414e-05
2	-9.4367e-06	-1.1316e-05
3	-5.0920e-06	-6.1100e-06
4	-6.4170e-06	-7.1393e-06
5	-5.2256e-06	-5.8023e-06

Table D.3: Doppler temperature coefficient comparison for fuel assemblies computed with direct difference and the adjoint method.

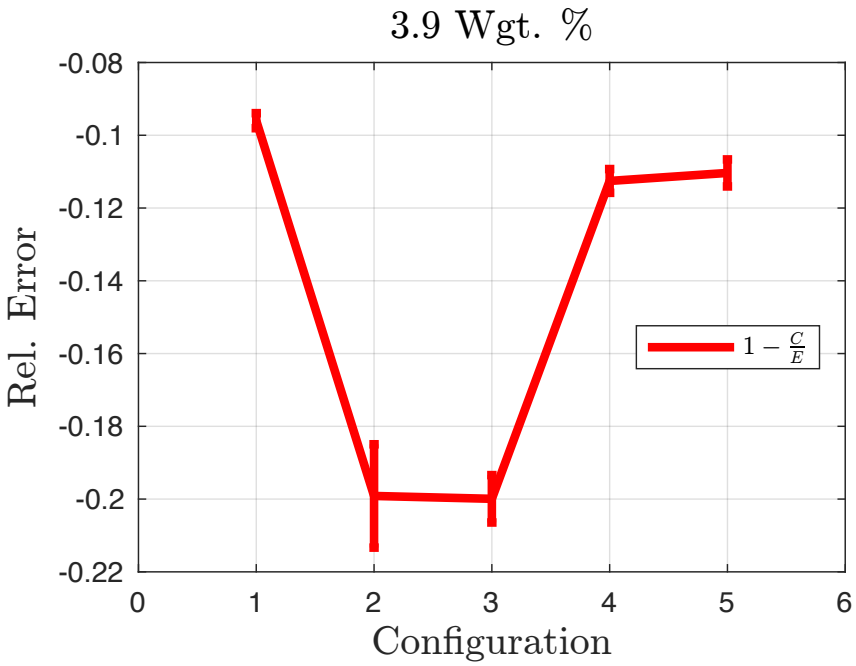

Figure D.6: Doppler temperature coefficient comparison with uranium containing 3.9 wgt. %

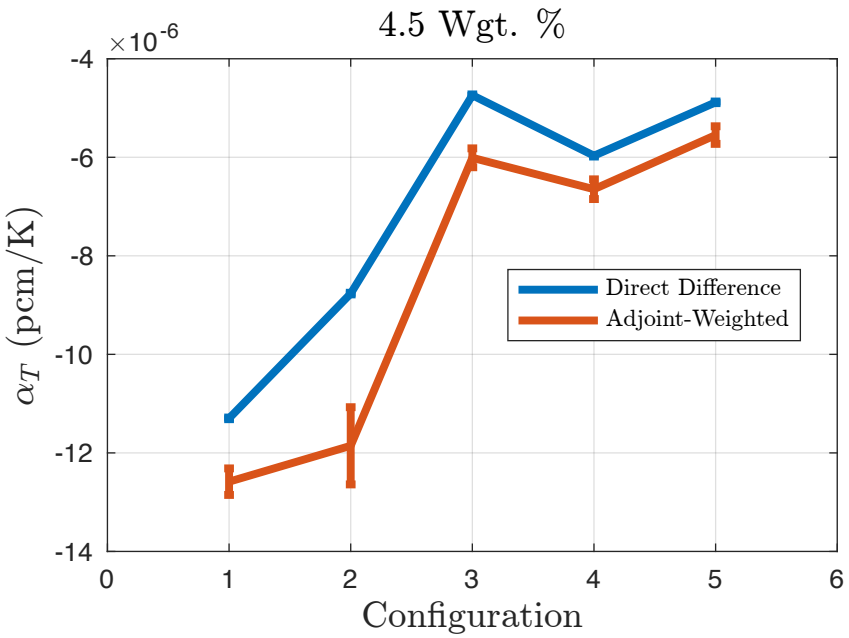

Figure D.7: Doppler temperature coefficient comparison with uranium containing 4.5 wgt. %

4.5 Wgt. %		
Config.	**Direct Difference** $(\Delta\rho/\Delta T)$ **(1/K)**	**Adjoint-Weighted** (α_T) **(1/K)**
1	-1.1299e-05	-1.2584e-05
2	-8.7663e-06	-1.1856e-05
3	-4.7406e-06	-6.0106e-06
4	-5.9682e-06	-6.6477e-06
5	-4.8846e-06	-5.5492e-06

Table D.4: Doppler temperature coefficient comparison for fuel assemblies computed with direct difference and the adjoint method.

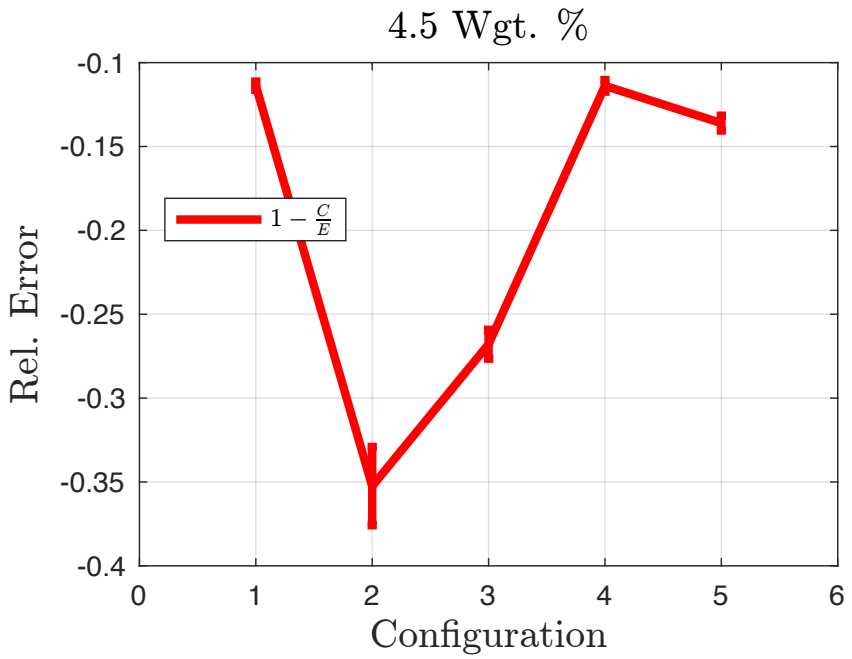

Figure D.8: Doppler temperature coefficient comparison with uranium containing 4.5 wgt. %

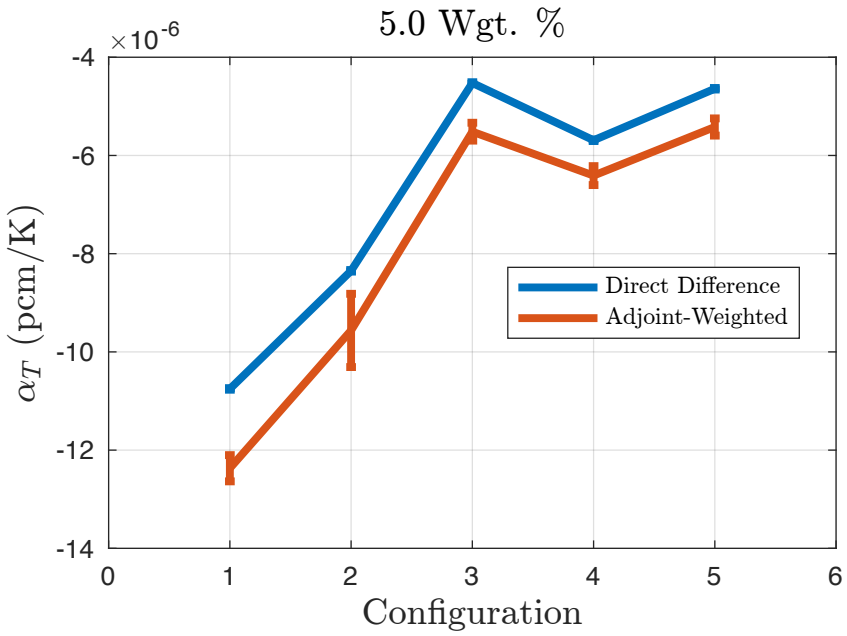

Figure D.9: Doppler temperature coefficient comparison with uranium containing 5.0 wgt. %

5.0 Wgt. %

Config.	**Direct Difference** $(\Delta\rho/\Delta T)$ **(1/K)**	**Adjoint-Weighted** (α_T) **(1/K)**
1	-1.0754e-05	-1.2369e-05
2	-8.3488e-06	-9.5628e-06
3	-4.5242e-06	-5.5157e-06
4	-5.6903e-06	-6.4098e-06
5	-4.6415e-06	-5.4203e-06

Table D.5: Doppler temperature coefficient comparison for fuel assemblies computed with direct difference and the adjoint method.

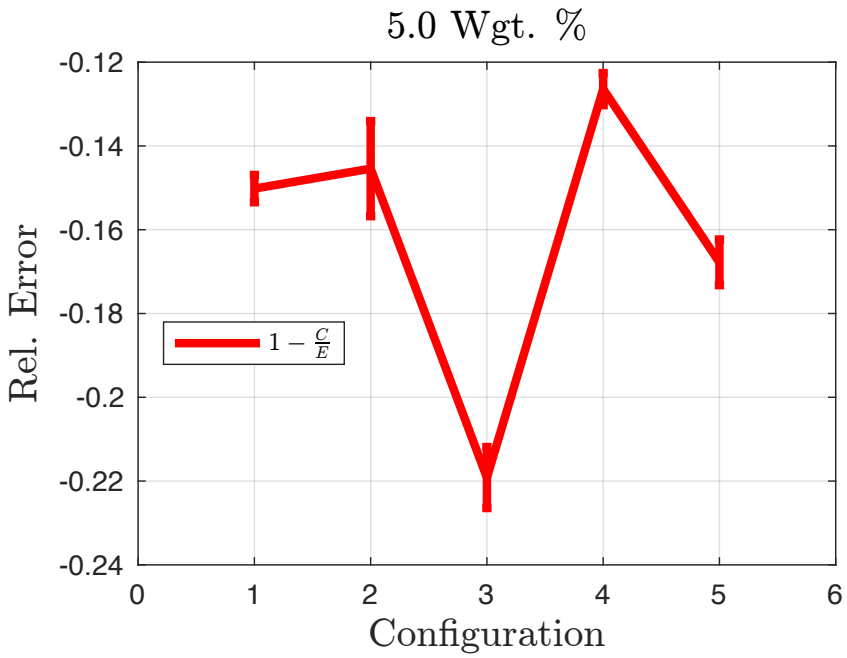

Figure D.10: Doppler temperature coefficient comparison with uranium containing 5.0 wgt. %

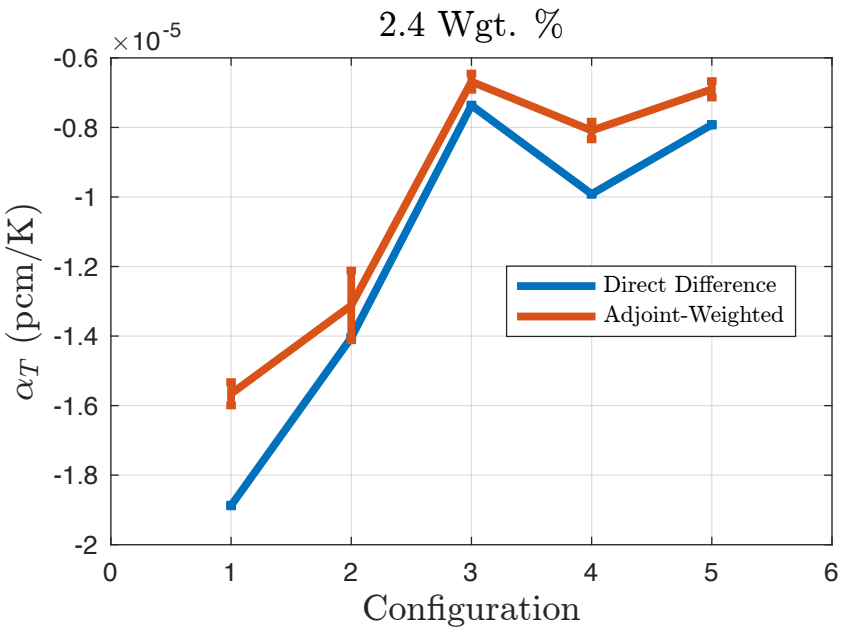

Figure D.11: Doppler temperature coefficient comparison with uranium carbide containing 2.4 wgt. %

2.4 Wgt. %

Config.	**Direct Difference** $(\Delta\rho/\Delta T)$ **(1/K)**	**Adjoint-Weighted** (α_T) **(1/K)**
1	-1.8873e-05	-1.5660e-05
2	-1.4046e-05	-1.3118e-05
3	-7.3659e-06	-6.6838e-06
4	-9.9151e-06	-8.0888e-06
5	-7.9223e-06	-6.9044e-06

Table D.6: Doppler temperature coefficient comparison for fuel assemblies computed with direct difference and the adjoint method.

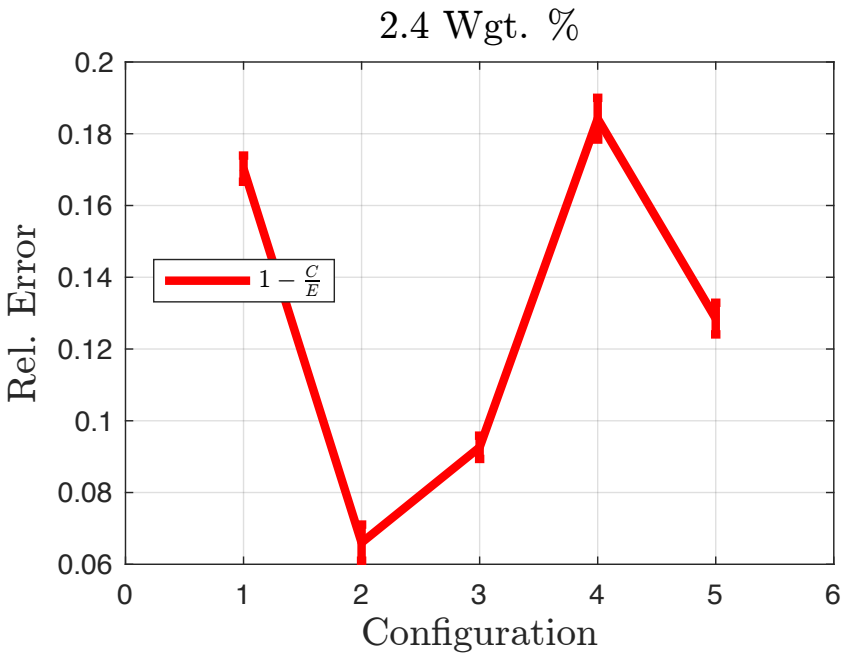

Figure D.12: Doppler temperature coefficient comparison with uranium carbide containing 2.4 wgt. %

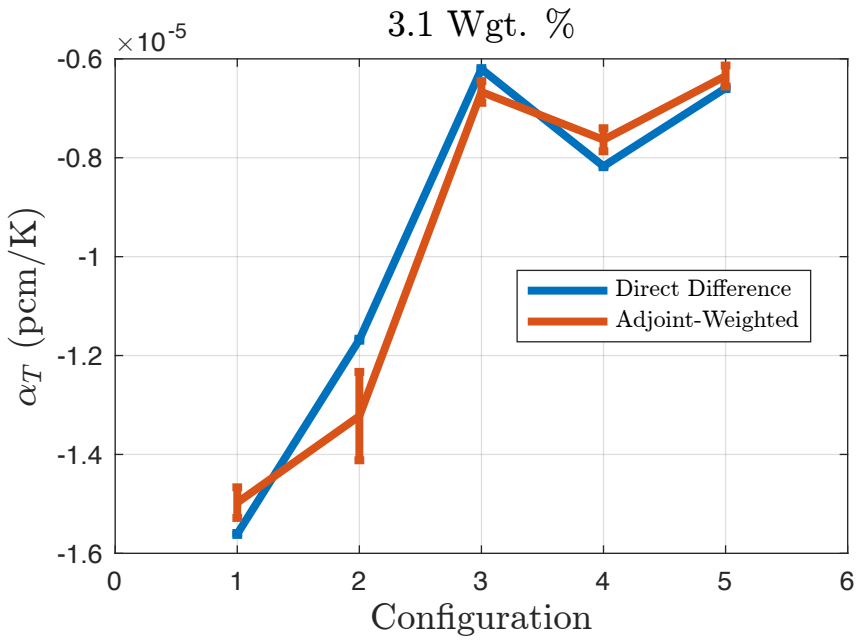

Figure D.13: Doppler temperature coefficient comparison with uranium carbide containing 3.1 wgt. %

3.1 Wgt. %

Config.	**Direct Difference** ($\Delta\rho/\Delta T$) **(pcm/K)**	**Adjoint-Weighted** (α_T) **(pcm/K)**
1	-1.560	-1.497
2	-1.168	-1.322
3	-0.620	-0.666
4	-0.817	-0.763
5	-0.659	-0.634

Table D.7: Doppler temperature coefficient comparison for fuel assemblies computed with direct difference and the adjoint method.

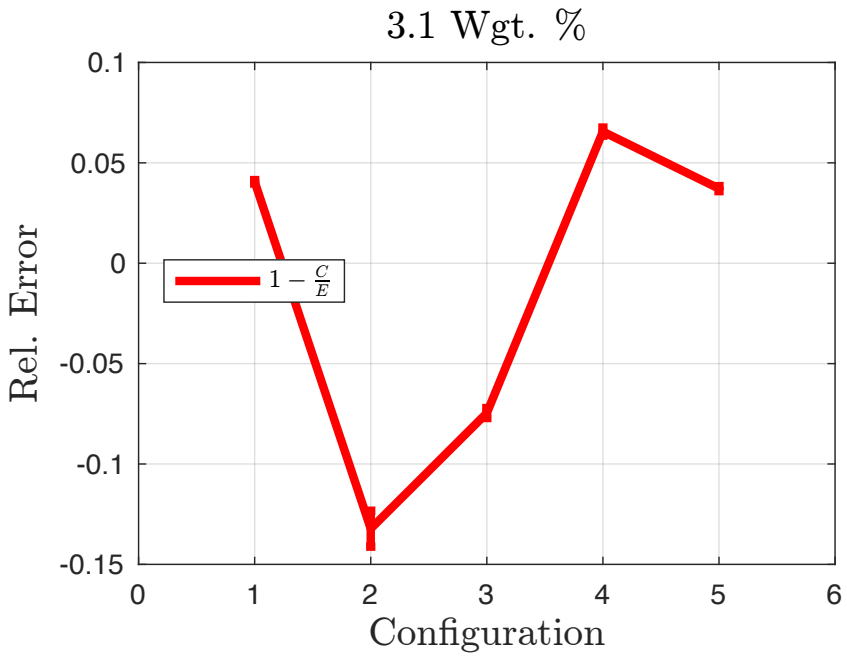

Figure D.14: Doppler temperature coefficient comparison with uranium carbide containing 3.1 wgt. %

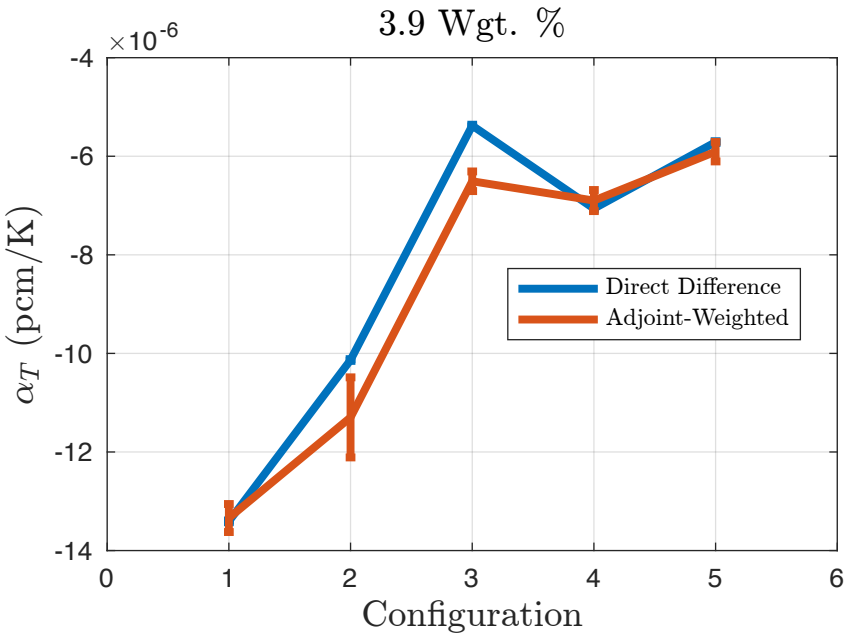

Figure D.15: Doppler temperature coefficient comparison with uranium carbide containing 3.9 wgt. %

3.9 Wgt. %

Config.	**Direct Difference** ($\Delta\rho/\Delta T$) **(pcm/K)**	**Adjoint-Weighted** (α_T) **(pcm/K)**
1	-1.340	-1.334
2	-1.013	-1.129
3	-0.538	-0.651
4	-0.706	-0.690
5	-0.571	-0.591

Table D.8: Doppler temperature coefficient comparison for fuel assemblies computed with direct difference and the adjoint method.

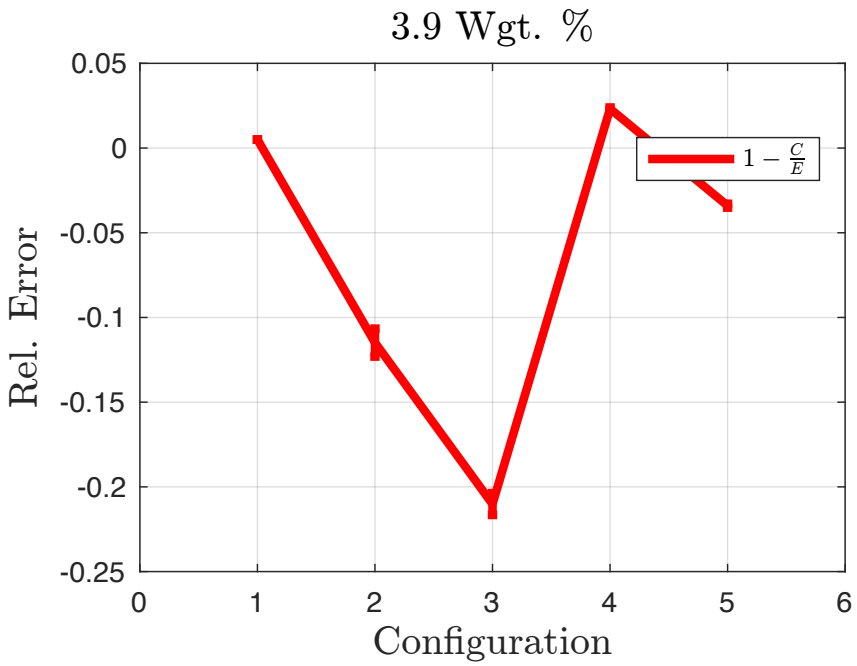

Figure D.16: Doppler temperature coefficient comparison with uranium carbide containing 3.9 wgt. %

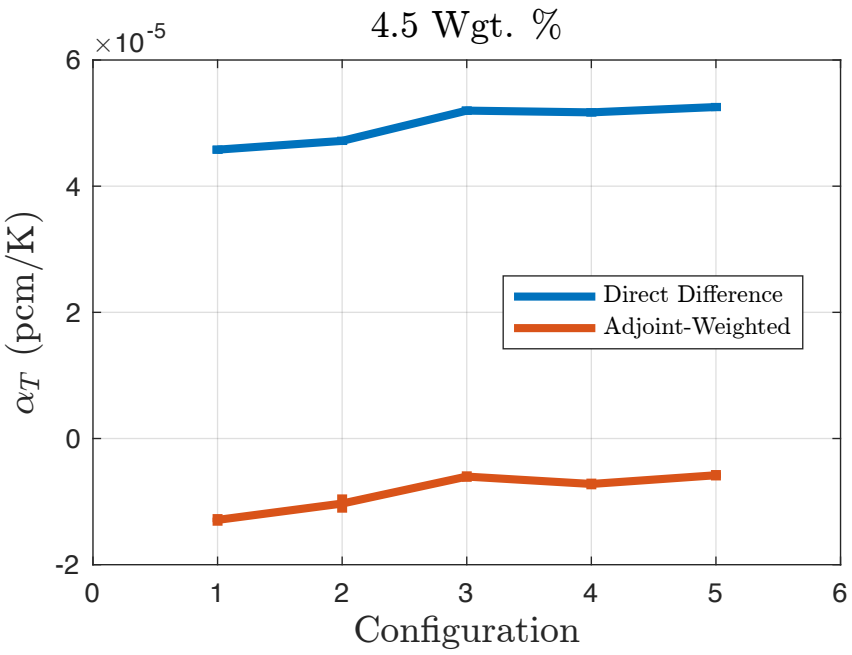

Figure D.17: Doppler temperature coefficient comparison with uranium carbide containing 4.5 wgt. %

4.5 Wgt. %

Config.	**Direct Difference** $(\Delta\rho/\Delta T)$ **(pcm/K)**	**Adjoint-Weighted** (α_T) **(pcm/K)**
1	-0.547	-1.290
2	-0.565	-1.030
3	-0.625	-0.633
4	-0.371	-0.721
5	-0.632	-0.582

Table D.9: Doppler temperature coefficient comparison for fuel assemblies computed with direct difference and the adjoint method.

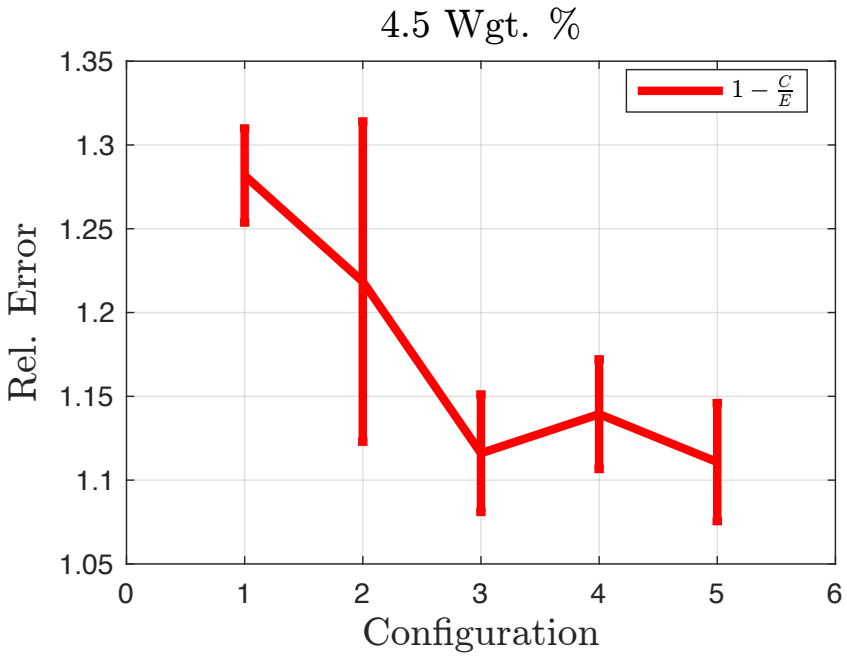

Figure D.18: Doppler temperature coefficient comparison with uranium carbide containing 4.5 wgt. %

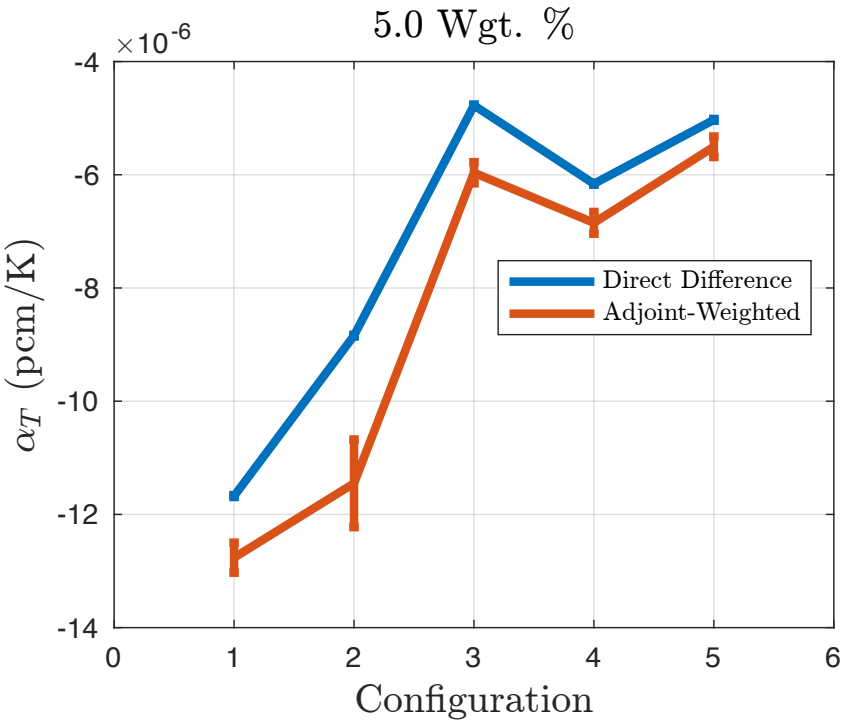

Figure D.19: Doppler temperature coefficient comparison with uranium carbide containing 5.0 wgt. %

5.0 Wgt. %		
Config.	**Direct Difference** ($\Delta\rho/\Delta T$) **(pcm/K)**	**Adjoint-Weighted** (α_T) **(pcm/K)**
1	-1.386	-1.276
2	-1.052	-1.145
3	-0.570	-0.596
4	-0.735	-0.685
5	-0.601	-0.551

Table D.10: Doppler temperature coefficient comparison for fuel assemblies computed with direct difference and the adjoint method.

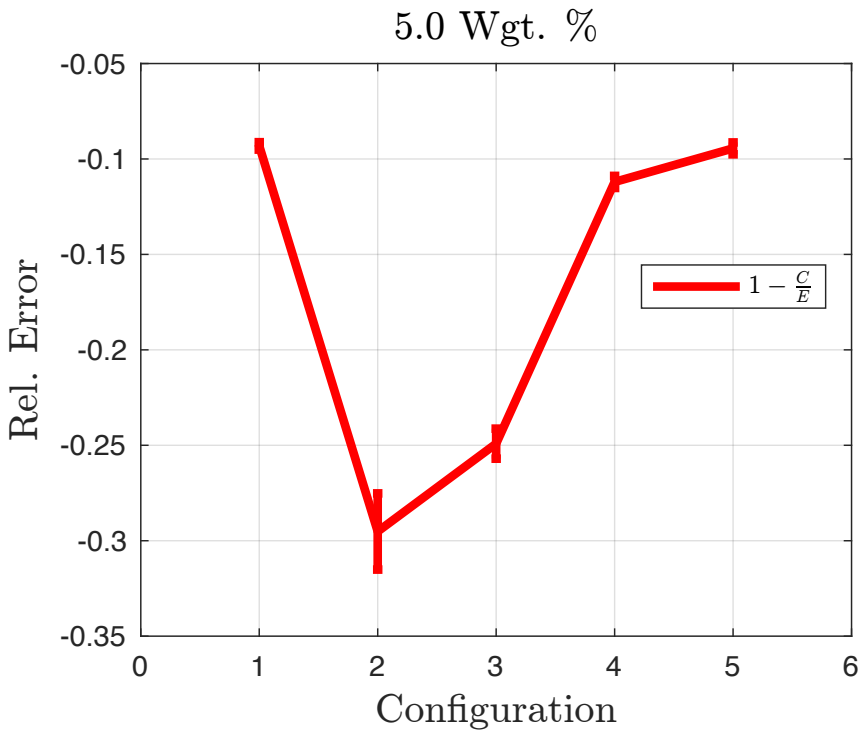

Figure D.20: Doppler temperature coefficient comparison with uranium carbide containing 5.0 wgt. %

References

[1] R. Baragiola, "Introduction and collision kinematics," 2003.

[2] T. Goorley, et al., "Initial MCNP6 Release Overview," *Nuclear Technology*, vol. 180, pp. 298–315, December 2012.

[3] B. Kiedrowski, "Advances in sensitivity analysis with mcnp," *Seminar for the Chemical and Nuclear Engineering Department at the University of New Mexico*, no. LA-UR-13-21327, 2013.

[4] G. Blackshaw and R. Murray, "Scattering functions for low-energy neutron collisions in a maxwellian monatomic gas," *Nucl. Sci. Eng.*, vol. 27, 1967.

[5] M. Ouisloumen and R. Sanchez, "A model for neutron scattering off heavy isotopes that accounts for thermal agitation effects.," *Nucl. Sci. Eng.*, vol. 107, 1991.

[6] E. Sunny, "Temperature effects of resonant scattering for epithermal neutrons in MCNP," in *Proc. Int. Conf. Advances in Reactor Physics: Linking Research, Industry, and Education (PHYSOR 2012)*, (Knoxville, Tennessee), April 15-12 2012.

[7] W. Rothenstein, "Proof of the formula for the ideal gas scattering kernel for nuclides with strongly energy dependent scattering cross sections.," *Ann. Nucl. Energy*, vol. 31, 2004.

[8] W. Rothenstein and R. Dagan, "Two-body kinetics treatment for neutron scattering from a heavy maxwellian gas," *Ann. Nucl. Energy*, vol. 22, 1995.

[9] S. Ghrayeb and et al, "The resonance neutron scattering angular moments using the deterministic approach," *Trans. Am. Nucl. Soc.*, vol. 103, 2010.

[10] S. Ghrayeb and et al, "Multigroup computation of the temperature-dependent resonance scattering (RSM) and its implementation," in *Proc. Int. Conf. Mathematics and Computiational Methods Applied to Nuclear Science & Engineering (M&C 2013)*, (Sun Valley, Idaho), May 5-9 2013.

[11] D. Lee, K. Smith, and J. Rhodes, "The impact of ^{235}U resonance elastic scattering approximations on thermal reactor doppler reactivity," *Ann. Nucl. Energy*, vol. 36, 2009.

[12] M. Ono, K. Wanda, and T. Akita, "Simplified treatment of exact resonance elastic scattering model in deterministic slowing down equation.," in *Proc. Int. Conf. Advances in Reactor Physics: Linking Research, Industry, and Education (PHYSOR 2012)*, (Knoxville, Tennessee), April 15-20 2012.

[13] R. Sanchez, C. Hewko, and S. Santandrea, "Numerical computation of doppler-broadening in the resonance domain," in *Proc. Int. Conf. Mathematics and Computiational Methods Applied to Nuclear Science & Engineering (M&C 2013)*, (Sun Valley, Idaho), May 5-9 2013.

[14] S. Ghrayeb and et al, "Multi-group formulation of the temperature-dependent resonance scattering model and its impact on reactor core parameters," *Ann. Nucl. Energy*, vol. 63, 2014.

[15] B. Becker, R. Dagan, and G. Lohnert, "Proof and implementation of the stochastic formula for ideal gas, energy dependent scattering kernel," *Ann. Nucl. Energy*, vol. 36, 2009.

[16] T. Mori and Y. Nagaya, "Comparison of resonance elastic scattering models newly implemented in MVP continuous-energy monte carlo code," *J. Nucl. Sci. Technol.*, vol. 46, 2009.

[17] A. Zoia, "Doppler broadening of neutron elastic scattering kernel in TRIPOLI-4," *Ann. Nucl. Energy*, vol. 54, 2013.

[18] S. Hart and et al, "Implementation of the doppler broadening rejection correction in KENO," *Trans. Am. Nucl. Soc.*, vol. 108, 2010.

[19] R. Mosteller, "Computational benchmarks for the doppler reactivity defect," in *ANS Joint Benchmark Committee*, 2006.

[20] H. Rief, "Generalized monte carlo perturbation algorithms for correlated sampling and a second-order taylor series approach," *Ann. Nucl. Energy*, vol. 11, no. 9, 1984.

[21] H. Shim, C. Gil, and C. Kim, "Nuclear data sensitivity and uncertainty analysis using adjoint flux estimated in monte carlo forward calculations," in *Int. Conf. on Nuclear Data for Science and Technology*, (Jeju Islan, Korea), April 26-30 2010.

[22] H. Shim and C. Kim, "Monte carlo fuel temperature coefficient estimation by an adjoint-weighted correlated sampling method," *Nuc. Sci. Eng.*, vol. 177, pp. 184–192, 2014.

[23] M. Gonzales and et al, "Monte carlo doppler temperature coefficients with perturbation theory," in *Transactions of the American Nuclear Society*, vol. 109, (Washington, D.C.), November 10-14 2013.

[24] B. Kiedrowski and F. Brown, "Adjoint-weighted kinetics parameters with continuous energy monte carlo," *Trans. Am. Nucl. Soc.*, vol. 100, 2009.

[25] Y. Nagaya and T. Mori, "Impact of perturbed fission source on the effective multiplication factor in monte carlo perturbation calculations," *J. Nucl. Sci. Technol.*, vol. 42, 2005.

[26] J. J. Duderstadt and L. J. Hamilton. Wiley, 1976.

[27] E. Lewis and W. Miller Jr., "Computational methods of neutron transport," 1993.

[28] M. Kalos and P. Whitlock, "Monte carlo methods," 1986.

[29] G. Bell and S. Glasstone. New York: Litton Educational Publishing, 1970.

[30] D. Pelowitz. 2013.

[31] F. Brown, "Lecture notes monte carlo techniques for nuclear systems," 2014.

[32] B. Kiedrowski and F. Brown, "Adjoint-based k-eigenvalue sensitivity coefficients to nuclear data using continuous-energy monte carlo," *Nucl. Sci. Eng.*, vol. 174, pp. 227–244, 2013.

[33] G. Yesilyurt, W. Martin, and F. Brown, "On-the-fly doppler broadening for monte carlo codes," *Nucl. Sci. Eng.*, vol. 171, pp. 239–257, 2012.

[34] D. Cullen and C. Weisbin, "Exact doppler broadening of tabulated cross sections," *Nucl. Sci. Eng.*, vol. 60, 1976.

[35] J. Rhodes, K. Smith, and D. Lee, "Casmo-5 development and applications," 2006.

[36] W. M. Stacey, *Neutron Thermalization*, pp. 453–481. Weinheim, Germany: Wiley-VCH Verlag GmbH & Co. KGaA, 2007.

[37] M. Williams. 1966.

[38] H. Hurwitz Jr., M. Nelkin, and G. Habetler, "Netron thermalizaion," 1956.

[39] E. Larsen and M. Williams, "New fokker-planck derivation of heavy gas models for neutron thermalizaion," 1990.

[40] J. Wilkins Jr., "Cp-2481,"

[41] L. J. Slater, *Confluent Hypergeometric Functions*, pp. 503–515. National Bureau of Standards, 1964.

[42] A. MacDonald, "Properties of the Confluent Hypergeometric Function," *Technical Report No. 84, Research Laboratory of Electronics, Massacusetts Institute of Technology*, 1948.

[43] W. Conkie, "Velocity dependent neutron transport theory"," *Nucl. Sci.Eng.*, vol. 7, 1959.

[44] A. Pappano, G. Blackshaw, and W. Squire, "p_1 total scattering probability for low-energy neutron scattering by a monatomic gas," *Journal Nucl. Eng.*, 1959.